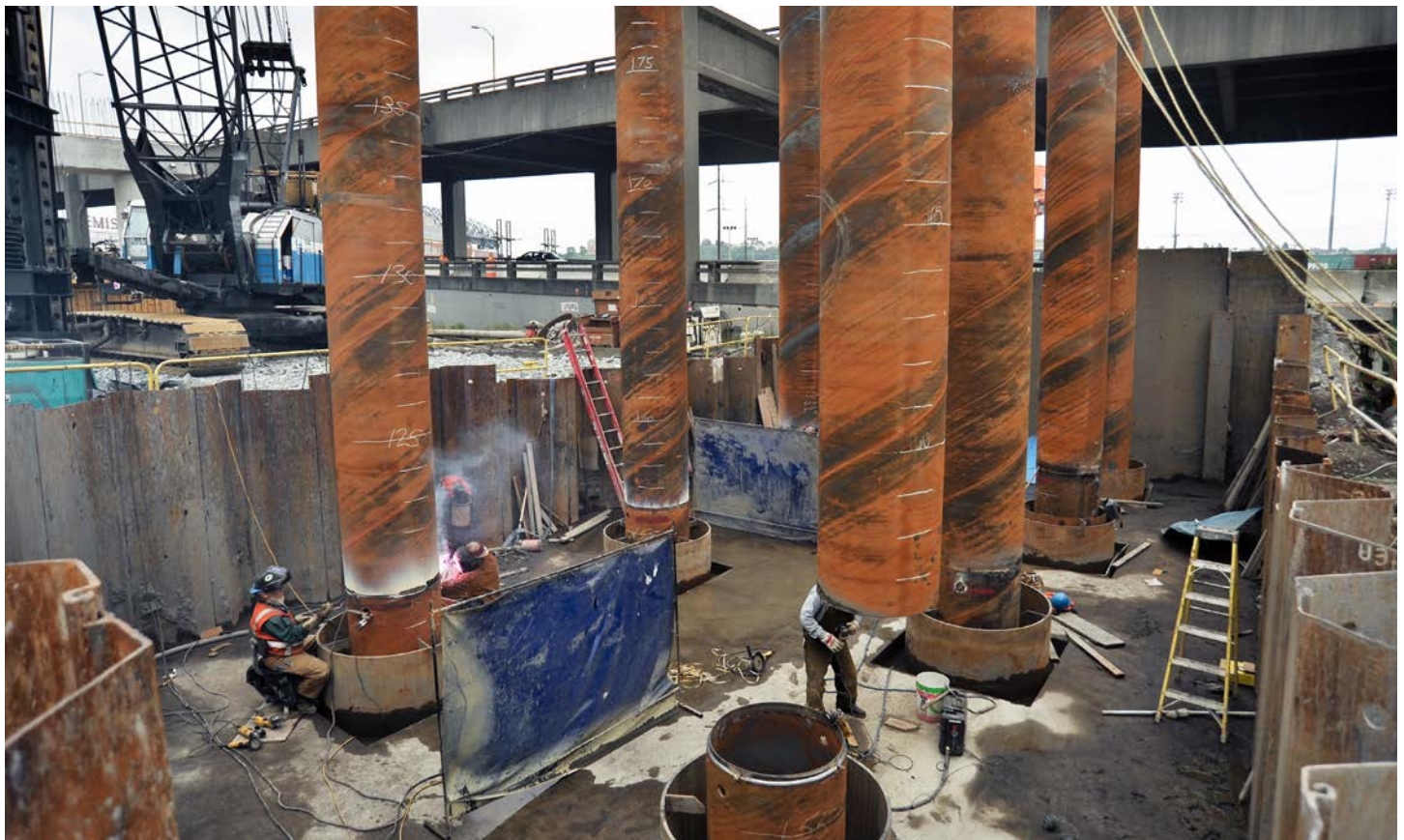


Shear Design Expressions for Concrete Filled Steel Tube and Reinforced Concrete Filled Tube Components

WA-RD 776.2

Charles Roeder
Dawn Lehman
Ashley Heid
Todd Maki

June 2016



**Washington State
Department of Transportation**

Office of Research & Library Services

WSDOT Research Report

Research Report
Agreement T1461, Task 04
Shear Design Expressions

**SHEAR DESIGN EXPRESSIONS FOR CONCRETE FILLED STEEL
TUBE AND REINFORCED CONCRETE FILLED TUBE
COMPONENTS**

by

Charles Roeder
Professor

Dawn Lehman
Professor

Ashley Heid
Graduate Student

Todd Maki
Graduate Student

Department of Civil and Environmental Engineering
University of Washington, Box 352700
Seattle, Washington 98195

Washington State Transportation Center (TRAC)
University of Washington, Box 354802
University District Building
1107 NE 45th Street, Suite 535
Seattle, Washington 98105-4631

Washington State Department of Transportation
Technical Monitor
Bijan Khaleghi
Bridge Design Engineer, Bridge Administration Section

Prepared for

The State of Washington
Department of Transportation
Roger Millar, Acting Secretary

June 2016

TECHNICAL REPORT STANDARD TITLE PAGE

1. REPORT NO. WA-RD 776.2	2. GOVERNMENT ACCESSION NO.	3. RECIPIENT'S CATALOG NO.	
4. TITLE AND SUBTITLE SHEAR DESIGN EXPRESSIONS FOR CONCRETE FILLED STEEL TUBE AND REINFORCED CONCRETE FILLED TUBE COMPONENTS		5. REPORT DATE June 2016	
		6. PERFORMING ORGANIZATION CODE	
7. AUTHOR(S) Charles Roeder, Dawn Lehman, Ashley Heid, Todd Maki		8. PERFORMING ORGANIZATION REPORT NO.	
9. PERFORMING ORGANIZATION NAME AND ADDRESS Washington State Transportation Center (TRAC) University of Washington, Box 354802 University District Building; 1107 NE 45th Street, Suite 535 Seattle, Washington 98105-4631		10. WORK UNIT NO.	
		11. CONTRACT OR GRANT NO. Agreement T1461, Task 04	
12. SPONSORING AGENCY NAME AND ADDRESS Research Office Washington State Department of Transportation Transportation Building, MS 47372 Olympia, Washington 98504-7372 Project Manager: Kim Willoughby, 360.705.7978		13. TYPE OF REPORT AND PERIOD COVERED Research Report	
		14. SPONSORING AGENCY CODE	
15. SUPPLEMENTARY NOTES This study was conducted in cooperation with the U.S. Department of Transportation, Federal Highway Administration.			
16. ABSTRACT: Concrete-filled steel tubes (CFSTs) and reinforced concrete-filled steel tubes (RCFSTs) are increasingly used in transportation structures as piers, piles, caissons or other foundation components. While the axial and flexural properties of CFTs have been well researched, research on their shear resistance is lacking. Currently accepted methods for calculating the shear capacity of CFSTs and RCFTs are adapted from shear strength equations used for structural steel or reinforced concrete components. Though, it is expected that CFSTs would retain the full shear capacity of the steel without local buckling of the section. In addition, because circular CFSTs provide optimum confinement to the concrete core, it is also expected that the full shear strength of plain or longitudinally reinforced concrete can also be developed. Since no equation currently accounts for both, it is probable that they significantly underestimate the effectiveness of the composite section, potentially increasing undesirable conservatism and cost. However, without experimental data to validate the design expressions, it is not possible to modify them. The research program described herein experimentally investigated the shear resistance and deformation of CFST and RCFST members with an eye towards developing an improved and more accurate shear strength expression. The experimental study included 22 large-scale CFTs subjected to four-point bending. The study parameters included: (1) the aspect ratio (a/D where a is the clear span from the point of loading to the point of support and D is the tube diameter), (2) concrete strength, (3) D/t (where t is the thickness of the steel tube), (4) interface condition (greased or contaminated with soil), (5) infill type (concrete or gravel), (6) internal reinforcement ratio, and (6) length of the tube beyond the support (tail length). The results indicate that the shear strength of CFSTs and RCFSTs is on average 2 times the current WSDOT expression. This new design expression for shear resistance has been proposed for implementation in the WSDOT Bridge Design Manual (BDM).			
17. KEY WORDS Concrete Filled Steel Tubes, CFST, RCFST, Shear resistance		18. DISTRIBUTION STATEMENT No restrictions. This document is available to the public through the National Technical Information Service, Springfield, VA 22616	
19. SECURITY CLASSIF. (of this report) None	20. SECURITY CLASSIF. (of this page) None	21. NO. OF PAGES	22. PRICE

DISCLAIMER

The contents of this report reflect the views of the authors, who are responsible for the facts and the accuracy of the data presented herein. The contents do not necessarily reflect the official views or policies of the Washington State Department of Transportation or Federal Highway Administration. This report does not constitute a standard, specification, or regulation.

TABLE OF CONTENTS

CHAPTER 1 INTRODUCTION.....	1
RESEARCH OBJECTIVES.....	3
FORMAT OF THIS REPORT.....	4
CHAPTER 2 PRIOR RESEARCH AND CURRENT DESIGN MODELS....	6
CURRENT DESIGN METHODS.....	6
PRIOR EXPERIMENTAL RESEARCH ON SHEAR CAPACITY OF CFST..	9
Qian, Cui, and Fang (2007).....	9
Xu, Haxiao, and Chengkui (2009).....	12
Xiao, Cai, Chen, and Xu (2012).....	16
Nakahara and Tokuda (2012).....	19
COMPARISON OF SHEAR PROVISIONS USING PREVIOUS RESEARCH RESULTS.....	21
DISCUSSION AND EVALUATION OF TEST SETUPS.....	24
CHAPTER 3 DEVELOPMENT OF EXPERIMENTAL PROGRAM.....	26
EXPERIMENTAL TEST SETUP.....	26
INSTRUMENTATION.....	30
TEST MATRIX.....	31
MATERIAL PROPERTIES.....	4
SPECIMEN CONSTRUCTION.....	37
CHAPTER 4 EXPERIMENTAL RESULTS.....	40
LOADING PROCEDURE.....	40
SPECIMEN FAILURE.....	40
PERFORMANCE CATEGORIZATION AND FAILURE MODE.....	48
Flexural Failure in CFST.....	49
Shear Failure in CFST.....	50
Flexural-Shear Interaction in CFST.....	51
Bond Slip in CFST.....	51
DISCUSSION OF SPECIFIC TEST RESULTS.....	54
Specimen 5 – CFST with Muddy Interface.....	54
Specimen 8 – RCFST Specimen with Combined Behavior.....	56
Specimen 9 – CFST Specimen with Greased Interface.....	59
Specimen 13 – CFST Specimen with Axial Load.....	62
Specimen 17 CFST with Flexural Behavior.....	65

Specimen 21 – Steel Tube with Gravel Fill	68
CHAPTER 5 FURTHER ANALYSIS OF RESEARCH RESULTS	72
COMPOSITE ACTION AND DEVELOPMENT LENGTH	72
COMPARISON OF RCFST AND CFST.....	75
CONTAMINATION OF STEEL-CONCRETE INTERFACE	76
EFFECT OF CONCRETE STRENGTH.....	78
EVALUATION OF DESIGN EXPRESSIONS	79
Evaluation of Current WSDOT Provisions.....	81
Recommended Provisions.....	83
CHAPTER 6 NONLINEAR ANALYSIS AND PARAMETER STUDY	90
INITIAL VERIFICATION AND IMPROVEMENT OF THE MODEL	94
VALIDATION OF THE FINAL MODEL.....	99
PARAMETER STUDY	100
Axial Load Ratio.....	102
Diameter to Thickness Ratio, D/t.....	103
Concrete Strength, f_c'	105
Yield Stress of Steel Tube, F_{yst}	106
Effect of Internal Reinforcement Ratio, ρ	108
IMPROVED DESIGN EXPRESSIONS	111
CHAPTER 7 SUMMARY, CONCLUSIONS, AND RECOMMENDATIONS	121
SUMMARY	121
CONCLUSIONS.....	122
RECOMMENDATIONS.....	124
REFERENCES.....	126

LIST OF FIGURES

Figure 2. 1: Models for prediction of resistance of CFST, a) Plastic Stress Distribution Method, b) AISC Strain Compatibility Method, and c) ACI Method	7
Figure 2. 2: Schematic of Test Rig for Qian et al. (2007)	10
Figure 2. 3: Dependence of V_c on a/D for Qian et al. (2007)	10
Figure 2. 4: Schematic of Test Rig for Xu et al. (2009)	13
Figure 2. 5: Effect of End-Caps for Xu et al. (2009)	13
Figure 2. 6: Effect of Concrete Type for Xu et al. (2009)	15
Figure 2. 7: Schematic of Test Rig for Xiao et al. (2012)	17
Figure 2. 8: Effect of Ruptured End-Cap weld for Xiao et al. (2012)	19
Figure 2. 9: Schematic of Test Rig for Nakahara and Tokuda (2012).....	20
Figure 3. 1: Experimental Setup	27
Figure 3. 2: Test Apparatus.....	29
Figure 3. 3: Deformed Specimen and Elastomeric Bearing Movement	29
Figure 3. 4: Photo of Typical Instrumentation.....	31
Figure 3. 5: Test Specimen Preparation a) Tubes Prepared for Casting, b) Concrete Placement	38
Figure 3. 6: Muddied CFST Interface, a) Creating Surfaces, b) Finished Surface.....	39
Figure 4. 1: Typical Moment Displacement Curve with Proportional Limit	41
Figure 4. 2: Displacement and Span Measurements	43
Figure 4. 3: Shear Span Deformation and Restraint	43
Figure 4. 4: Characteristics of Flexural Mode	49
Figure 4. 5: Characteristics of Shear Failure in CFST	50
Figure 4. 6: Characteristics of Slip within CFST, a) Slip between the Concrete Sill and Steel Tube, b) Rigid Movements of Concrete Blocks with no Shear or Flexural Cracking	51
Figure 4. 7: Behavior of Specimen 5	55
Figure 4. 8: Specimen 5 Photos	56
Figure 4. 9: Behavior of Specimen 8	58

Figure 4. 10: Specimen 8 Photos	59
Figure 4. 11: Behavior of Specimen 9	61
Figure 4. 12: Specimen 9 Photos	62
Figure 4. 13: Behavior of Specimen 13	64
Figure 4. 14: Specimen 13 Photos	65
Figure 4. 15: Behavior of Specimen 17	67
Figure 4. 16: Specimen 17 photos.....	68
Figure 4. 17: Behavior of Specimen 21	70
Figure 4. 18: Photos of Specimen 21	71
Figure 5. 1: Tail Length Comparisons	74
Figure 5. 2: Moment-Displacement Behavior of Interface Series Specimens.....	77
Figure 5. 3: Comparison of Current WSDOT Design Equation to UW Experiments.....	82
Figure 5. 4: Comparison of Current WSDOT Design Equation to Prior Experimental Results.....	83
Figure 5. 5: Comparison of Possible Design Equation to UW Experiments	85
Figure 5. 6: Comparison of Possible Equation to Prior Experimental Results.....	86
Figure 5. 7: Comparison of Proposed Design Equation to UW Experiments	88
Figure 5. 8: Comparison of Proposed Equation to Prior Experimental Results	89
Figure 6.1: Base Model in ABAQUS	90
Figure 6.2: Material Models	91
Figure 6.3: Computed and Measured Response of Specimen 17	96
Figure 6.4: Force-Deflection Behavior of Specimen 16.....	97
Figure 6.5: Observed Asymmetric Deformations of Shear Dominated Specimens .	97
Figure 6.6: Replacement of the Support Cradle with Axial Springs	98
Figure 6.7: Confinement Model Used for Specimen 17 Based on Han 2007b.....	99
Figure 6.8: V_{pmax} vs. Axial Load Ratio	102
Figure 6.9: η vs. Axial Load Ratio	103
Figure 6.10: Bilinear Relationship of η vs. Axial Load Ratio for $a/D=.375$	103
Figure 6.11: Shear Resistance vs. Axial Load with Different D/t Ratios.....	104

Figure 6.12: η vs. Axial Load Ratio with Different D/t Ratios	105
Figure 6.13: η vs. Axial Load Ratio with Different Concrete Strength	106
Figure 6.14: Shear Resistance vs. Axial Load Ratio with Different Yield Stress, F_{yst}	107
Figure 6.15: η vs. Axial Load Ratio for Various Steel Yield Stresses	108
Figure 6.16: Shear Resistance vs. Axial Load Ratio for RCFST Specimens	110
Figure 6.17: η vs. Axial Load Ratio of RCFST Specimens	111
Figure 6.18: Example of Least Squares Linear Regression Fit Line Using CFST	112
Figure 6.19: Comparison of $\eta = 5(1 + 5 \cdot P/P_0) \leq 10$ for Shear-Controlled Models ...	113
Figure 6.20: Comparison of $V_{n(prop)}$ to Experimental Results Meeting Proposed Limit State Criterion, Including Axial Load	115
Figure 6.21: Comparison of $V_{n(prop)}$ to Shear Controlled Models, Meeting Limit State Criterion.....	116
Figure 6.22: Comparison of $V_{n(prop)}$ to Experimental and Analytical RCFST Shear Specimens, Meeting Proposed Limit State Criterion	117
Figure 6.23: Comparison of $V_{n(prop)}$ to Experimental and Analytical Shear Specimens, Meeting Proposed Limit State Criterion	118
Figure 6.24: Contribution of Tube Steel, Internal Reinforcement, and Concrete to Total Shear Resistance According to $V_{n(prop)}$	119
Figure 6.25: Contribution of Tube Steel, Internal Reinforcement, and Concrete to Total Shear Resistance According to $V_{n(prop)}$ Using All Data.....	119
Figure 6.26: Contribution of Tube Steel, Internal Reinforcement, and Concrete to Total Shear Resistance According to $V_{n(prop)}$ Using Typical CFST Design.....	120

LIST OF TABLES

Table 2. 1: Results for Qian et al. (2007).....	11
Table 2. 2: Results for Xu et al. (2009).....	14
Table 2. 3: Results for Xiao et al. (2012).....	17
Table 2. 4: Results for Nakahara and Tokuda (2012).....	21
Table 2. 5: Results for WSDOT Without Axial Load or Expansive Concrete.....	22
Table 2. 6: Results for AISC Method 1 Without Axial Load or Expansive Concrete.....	22
Table 2. 7: Results for AISC Method 2 Without Axial Load or Expansive Concrete.....	22
Table 3. 1: Test Matrix.....	32
Table 3. 2: CFST Material Properties.....	36
Table 3. 3: CFST Reinforcing Bar Properties.....	37
Table 4. 1: Summary of Key Performance States.....	46
Table 4. 2: Summary of Concrete States	47
Table 4. 3: Specimen Failure Classification	53
Table 5. 1: Tail Length Series Specimens and Comparisons.....	73
Table 5. 2: RCFST Specimen Properties	76
Table 5. 3: Interface Series Specimen Properties	77
Table 5. 4: Concrete Strength Series Specimen Properties.....	79
Table 6.1: Concrete Damaged Plasticity Parameters.....	92
Table 6.2: Specimens for Verification Study.....	94
Table 6.3: Summary of Error in Predicted Ultimate Shear Resistance.....	100

CHAPTER 1

INTRODUCTION

Concrete-filled steel tubes (CFST) have been used extensively throughout the world in building and transportation structures as columns, beams, braces, truss elements, and foundation components. CFSTs combine steel and concrete to create efficient and economical composite structural members. They utilize the high strength and ductility of steel and the ability concrete to efficiently carry compressive load and flexure. The concrete restrains local buckling of the steel tube while the steel tube provides longitudinal and transverse reinforcement of the concrete. The steel tube provides formwork and shoring during construction, thus speeding construction and reducing costs.

Reinforced concrete-filled steel tubes (RCFSTs) are less commonly employed, but can be found when other structural components are connected to CFSTs or when an increased strength is required due to geometric limitations. While CFSTs can be constructed with either rectangular or circular steel tubes, research (Roeder et al. 2009) has shown that circular CFSTs offer better confinement of the concrete and better bond stress between the concrete and steel, increasing the effective composite action in the member.

The axial and flexural properties of CFSTs have been well researched and reported in the literature but little research has been performed on the shear strength and behavior of CFST and RCFST. The *Specification for Structural Steel Buildings* by the American Institute of Steel Construction (AISC 2010) provides three methods for calculating the shear capacity of CFST members, but only two of these methods are

currently permitted by the AASHTO LRFD provisions. The Washington Department of Transportation (WSDOT 2012), in a design memorandum addressing the use of CFST and RCFST in bridge foundations, recommends using a variation of the third AISC method, where the design expression that sums the shear capacities of the individual steel and concrete components without accounting for any interaction. All methods neglect the composite behavior and are likely to significantly underestimate the shear capacity of the composite section, potentially increasing undesirable conservatism and cost.

Current research on the shear resistance of CFST has been focused primarily in Japan and China, where CFSTs are used more frequently in construction than in the United States. With more research and awareness of their benefits, CFSTs are gaining wider acceptance in the U.S. for transportation. CFST and RCFST offer great benefits for the design of bridge piles, drilled shafts and pier columns. The primary advantages are: (1) superior composite strength and stiffness relative to a reinforced concrete column of the same size, (2) inherent local stabilization of the thin wall steel tube by the concrete fill, (3) optimized confinement of the concrete fill by the circular tube, and (4) more rapid and economical construction. Under extreme loading, RCFST and CFST members develop excellent inelastic deformation capacity while mitigating damage and deterioration. They are an efficient solution for many components in bridge design.

An unrealized potential of CFST and RCFST components is their inherently large shear strength. Accurate expression that account for the true shear strength could decrease the size of these components. For example, piles and drilled shafts subjected to seismic loads, soil liquefaction, and/or lateral spreading of the soil may experience very large, local shear forces, which may require large diameter members. The diameter

impacts constructability and construction costs. If research could provide a more realistic and larger estimate of the shear capacity, the diameter could be decreased. This could result in significant cost savings due to reduced materials and labor as well as other reductions in other construction costs.

In addition to the shear capacity alone, the impact of large shear demands on the flexural strength (i.e., normal stresses) and the interface shear, or bond, capacity must be understood. It is critical to sustain the bond strength between the steel tube and concrete fill to ensure the development of the composite strength and stiffness of CFST. In addition, the length required to fully develop the shear (and moment) capacity of a CFST or RCFST is needed.

To date, a very few small-scale shear tests have been conducted. Prior testing to study shear resistance of CFST is limited to small diameter tubes (typically 4 to 8 inches in diameter). Because piles and caissons used in bridge construction are of much larger diameter than the limited prior test programs, these prior tests results are not clearly applicable.

RESEARCH OBJECTIVES

This research used integrated experimental testing methods combined with high-resolution analytical models to investigate the shear capacity of CFST and RCFST members. The research program includes the five primary tasks:

1. A thorough study and evaluation of prior research work and existing shear strength design methods.

2. Development of an experimental program of large-scale CFST and RCFST subjected to transverse shear load.
3. Completion of a test program to evaluate parameters that affect the shear capacity of CFST and RCFST.
4. Study of the results using of high-resolution finite element models to support and supplement the experimental results.
5. Combine the experimental and analytical results with prior research results to develop design expressions for shear resistance and behavior.

The relevant parameters for experimental and analytical research include effect of axial compression, effect of internal reinforcement, material strength, D/t , development length needed to assure the full shear and flexural resistance of CFST, and the effects of contamination of the contact surface between steel and concrete possible during construction. The D/t ratios used in this research were somewhat larger than commonly used in piles and drilled shafts, because most piles and drilled shafts may require an allowance for corrosion and additional thickness to facilitate driving and handling the tube. In addition, the predicted strengths and deformations may be based on this final corroded state. Further, the experiments are large-scale to simulate bridge construction.

FORMAT OF THIS REPORT

This report is divided in six chapters. This Chapter 1 introduces the research and the technical question. Chapter 2 proved a detailed discussion of prior research existing models for predicting shear capacity of CFST and RCFST. Chapter 3 describes the test setup, instrumentation, test specimens and test matrix on the experimental research program. Chapter 4 provides a detailed summary of individual test results. Chapter 5

provides an analysis of the experimental test results in greater detail. The results are combined with analytical results and the results of other prior experimental research to evaluate and develop design expressions for shear strength and behavior. Chapter 6 will summarize the design recommendations and the conclusions and results of this research.

CHAPTER 2

PRIOR RESEARCH AND CURRENT DESIGN MODELS

CURRENT DESIGN METHODS

Substantial research on the flexural, axial and combined flexural axial strength of CFST has been completed (Roeder et al. 2010, Moon et al. 2014). Design provisions for the CFST are included in the American Institute of Steel Construction (AISC) specifications (AISC 2010) the American Concrete Institute (ACI) specifications (ACI 2010), and the American Association of State Highway and Transportation Officials (AASHTO) specifications (AASHTO 2016), and there has historically been wide variation among these three specifications. However, recent changes to the AASHTO LRFD specification have dramatically narrowed the variations between the AASHTO and AISC provisions, because of research demonstrating the greater accuracy of the AISC provisions (Bishop 2009).

The AASHTO and AISC provisions permit both the plastic stress distribution method (PSDM) and the strain compatibility methods for evaluating the basic axial, flexural and combined axial and flexural capacity of CFST and RCFST. Research (Bishop 2009, and Roeder et al. 2010) has shown that the PSDM provides a consistently more accurate yet conservative prediction of resistance with less scatter when compared to experimental results than the strain compatibility method, because the strain compatibility method requires a strain or deformation limit. Strain or deformation limits on steel or concrete are inherently less meaningful for CFST and RCFST than for reinforced concrete members, because the concrete fill is extremely well confined and spalling cannot occur.

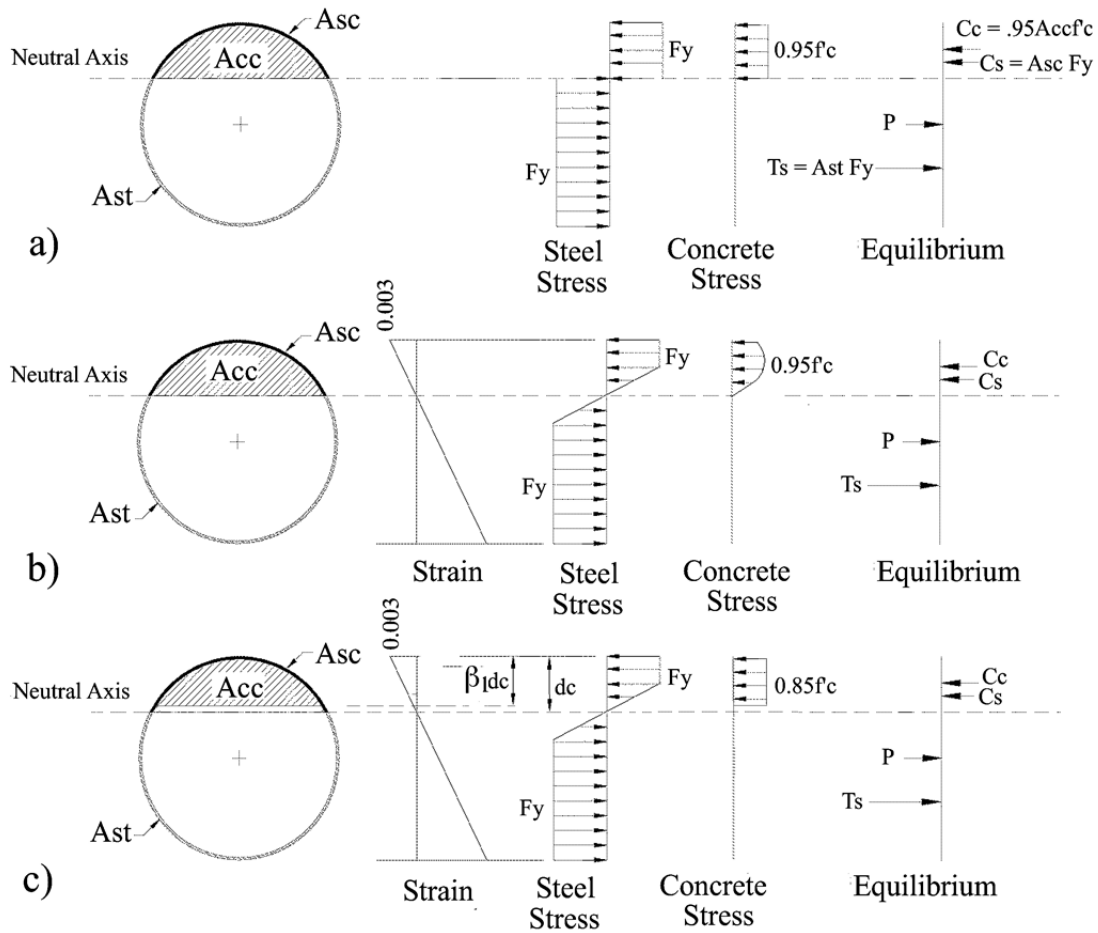


Figure 2. 1: Models for prediction of resistance of CFST, a) Plastic Stress Distribution Method, b) AISC Strain Compatibility Method, and c) ACI Method

Methods for predicting shear resistance of CFST are still quite variable because of the limited research in this area. The AISC provision (2010) permit three methods for calculating the shear strength of CFST and RCFST members. The first, shown in Equations 2.1, relies only upon the available shear strength of the steel tube, neglecting any contribution by the concrete fill. The second method, shown in Equations 2.2, utilizes the shear strength of the concrete and any internal shear reinforcement, ignoring the steel tube. The third method, shown in Equations 2.3, is a hybrid of the first two, utilizing the shear strength of the steel tube and the contribution from any transverse reinforcement that is in the concrete fill.

AISC Method 1

$$V_n (AISC_1) = V_s \quad (2.1a)$$

$$\text{where } V_s = 0.6f_y(0.5A_s) \quad (2.1b)$$

AISC Method 2

$$V_n (AISC_2) = V_c + V_{sr} \quad (2.2a)$$

$$\text{where } V_c = 2\sqrt{f'_c}A_c \quad (2.2b)$$

$$V_{sr} = \frac{A_y f_y D}{s} \quad (2.2c)$$

AISC Method 3

$$V_n (AISC_3) = V_s + V_{sr} \quad (2.3a)$$

$$\text{where } V_s = 0.6f_y(0.5A_s) \quad (2.3b)$$

$$V_{sr} = \frac{A_y f_y D}{s} \quad (2.3c)$$

The ACI specification (2011) limits the shear resistance of CFST to that of the concrete fill, and its shear resistance is comparable to that of AISC Method 2.

The AASHTO Specification (2016) limits the shear resistance of CFST and RCFST to that of the steel only and is comparable to the prediction provided by AISC Method 1.

The WSDOT shear design expression combines the respective strengths of the concrete fill and the steel tube but neglects the positive effects the concrete fill and the

steel tube have on each other. Equations 2.4 show the WSDOT design expression for CFST and RCFST members.

$$V_n (WSDOT) = V_s + 0.5V_c \quad (2.4a)$$

$$\text{where } V_s = 0.6f_y(0.5A_s) \quad (2.4b)$$

$$V_c = 0.0316\beta\sqrt{f'_c}A_c \text{ if } P_u \text{ is compressive} \quad (2.4c)$$

and f'_c is in ksi and $\beta = 2$.

where A_s is the cross sectional area of the steel tube, A_c is the area of the concrete fill, f_y is yield stress of the respective steel element, f'_c is the compressive strength of the concrete, and A_y is the total cross sectional area of the internal reinforcement.

PRIOR EXPERIMENTAL RESEARCH ON SHEAR CAPACITY OF CFST

Few research programs have been performed to investigate the shear resistance of circular, concrete-filled steel tubes. This section reviews the results and conclusions of four experimental programs that employed small-scale CFSTs. For axially loaded specimens, the axial load ratio, P/P_0 , is reported with P_0 is the crush capacity of the composite member as computed by the PSDM. The results of the WSDOT shear expression are presented for each specimen. A brief evaluation of the comparison of the current design models to these experimental results is present in a later section.

Qian, Cui, and Fang (2007)

Qian et al. (2007) performed thirty-five tests of circular CFSTs to investigate their shear strength. The tests used a three-point bending setup with monotonic loading, as shown in Figure 2.2. These specimens were tested with and without axial compressive load. The test

parameters included shear span to depth ratio, concrete strength, axial force ratio, and tube wall thickness. All the specimens had an outer diameter of 194 mm (7.64 in.) and most specimens had end-caps, which limited or prevented slip between the concrete fill and the steel tube. Fifteen specimens were tested with no axial load. The shear span to depth ratio, a/D , ratios included in the program varied from 0.1 to 1.0.

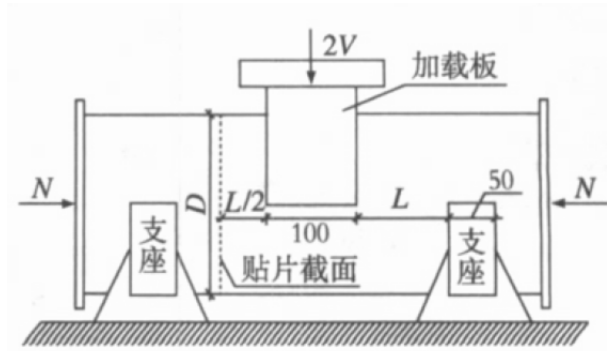


Figure 2. 2: Schematic of Test Rig for Qian et al. (2007)

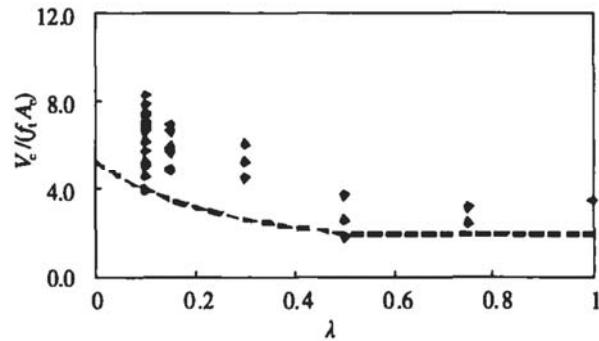


Figure 2. 3: Dependence of V_c on a/D for Qian et al. (2007)

The authors reported that twenty-seven specimens failed in shear, three failed in flexure-shear, and five failed in flexure. For specimens with no axial load, shear span to depth ratio had the largest effect on failure mode; when $a/D \leq 0.3$, the CFST failed in shear; when $a/D = 0.5$, the CFST failed in flexure-shear interaction; and when $a/D \geq 0.75$, the CFST failed in flexure. When axial load was present, specimens with $a/D = 0.75$ also

failed in flexure-shear interaction. Table 2.1 shows the specimen properties and the test results of the reported shear failures.

Table 2. 1: Results for Qian et al. (2007)

Specimen	a (in)	a/D	t (in)	D/t	f_{ym} (ksi)	f'_{cm} (ksi)	P/P_0	V_{exp} (kip)	V_n (WSDOT) (kip)	V_{exp}/V_n (WSDOT)	
Q1	0.76	0.100	0.217	35.3	47.9	5.87	0	286	76	3.78	
Q2	0.76	0.100	0.295	25.9	61.2	5.87		289	128	2.26	
Q7	1.15	0.150	0.217	35.3	47.9	5.87		439	76	5.81	
Q8	1.15	0.150	0.295	25.9	61.2	5.87		458	128	3.58	
Q9	0.76	0.100	0.217	35.3	47.9	8.06		501	76	6.57	
Q10	0.76	0.100	0.295	25.9	61.2	8.06		283	129	2.20	
Q15	1.15	0.150	0.217	35.3	47.9	8.06		230	76	3.02	
Q16	1.15	0.150	0.295	25.9	61.2	8.06		225	129	1.75	
Q17	2.29	0.300	0.295	25.9	61.2	8.06		395	129	3.07	
Q28	0.76	0.100	0.217	35.3	47.9	9.79		326	77	4.26	
Q29	0.76	0.100	0.295	25.9	61.2	9.79		398	129	3.09	
Q34	1.15	0.150	0.217	35.3	47.9	9.79		289	77	3.78	
Q35	1.15	0.150	0.295	25.9	61.2	9.79		220	129	1.71	
Q3	0.76	0.100	0.217	35.3	47.9	5.87		0.431	281	76	3.72
Q4	0.76	0.100	0.295	25.9	61.2	5.87		0.463	375	128	2.93
Q5	0.76	0.100	0.217	35.3	47.9	5.87	0.719	378	76	5.00	
Q6	0.76	0.100	0.295	25.9	61.2	5.87	0.772	409	128	3.20	
Q11	0.76	0.100	0.217	35.3	47.9	8.06	0.414	272	76	3.57	
Q12	0.76	0.100	0.295	25.9	61.2	8.06	0.446	277	129	2.15	
Q13	0.76	0.100	0.217	35.3	47.9	8.06	0.689	336	76	4.41	
Q14	0.76	0.100	0.295	25.9	61.2	8.06	0.297	263	129	2.05	
Q18	2.29	0.300	0.295	25.9	61.2	8.06	0.446	387	129	3.01	
Q19	2.29	0.300	0.217	35.3	47.9	8.06	0.689	391	76	5.13	
Q30	0.76	0.100	0.217	35.3	47.9	9.79	0.403	376	77	4.92	
Q31	0.76	0.100	0.295	25.9	61.2	9.79	0.435	271	129	2.10	
Q32	0.76	0.100	0.217	35.3	47.9	9.79	0.672	226	77	2.95	
Q33	0.76	0.100	0.295	25.9	61.2	9.79	0.290	291	129	2.26	

The researchers concluded that:

- CFSTs that fail in shear have a large deformation capacity.
- For a/D ratios less than 0.5 the concrete shear strength is dependent upon the shear span to depth ratios, as shown in Figure 2.5.
- The shear strength of the CFST increases with increasing axial load.

Xu, Haixiao, and Chengkui (2009)

Xu et al. (2009) investigated the shear behavior of self-stressing circular concrete-filled steel tubes (SSCFSTs). That is, the SSCFSTs were filled with an expansive concrete used to counteract the negative effects (i.e. reduced bond capacity) of concrete shrinkage on the composite behavior and to investigate potential performance increase resulting from the radial pre-stressing of the section. They reported test results on thirty-five specimens with diameters ranging from 140 mm (5.5 in.) to 165.5 mm (6.5 in.). Twenty-seven of the specimens were SSCFSTs and the remaining eight were standard CFSTs. The CFSTs used a conventional concrete. The primary test parameters were the self-stressing and the shear span to depth ratio. The specimens were subjected to a three-point bending test with monotonic loading, as shown in Figure 2.4.

The authors reported thirty-one shear failures and four flexural failures. Only seven of the shear failures contained conventional concrete. Table 2.2 summarizes the specimen properties and the test results of the reported shear failures. None of the specimens were axially loaded.

All but five of the specimens tested had end-caps. Notable differences were observed in the ultimate shear strength and plastic deformation of specimens with and without end-caps. Figure 2.5 shows force-displacement plots of Specimen Sc-2 (Xu12 in the table), with end-caps, and Specimen Uc-2 (Xu25 in the table), without end-caps. Other variable parameters were consistent, and both specimens used expansive concrete.

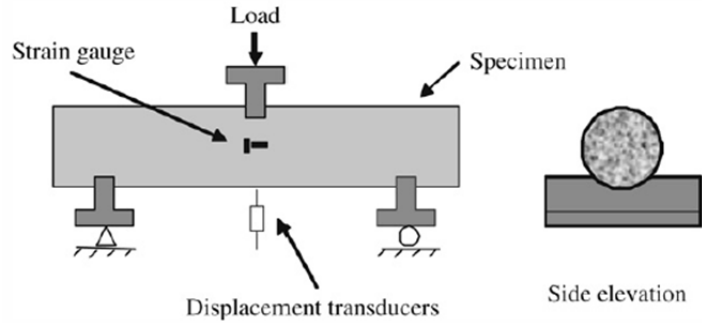


Figure 2. 4: Schematic of Test Rig for Xu et al. (2009)

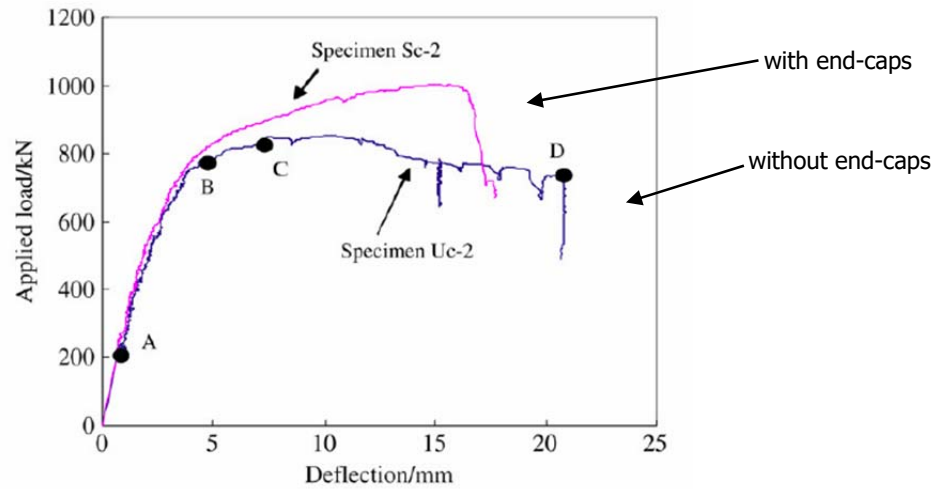


Figure 2. 5: Effect of End-Caps for Xu et al. (2009)

Eight of the specimens used conventional concrete. The CFST specimens had lower ultimate shear capacity and higher ultimate deformation when compared to the SSCFST specimens. Figure 2.6a shows the force-displacement plots two specimens with end-caps: Specimen Sb-2 (Xu7 in the table), with expansive concrete, and Specimen So-2 (Xu17 in the table), with conventional concrete. Figure 2.6b shows the force-displacement plots two specimens without end-caps: Specimen Ub-2 (Xu22 in the table), with expansive concrete, and Specimen Uo-2 (Xu27 in the table), with conventional concrete.

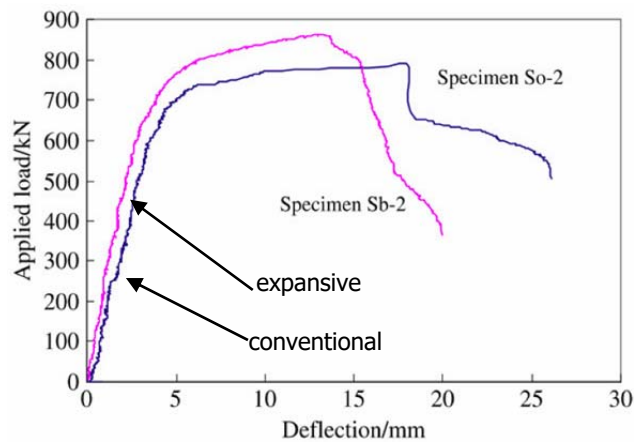
Table 2. 2: Results for Xu et al. (2009)

Specimen	a (in)	a/D	t (in)	D/t	f_{ym} (ksi)	f'_{cm} (ksi)	Radial Stress (ksi)	end-cap	V_{exp} (kip)	V_n (WSDOT) (kip)	V_{exp}/V_n (WSDOT)
Xu16	0.55	0.1	0.145	38	52.8	4.88	0	Yes	40	93	2.31
Xu17	1.1	0.2	0.145	38	52.8	4.88		Yes	40	83	2.07
Xu18	1.65	0.3	0.145	38	52.8	4.88		Yes	40	80	1.99
Xu19	2.76	0.5	0.145	38	52.8	4.88		Yes	40	68	1.70
Xu26	0.55	0.1	0.145	38	52.8	4.88		No	40	88	2.20
Xu27	1.1	0.2	0.145	38	52.8	4.88		No	40	79	1.96
Xu28	1.65	0.3	0.145	38	52.8	4.88		No	40	75	1.87
Xu1	0.55	0.1	0.145	38	52.8	5.19	0.81	Yes	40	104	2.58
Xu2	1.1	0.2	0.145	38	52.8	5.19	0.81	Yes	40	97	2.42
Xu3	1.65	0.3	0.145	38	52.8	5.19	0.81	Yes	40	89	2.22
Xu4	2.76	0.5	0.145	38	52.8	5.19	0.81	Yes	40	69	1.71
Xu6	0.55	0.1	0.145	38	52.8	4.94	0.88	Yes	40	109	2.71
Xu7	1.1	0.2	0.145	38	52.8	4.94	0.88	Yes	40	91	2.25
Xu8	1.65	0.3	0.145	38	52.8	4.94	0.88	Yes	40	84	2.09
Xu9	2.76	0.5	0.145	38	52.8	4.94	0.88	Yes	40	76	1.88
Xu11	0.55	0.1	0.145	38	52.8	5.76	0.99	Yes	40	109	2.71
Xu12	1.1	0.2	0.145	38	52.8	5.76	0.99	Yes	40	100	2.48
Xu13	1.65	0.3	0.145	38	52.8	5.76	0.99	Yes	40	94	2.32
Xu14	2.76	0.5	0.145	38	52.8	5.76	0.99	Yes	40	69	1.72
Xu21	0.55	0.1	0.145	38	52.8	4.94	0.68	No	40	100	2.49
Xu22	1.1	0.2	0.145	38	52.8	4.94	0.68	No	40	88	2.18
Xu23	1.65	0.3	0.145	38	52.8	4.94	0.68	No	40	82	2.05
Xu24	0.55	0.1	0.145	38	52.8	5.76	0.84	No	40	110	2.73
Xu25	1.1	0.2	0.145	38	52.8	5.76	0.84	No	40	92	2.29
Xu29	0.65	0.1	0.117	56	52.8	5.19	0.68	Yes	39	107	2.71
Xu30	1.3	0.2	0.117	56	53.8	5.19	0.68	Yes	40	99	2.48
Xu31	1.95	0.3	0.117	56	53.8	5.19	0.68	Yes	40	91	2.26
Xu32	3.26	0.5	0.117	56	53.8	5.19	0.68	Yes	40	78	1.94
Xu33	0.65	0.1	0.117	56	53.8	5.76	0.75	Yes	40	111	2.77
Xu34	1.3	0.2	0.117	56	53.8	5.76	0.75	Yes	40	94	2.35
Xu35	1.95	0.3	0.117	56	53.8	5.76	0.75	Yes	40	88	2.18

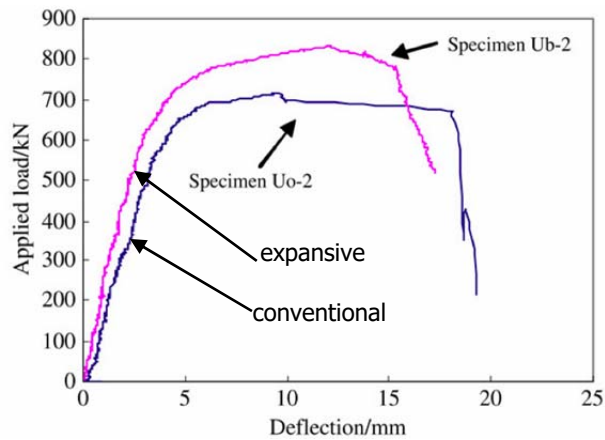
Note: The radial stress is normal to the concrete surface and positive outwards.

The researchers concluded that:

- CFSTs with $a/D < 0.5$ fail in shear.
- CFSTs with $0.5 \leq a/D \leq 1.0$ fail in flexure.
- CFSTs with expansive concrete fill have higher shear capacity.
- The shear capacity of CFSTs with short a/D ratios varies with a/D .
- Slip between the concrete core and the steel tube decreases shear capacity.



a) With End-Caps



b) Without End-Caps

Figure 2. 6: Effect of Concrete Type for Xu et al. (2009)

Xiao, Cai, Chen, and Xu (2012)

Xiao et al. (2012) investigated the shear capacity, ductility, and damage modes of fifty-eight CFST specimens. The test parameters included tube wall thickness, shear span to depth ratio, concrete strength, and axial compression ratio. The tube diameters ranged from 160 mm (6.3 in.) to 166 mm (6.5 in.). They employed a three-point loading bending rig which applied an axial load applied through end caps and with monotonically applied transverse loading, as seen in Figure 2.7. Twenty-five specimens had no axial load.

All specimens and were outfitted with welded end-caps. The welds connecting the end-caps to the tubes failed prematurely on three test specimens allowing differential movement between the concrete fill and the steel tube. They are X25, X26, and X27 in the results table and exhibited less ultimate shear strength than comparable specimens with no weld failure. The welds on the remaining test specimens were strengthened to preclude such a failure. Figure 2.8 shows the force-displacement plots for specimens X27 and X28.

The authors reported fifty-one shear failures, three weld failures, two flexure failures and two flexure-shear failures. Table 2.3 summarizes the specimen properties and the test results of the reported shear failures. Flexural failures were indicated by a steel rupture in the tension zone and a uniform pattern of dense, transverse cracks in the concrete fill, both occurring in the middle of the span. Shear failures exhibited large shear deformations between the load and supports points and the steel tube sheared open at a support. If the steel tube tore at a support, the concrete fill flowed out in powder form, having been crushed. If the steel tube did not tear, the concrete fill contained thin, irregular cracks.

For shear failures with $a/D = 0.14$, the concrete exhibited a direct shear failure.

For shear failures with $a/D = 0.40$, the concrete exhibited diagonal compression failure.

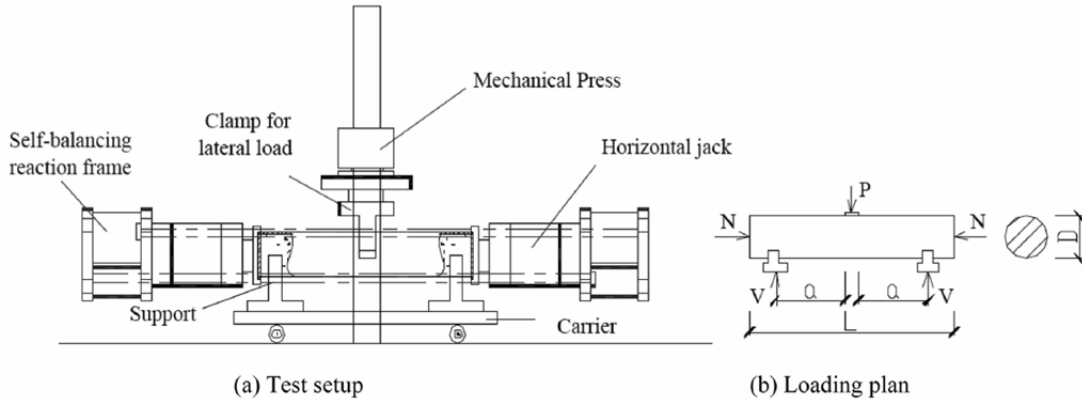


Figure 2. 7: Schematic of Test Rig for Xiao et al. (2012)

Table 2. 3: Results for Xiao et al. (2012)

Specimen	a (in)	a/D	t (in)	D/t	f_{ym} (ksi)	f'_{cm} (ksi)	P/P_0	V_{exp} (kip)	V_n (WSDOT) (kip)	V_{exp} / V_n (WSDOT)
X1	2.52	0.40	0.217	29.1	54.7	3.76	0	221	70	3.17
X2	2.52	0.40	0.217	29.1	54.7	4.70		211	70	3.03
X3	2.52	0.40	0.217	29.1	54.7	4.28		209	70	3.00
X4	2.61	0.40	0.173	37.7	50.0	3.76		169	54	3.13
X5	2.61	0.40	0.173	37.7	50.0	4.70		174	54	3.22
X6	2.61	0.40	0.173	37.7	50.0	4.28		168	54	3.11
X7	2.6	0.40	0.118	55.0	59.2	3.76		115	44	2.61
X8	2.6	0.40	0.118	55.0	59.2	4.70		123	44	2.79
X9	2.6	0.40	0.118	55.0	59.2	4.28		118	44	2.68
X25	0.88	0.14	0.217	29.1	54.7	3.76		170	70	2.44
X26	0.88	0.14	0.217	29.1	54.7	4.70		174	70	2.49
X27	0.88	0.14	0.217	29.1	54.7	4.28		170	70	2.43
X28	0.88	0.14	0.217	29.1	54.7	4.28		289	70	4.15
X29	0.91	0.14	0.173	37.7	50.0	4.28		225	54	4.18
X30	0.91	0.14	0.118	55.0	59.2	4.28		155	44	3.53
X31	0.91	0.14	0.173	37.7	50.0	3.76		220	54	4.09
X32	0.91	0.14	0.173	37.7	50.0	4.70		220	54	4.07
X33	0.91	0.14	0.173	37.7	50.0	4.28		212	54	3.93
X34	0.91	0.14	0.118	55.0	59.2	3.76		154	44	3.51
X35	0.91	0.14	0.118	55.0	59.2	4.70		157	44	3.55
X36	0.91	0.14	0.118	55.0	59.2	4.28	169	44	3.85	

X10	2.52	0.40	0.173	29.1	54.7	3.76	0.31	228	70	3.28
X11	2.52	0.40	0.118	29.1	54.7	4.70	0.30	218	70	3.12
X12	2.52	0.40	0.118	29.1	54.7	4.28	0.30	230	70	3.30
X13	2.61	0.40	0.118	37.7	50.0	3.76	0.30	195	54	3.62
X14	2.61	0.40	0.217	37.7	50.0	4.70	0.29	183	54	3.38
X15	2.61	0.40	0.217	37.7	50.0	4.28	0.29	190	54	3.52
X16	2.6	0.40	0.173	55.0	59.2	3.76	0.30	141	44	3.22
X17	2.6	0.40	0.173	55.0	59.2	4.70	0.28	133	44	3.01
X18	2.6	0.40	0.118	55.0	59.2	4.28	0.28	133	44	3.02
X19	2.52	0.40	0.118	29.1	54.7	3.76	0.62	198	70	2.85
X20	2.52	0.14	0.217	29.1	54.7	4.70	0.60	234	70	3.35
X21	2.61	0.14	0.217	37.7	50.0	3.76	0.61	184	54	3.42
X22	2.61	0.14	0.217	37.7	50.0	4.70	0.58	204	54	3.78
X23	2.6	0.14	0.173	55.0	59.2	3.76	0.60	144	44	3.29
X24	2.6	0.14	0.173	55.0	59.2	4.70	0.56	153	44	3.46
X37	0.88	0.14	0.173	29.1	54.7	3.76	0.31	327	70	4.71
X38	0.88	0.14	0.118	29.1	54.7	4.70	0.30	328	70	4.71
X39	0.88	0.14	0.118	29.1	54.7	4.28	0.30	337	70	4.84
X40	0.91	0.14	0.118	37.7	50.0	3.76	0.30	280	54	5.20
X41	0.91	0.14	0.217	37.7	50.0	4.70	0.29	284	54	5.26
X42	0.91	0.14	0.217	37.7	50.0	4.28	0.29	281	54	5.20
X43	0.91	0.14	0.217	55.0	59.2	3.76	0.30	216	44	4.91
X44	0.91	0.14	0.173	55.0	59.2	4.70	0.28	205	44	4.65
X45	0.91	0.14	0.173	55.0	59.2	4.28	0.28	214	44	4.87
X46	0.88	0.14	0.173	29.1	54.7	3.76	0.62	336	70	4.84
X47	0.88	0.14	0.118	29.1	54.7	4.70	0.60	405	70	5.80
X48	0.88	0.14	0.118	29.1	54.7	4.28	0.60	384	70	5.52
X49	0.91	0.14	0.118	37.7	50.0	3.76	0.61	333	54	6.19
X50	0.91	0.14	0.173	37.7	50.0	4.70	0.58	323	54	5.97
X51	0.91	0.14	0.173	37.7	50.0	4.28	0.58	233	54	4.31
X52	0.91	0.14	0.118	55.0	59.2	3.76	0.60	240	44	5.47
X53	0.91	0.14	0.118	55.0	59.2	4.70	0.56	222	44	5.03
X54	0.91	0.14	0.118	55.0	59.2	4.28	0.56	233	44	5.30

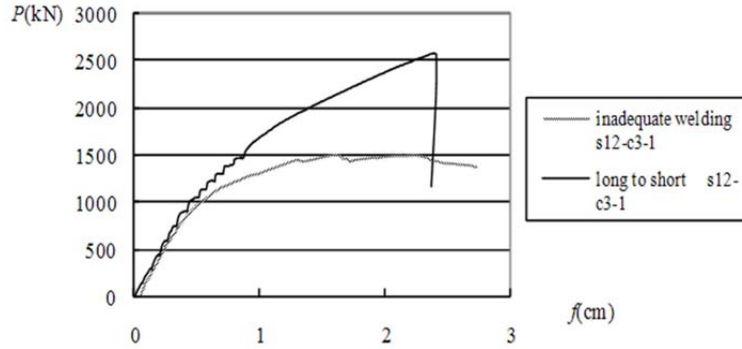


Figure 2. 8: Effect of Ruptured End-Cap weld for Xiao et al. (2012)

The researchers concluded that:

- CFSTs with small a/D ratios, e.g. less than 0.5, fail in shear.
- CFSTs with a small a/D ratio greater than or equal to 0.5 fail in flexure or flexure-shear.
- The shear capacity of CFSTs with small a/D ratios varies with a/D .
- The shear strength of CFSTs increases with increasing axial load.

Nakahara and Tokuda (2012)

Nakahara and Tokuda (2012) tested five CFSTs subjected to shear loading to investigate their shear capacity and deformation behavior. The steel tubes all had a diameter of either 165 mm (6.5 in.) or 166 mm (6.5 in.) and the shear span to depth ratio was 0.5 for all specimens. They only varied concrete strength and axial load ratio in their experimental program. A double-curvature apparatus was employed as seen in Figure 2.9 and a cyclic shear load was applied. All specimens had end-caps.

- (1) Specimen (2) Double-Acting Hydraulic Jack(IMN) (3) Load Cell
 (4) Roller (5) Parallel Supporting Mechanism (6) 5MN Universal-Testing Machine
 (7) Counter Balance

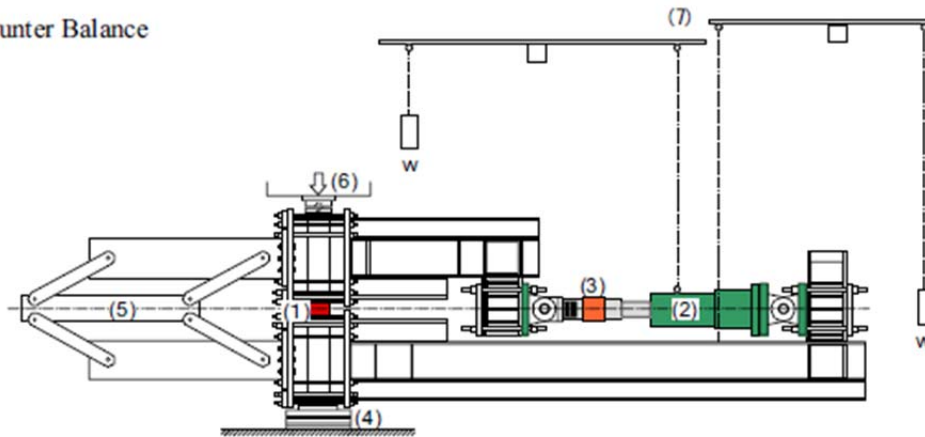


Figure 2. 9: Schematic of Test Rig for Nakahara and Tokuda (2012)

The authors reported that all specimens failed in shear. The CFSTs without axial load showed a stable but mildly pinched hysteretic response. The tube steel did not tear in any of the tests and they do not discuss the state of the concrete fill at the end of each test. Each CFST was tested until the drift equal 0.04 radians. Table 2.5 summarizes the properties and test results of each of the CFST specimens.

Nakahara and Tokuda concluded that:

- All specimens failed in shear before flexural yielding occurred.
- The shear strength of the CFSTs increased after shear yielding of the steel tube occurred, achieving maximum shear strength at a drift of 0.02 radians followed by stable deterioration until the tests were ended.
- The hysteresis properties of the short CFSTs were sufficient to be used as damping devices in seismic regions.

- Low axial load ratios ($P/P_0 \leq 0.4$) increased the shear strength of the CFST. Higher axial load ratios decreased the available shear strength.

Table 2. 4: Results for Nakahara and Tokuda (2012)

Specimen	a (in)	a/D	t (in)	D/t	f_{ym} (ksi)	f'_{cm} (ksi)	P/P_0	V_{exp} (kip)	V_n (WSDOT) (kip)	V_{exp} / V_n (WSDOT)
N1	3.27	0.5	0.193	34	77.5	9.34	0	154	92	1.67
N2	3.27	0.5	0.193	34	77.5	9.34	0.3	158	92	1.77
N3	3.25	0.5	0.197	33	78.6	7.03	0.1	152	94	1.65
N4	3.25	0.5	0.197	33	78.6	7.03	0.2	155	94	1.69
N5	3.25	0.5	0.197	33	78.6	7.03	0.4	144	94	1.57

COMPARISON OF SHEAR PROVISIONS USING PREVIOUS RESEARCH RESULTS

The experimental shear for each of the reported shear failures without axial load or expansive concrete was compared to the current shear design expressions, and a brief analysis was provided to assess their validity. The shear resistance was calculated per the current expressions for each of the thirty-nine specimens. The experimental shears were normalized by those capacities, and the results are summarized in Tables 2.5, 2.6 and 2.7. The current design expressions are extremely conservative. AISC Method 3 without shear reinforcement is the same as Method 1.

Table 2. 5: Results for WSDOT Without Axial Load or Expansive Concrete

Research Program	$V_{exp} / V_n (WSDOT)$						
	# of tests	Mean	Median	Min	Max	Std. Dev.	C.O.V.
Qian et al.	13	3.42	3.09	1.71	6.57	1.27	0.37
Xu et al.	7	2.01	1.99	1.70	2.31	0.21	0.10
Xiao et al.	18	3.42	3.37	2.61	4.18	0.52	0.15
Nakahara and Tokuda	1	1.67	1.67	1.67	1.67	N/A	N/A
All Specimens	39	3.28	3.07	1.53	6.57	1.21	0.37

Table 2. 6: Results for AISC Method 1 Without Axial Load or Expansive Concrete

Research Program	$V_{exp} / V_n (AISC_1)$						
	# of tests	Mean	Median	Min	Max	Std. Dev.	C.O.V.
Qian et al.	13	3.60	3.19	1.76	6.91	1.55	0.43
Xu et al.	7	2.09	2.11	1.76	2.40	0.27	0.13
Xiao et al.	18	3.56	3.51	2.73	4.34	0.54	0.15
Nakahara and Tokuda	1	1.73	1.73	1.73	1.73	N/A	N/A
All Specimens	39	3.37	3.24	1.76	6.91	1.11	0.33

Table 2. 7: Results for AISC Method 2 Without Axial Load or Expansive Concrete

Research Program	$V_{exp} / V_n (AISC_2)$						
	# of tests	Mean	Median	Min	Max	Std. Dev.	C.O.V.
Qian et al.	13	48.2	45.7	28.0	76.6	13.6	0.29
Xu et al.	7	27.1	27.2	22.8	31.1	3.42	0.13
Xiao et al.	18	43.3	40.1	27.1	71.2	11.6	0.27
Nakahara and Tokuda	1	26.8	26.8	26.8	26.8	N/A	N/A
All Specimens	39	42.9	39.8	22.8	76.6	14.0	0.33

This evaluation shows that current design models are not very accurate, because the experimental resistance was always significantly larger than that provided by current design models. The current WSDOT model was the more accurate model, but the average resistance predicted by this model was still only about $1/3$ of the average measured resistance.

It must be noted that the maximum shear capacity may be controlled by maximum flexural resistance for any of the test setups used in this prior research. Hence, some of the measured shear resistances are controlled by flexure or combined shear-flexure rather than shear resistance. Therefore, the predictive models are clearly more conservative than noted in Tables 2.5, 2.6 and 2.7.

Individual researchers predicted whether shear, flexure or combined shear-flexure controlled individual experiments. However, careful review of the work calls the precisions of this determination into question. This determination appears largely to be based upon deflected shape and the relationship of the bending moment and shear for individual test. The deflected shape is approximate at best, since flexural yielding combined with large shear will appear to have shear deformation. The large loads required to develop shear failure also require that load application be distributed over a finite length, and so the relationship between moment and shear for each specimen is imprecise. Evaluation of this data suggests that some specimens identified as shear failures may well be controlled by flexure or combined shear-flexural behavior.

The resistance predicted by the AISC Method 2 relies only on the shear capacity of the concrete fill. Table 2.7 shows that this method is extremely conservative, since the average predicted resistance is only about 2.5% of the average measured resistance.

Finally, it should be emphasized that the data with axial load and expansive concrete are excluded from these tables and comparisons. These effects increased the measured resistance of the CFST specimens, and much greater scatter and variation would result if they were included in the data. Most specimens included in these comparisons had end caps. Normally, end caps are expected to increase the measured

shear resistance. Comparison of figures 2.6a and 2.6b provide some support for this conclusion, but careful review of the reference articles show that the broad applicability of this conclusion is not clear. The articles note that the end caps were sometimes damaged and ineffective in constraining the concrete fill, and the end caps may not have provided direct bearing on the concrete in other cases. Hence their impact on the results is not certain.

DISCUSSION AND EVALUATION OF TEST SETUPS

The above comparison shows that current design models are extremely conservative. Further they demonstrate considerable scatter in the measured shear resistance since the standard deviation and coefficient of variation was relatively large for some test programs. Prior discussion notes that some of this variation may be caused by the uncertainty in the relationship between the maximum moment and maximum shear in the test specimens, and the fact that flexural resistance may control more specimens than suggested by the individual researchers.

Two different test setups were used in the prior research. Qian et al., Xiao et al., and Xu et al. used a simple beam with 3-point loading to load the CFST specimens in shear. Qian and Xiao also included axial compression on the beam with some of the tests. Nakahara and Tokuda used a specimen with ends restrained against end rotation and double curvature in the beam, as shown in Figure 2.9.

These setups were evaluated in considerable detail to determine the experimental setup to be used in this research study. Detailed finite element analyses were performed with CFST specimens of larger size and diameter as planned for this research to examine consequences of the setup and test procedures. The diameter of CFST specimens in prior

research were approximately 6 inches, while the proposed specimens for this research were more than 3 times this diameter. The prior research shows that if all factors except diameter, D , are constant, the shear resistance should increase by the square of the diameter. Therefore, the applied loads necessary to cause shear failure would be in order of 10 times the magnitude of loads used in prior research. These large loads were a major problem in defining a test setup. The analytical predictions suggested that the experimental control of the shear in the specimen is significantly better with the double curvature apparatus used by Nakarahara.

Further, the applied load required with this setup is smaller than that required with 3-point loading. However, the double curvature apparatus (see Figure 2.9) requires building a complex mechanism to permit development of shear while restraining the specimens against rotation. Building a mechanism to develop a shear of 150 kips appeared quite expensive, but building a mechanism to develop a shear of more than 1000 kips as anticipated for this research was very expensive and greatly exceeded the available budget for this research. The three-point loading specimens require a much larger load to develop a 1000 kip shear force, and the application of this large load and reaction of supports resisting this load can damage the specimen before developing the shear resistance.

To prevent the load and reactions must be distributed over a significant length. This also adds considerable cost to the development of the test apparatus, and it compounds the uncertainty in establishing the maximum moment and moment diagram for the test specimens. As a result of this analysis, it was clear that neither of these setups were appropriate for the planned test program.

CHAPTER 3

DEVELOPMENT OF EXPERIMENTAL PROGRAM

The test program was developed to (1) evaluate the shear strength of CFSTs, and (2) investigate parameters that could impact the shear strength, in particular interior surface condition, concrete strength, and the length beyond the support point (also referred to as the tail length).

EXPERIMENTAL TEST SETUP

The 4 point-load configuration illustrated in Figure 3.1 was chosen for the final test setup, because it was significantly less expensive than a double-curvature apparatus and it significantly reduced the applied-moment distribution issue, which complicates determination of the maximum moment in the specimen in the double-curvature test setup. Accurate determination of the maximum moment is critical to determine whether shear or flexure controls the behavior. The 4-point load setup also offered the following benefits over a 3 point-load or double-curvature configurations.

- More accurate determination of the response mode (flexure or shear) since the middle portion of the specimen (between the load cradels) is subjected to a constant moment and therefore the applied moment is more reliably determined.
- The maximum shear demand during testing was expected to approach 1000 kips. A 3-point configuration would have had twice the shear demand applied directly to the specimen resulting in a highly disturbed the load region more than required.

- Any flexural buckling for flexural and combined shear-flexural specimens should occur within the pure bending moment region (outside the shear zone), thus allowing the concrete to remain confined by the steel in the shear spans.

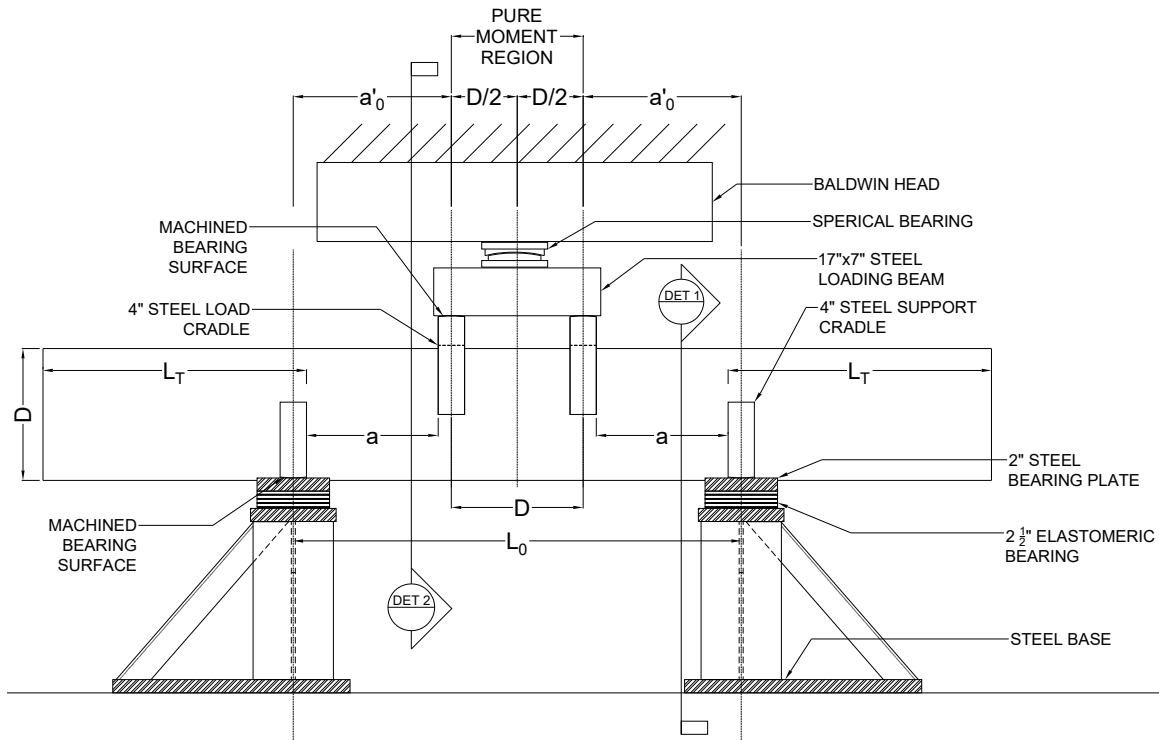


Figure 3. 1: Experimental Setup

Several dimensions critical to the specimen design are illustrated in Figure 3.1. In the figure, a is the approximate shear span, a_0 is the initial center-to-center distance from support cradle to load cradle and is used for an initial estimate of the maximum bending moment, D is the outside diameter of the steel tube, L_0 is the initial (un-deformed) center-to-center span length, and L_T is the overhang or tail length.

While the actual shear capacity of circular CFSTs and RCFSTs is not known, Bishop (2009) found that the mean flexural capacity of CFST was 123% of the plastic moment calculated by the plastic stress distribution method, M_{PSDM} . The apparatus was

thus designed to accommodate $V_{pr, 1.25M_{PSDM}}$, the shear force corresponding to the development of 125% of M_{PSDM} for most of the specimens. It was expected that specimens controlled by flexure would reach this shear force, while specimens controlled by shear would fail in shear at a force less than $V_{pr, M_{PSDM}}$ (shear strength corresponding to the development of M_{PSDM})

The tests were conducted using the 2.4-million pound Baldwin hydraulic test machine in the structures laboratory at the University of Washington (indicated as “Baldwin Head” in Figure 3.1). The machine is calibrated annually using NIST-traceable load cells.

The preliminary *ABAQUS* analyses showed substantial rotations at the load and support cradles, large longitudinal strains at the bottom of the tube, and flexural buckling in the constant-moment region. Elastomeric bearings were employed to allow longitudinal extension without providing excessive horizontal restraint. The stresses in the elastomeric bearing were quite high for some of the specimens, due to the limited bearing area (4 in.) and the expected rotation of the CFSTs at the support cradles. A radius was cut on the bearing surfaces of the cradles so they would rotate and remain locally perpendicular to the CFSTs. Cotton duck bearing pads were placed between the CFST specimens and the load cradles to distribute the bearing stresses and allow some differential rotation where needed. Figure 3.2 shows Specimen 4 in the test apparatus, and Figure 3.3. shows the the deformed specimen in the test apparatus.

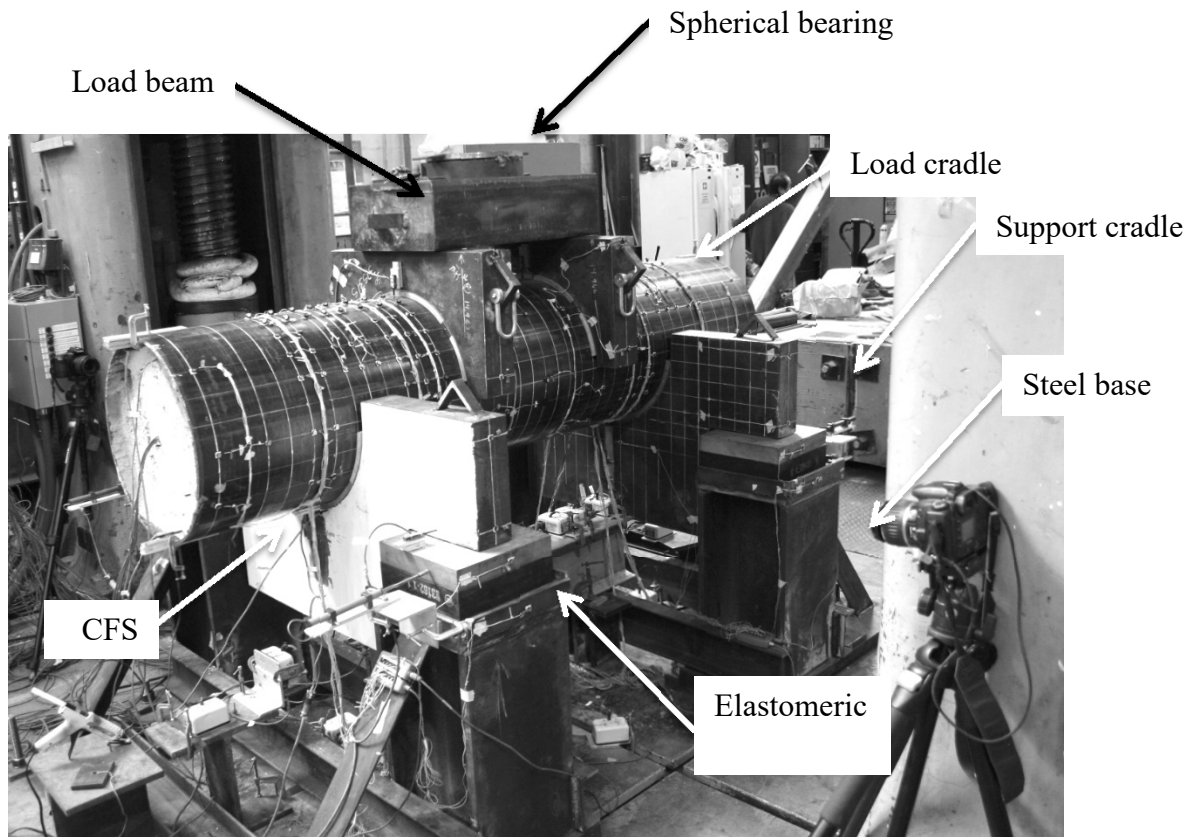


Figure 3. 2: Test Apparatus

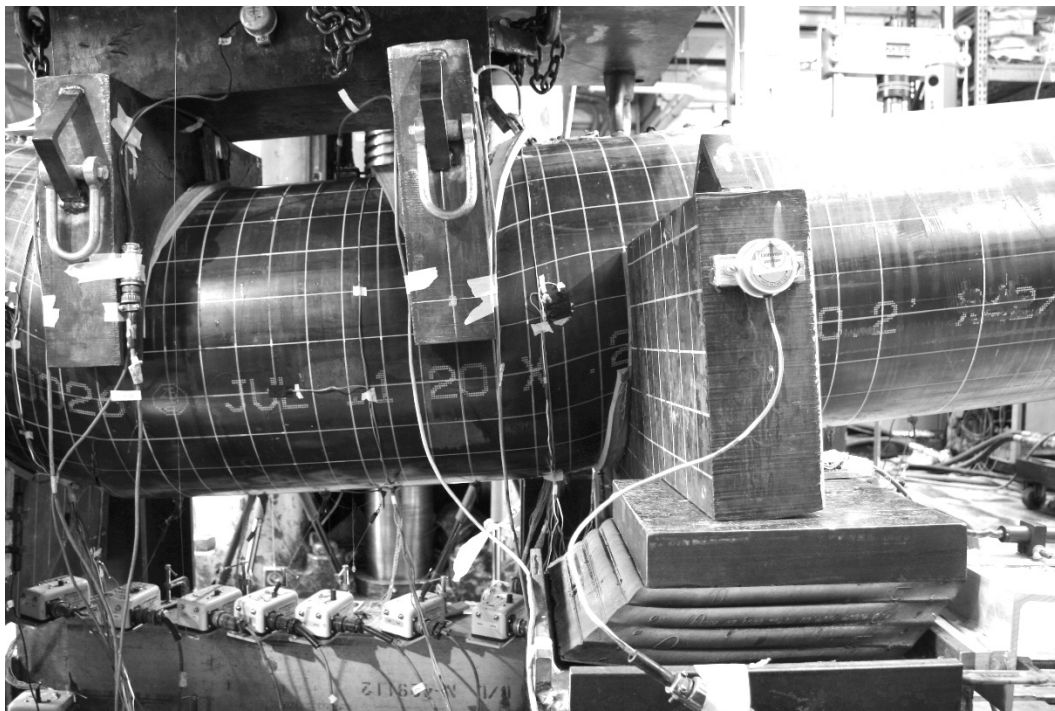


Figure 3. 3: Deformed Specimen and Elastomeric Bearing Movement

INSTRUMENTATION

Extensive instrumentation was applied to each specimen as illustrated by the photo of one half of a typical specimen in Figure 3.4. TML steel strain gauges were attached to each steel tube to measure local steel strains. Single element gauges were employed at mid-span and at the top and bottom of the shear spans for the shorter a/D ratios of 0.375 and 0.25, to develop strain profiles. Three-element rosettes were employed at the center of the shear spans on each side of the steel tube.

Geokon vibrating wire strain gauges were placed within the concrete in the shear spans of several CFSTs to better understand the concrete strain behavior at discrete locations. Some were oriented diagonally to evaluate shear strains and to capture the tensile strains and cracking that occur during strutting action. Linear displacement transducers, Duncan linear potentiometers, and inclinometers were used on each specimen and on the apparatus to measure displacements and rotations.

The NDI Optotrak Certus system was used to capture displacement at over 130 discrete locations of each specimen. A grid was drawn on each specimen to aid in the visualization and understanding of the deformation patterns and to provide discrete locations for the Optotrak targets. These displacements can be used to determine deflections and deformations, to calculate large inelastic strains throughout each test, and to provide local data for validation of analytical models. Instruments were placed on the test specimen as well as the test apparatus to measure cradle rotations, bearing deformations and other effects.

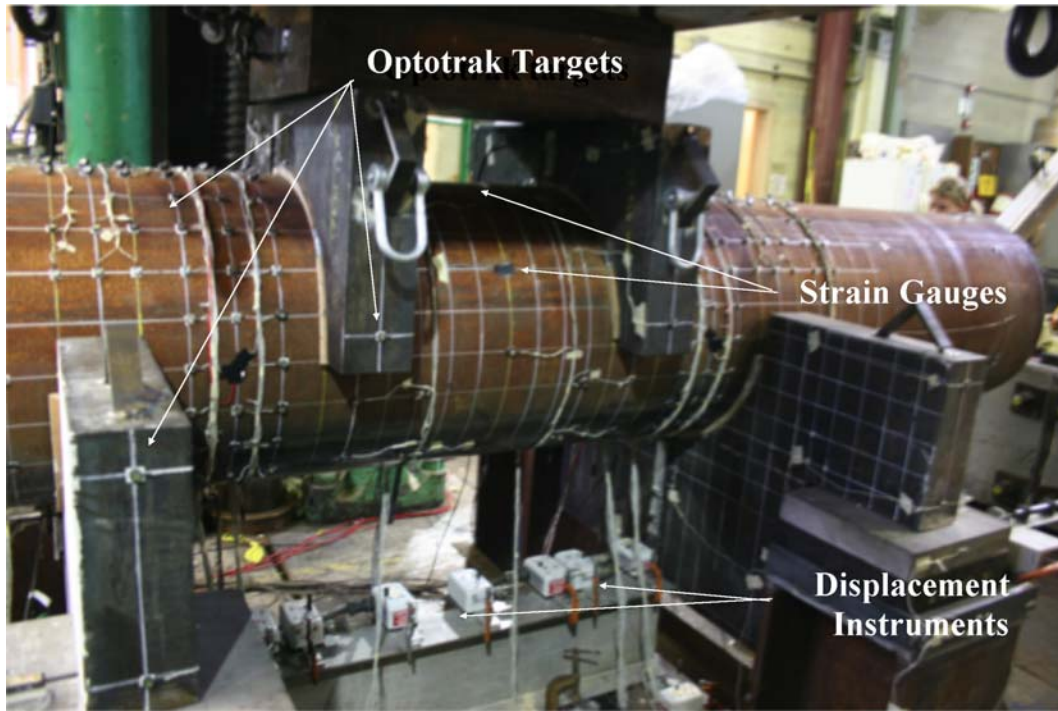


Figure 3. 4: Photo of Typical Instrumentation

TEST MATRIX

Twenty-two specimens were built and tested. The test specimens were selected in to meet the overall goals of the project, and they were selected as part two separate meetings with WSDOT engineers to discuss the goals and focus of the work. The test matrix is summarized in Table 3.1, and critical information for each specimen is provided there. Specimen 1 was a reference specimen with an a/D of 1.0, expected to respond in flexure. Parameters that deviated from this reference specimen are highlighted in the table. The test parameters included:

1. a/D ratio (1, 0.5, 0.375, 0.25)
2. Concrete strength (10, 6, 2.5 and 0 ksi where 0 is the specimen with gravel in the shear span)
3. Tail length (D , $0.5D$, $0.25D$)
4. Interior tube or “interface” condition: clean, greased or muddied

5. Axial load ratio (0 or 8.5% of gross axial capacity)
6. D/t ratio (80, 53)
7. Tube type (spiral, straight seam)

Table 3. 1: Test Matrix

Specimen	D (in)	t (in)	a (in)	D/t	a/D	f _y (ksi)	f' _c (ksi)	P/P ₀	L _T	ρ _{int}	Interface
1	20	0.25	20.0	80	1.0	42	6.0	0%	2D	0%	Clean
22	20	0.25	20.0	80	1.0	70	10.0	0%	4D	0%	Spiral
2	20	0.25	10.0	80	0.5	42	6.0	0%	2D	0%	Clean
3	20	0.25	10.0	80	0.5	42	6.0	0%	D/2	0%	Clean
4	20	0.25	10.0	80	0.5	42	6.0	0%	D	0%	Clean
5	20	0.25	10.0	80	0.5	42	6.0	0%	2D	0%	Muddy
6	20	0.25	10.0	80	0.5	70	6.0	0%	2D	0%	Spiral
9	20	0.25	10.0	80	0.5	42	6.0	0%	2D	0%	Greased
12	20	0.25	10.0	80	0.5	42	6.0	0%	2D	1.13%	Clean
17	20	0.25	10.0	80	0.5	42	12.0	0%	2D	0%	Clean
18	20	0.375	10.0	53.3	0.5	42	12.0	0%	2D	0%	Clean
19	20	0.375	10.0	53.3	0.5	42	12.0	0%	2D	1.07%	Clean
7	20	0.25	7.5	80	0.375	42	6.0	0%	2D	1.04%	Clean
8	20	0.25	7.5	80	0.375	42	6.0	0%	2D	2.01%	Clean
10	20	0.25	7.5	80	0.375	42	6.0	0%	2D	0%	Clean
11	20	0.25	7.5	80	0.375	42	6.0	0%	D/2	0%	Clean
13	20	0.25	7.5	80	0.375	42	6.0	8.5%	D/2	0%	Clean
16	20	0.25	7.5	80	0.375	42	12.0	0%	2D	0%	Clean
21	20	0.25	7.5	80	0.375	42	0	0%	2D	0%	Clean
14	20	0.25	5.0	80	0.25	42	12.0	0%	2D	0%	Clean
15	20	0.25	5.0	80	0.25	42	12.0	0%	D/2	0%	Clean
20	20	0.25	5.0	80	0.25	42	2.5	0%	2D	0%	Clean

- Notes: 1) Specimen 10 was the baseline test. While not all specimens will be compared to it, test parameters that vary from those of specimen 10 are highlighted.
- 2) All specimens used straight-seam steel tubes unless noted otherwise.
- 3) All tube steel conformed to both API 5L X42 and ASTM A53B, except Specimens 6 and 22 which conformed to ASTM A1011 HSLAS Gr 70 C1/C2.

The response of specimens with small a/D ratios (0.25 and 0.375) was expected to be dominated by shear while the response of specimens with large a/D ratios (1.0, 0.5) was expected to be dominated by flexure. It was expected that some of the specimens (0.5 and 0.375) would response in a combine shear-flexural mode. Specimens 1, 2, 10, 14, 16, 17, 20, and 21 can be combined to evaluate these effects.

The length beyond the support, or the tail length, L_T , is important, since composite action in CFSTs requires strain compatibility and stress transfer across the concrete-steel interface. The development length required to insure this transfer has not considered in past research and was an important parameter of this study. Specimens 2, 3, 4, 6, 10, 11, 13, 14, and 15 were used to address this parameter.

RCFSTS have internal reinforcement which may affect the shear and moment resistances of the composite member. Specimens 7, 8, 12 and 19 are RCFST specimens, and Specimens 2 and 10 provide a baseline CFST.

A major application of composite CFST and RCFST members are piles and drilled shafts. Composite members require stress transfer between the steel tube and concrete fill, but contamination due to soil and mud may occur. The effect of the bond surface conditions was studied with Specimens 2, 5, 6, and 9 by comparing their results with specimens with clean steel surfaces. The contaminated surfaces included muddy, straight-seam tubes and greased, straight-seam tubes.

Spirally welded tubes were also tested, and research consistently shows they have greater capacity for bond stress transfer under a wide range of load conditions than straight-seam tubes. Specimens 2 and 6 allow a comparison of straight seam and spiral welded tubes.

Compressive axial load increases the shear capacity of concrete, and Specimens 10, 11, and 13 were tested with a compressive axial load on the concrete to demonstrate this effect. This is particularly important for CFST because they typically are used in applications with significant bending moment and axial load. Tables 2.5, 2.6 and 2.7 suggest that the bulk of the shear resistance is provided by the steel tube, but is important to define how much of the shear resistance is provided by concrete. Therefore, the concrete strength is an important test parameter. Self-consolidating or low-shrinkage concretes are frequently used with CFST but seldom used in deep foundations for cost reasons. Therefore, conventional concrete with various compressive strengths was employed in Specimens 2, 17, 10, 16, 21, 14, and 20. The relative strength of the steel to concrete also varied in these tests, and they were also used to examine this parameter.

The D/t ratio can impact local stability (tube buckling) of CFSTs under axial and flexural loading conditions (Moon et al. 2012; Brown et al. 2015) and bond stress transfer (Roeder et al. 2009). While local stability was not expected to influence the shear resistance of the CFSTs, as the concrete fill restrains shear buckling, the bond stress transfer was likely to play a key role. The majority of the specimens used D/t ratio of 80; Specimens 18 and 19 had D/t ratios of 53 (which was the only variable changed from Specimens 2, 12 to Specimens 18 and 19).

MATERIAL PROPERTIES

Twenty of the test specimens were straight seam tubes made of steel conforming to API 5L X42 and ASTM A53B standards. Two specimens were spirally welded from ASTM A1011 HSLAS Gr 70 C1/C2 coil steel using a double submerged arc weld. Specimens 6 and 22 were tested using the higher strength steel tube. The steel tube for

Specimen 22 was galvanized and filled with a high-strength, self-consolidating, low-shrinkage concrete mix with a 28-day design strength of 10,000 psi. It was previously fabricated for use in an earlier research program (Thody 2006) and was used and initial test to validate the testing apparatus and procedure. Specimen 6 used the same ungalvanized steel tube and was filled with concrete as part of the current testing program. The reinforcing bar used in the four RCFSTs conformed to either ASTM A615 Gr 60 or ASTM A706 Gr 60. Coupons were cut from each length of steel tube and tension tests were performed with the measured properties summarized in Table 3.2.

Three concrete design mixes with normal weight aggregate were used in the testing program. Standard 6 in. diameter by 12 in. long cylinders were prepared at each casting date and tested in compression until failure at 3, 7, and 21 days as well as on the date of testing. The concrete used in the third casting had a 28-day specified strength of 12,000 psi, but the test cylinders resulted in much lower strengths than expected. The properties from these compression tests are also summarized in Table 3.2.

Samples were cut from at least two reinforcing bars in each RCFST specimen and tested in tension until failure. Table 3.3 shows the nominal yield strength and the results of the reinforcing bar tension tests.

Table 3. 2: CFST Material Properties

Specimen	Steel Tube				Concrete Fill				
	Tube ID	f_y (ksi)	f_{ym} (ksi)	f_{um} (ksi)	Mix ID	f'_c (psi)	f'_{cm} (psi)	f_{tm} (psi)	Age (days)
1	SS-1	42	49.6	61.0	563375	6000	6012	630	22
2	SS-1	42	49.6	61.0	563375	6000	6220	561	31
3	SS-2	42	50.1	61.0	563375	6000	6655	554	45
4	SS-2	42	50.1	61.0	563375	6000	6558	N/A	59
5	SS-1	42	49.6	61.0	563375	6000	7041	704	101
6	SW-1	70	70.8	83.5	563375	6000	7182	554	115
7	SS-2	42	50.1	61.0	563375	6000	6447	704	50
8	SS-3	42	53.9	66.1	563375	6000	6484	552	56
9	SS-2	42	50.1	61.0	563375	6000	6317	506	33
10	SS-3	42	53.9	66.1	563375	6000	6151	608	42
11	SS-4	42	56.8	66.4	563375	6000	6609	645	47
12	SS-3	42	53.9	66.1	563375	6000	6177	592	28
13	SS-3	42	53.9	66.1	563375	6000	5326	570	64
14	SS-6	42	55.4	71.3	880378X	12000	8596	694	41
15	SS-6	42	55.4	71.3	880378X	12000	8792	796	47
16	SS-4	42	56.8	66.4	880378X	12000	8609	737	34
17	SS-6	42	55.4	71.3	880378X	12000	9450	753	50
18	SS-5	42	57.2	70.2	880378X	12000	8641	760	54
19	SS-5	42	57.2	70.2	880378X	12000	9131	706	56
20	SS-4	42	56.8	66.4	3051	2500	2787	347	37
21	SS-4	42	56.8	66.4	N/A	0	0	0	N/A
22	N/A	70	75.6	84.8	N/A	10000	13000	N/A	N/A

Table 3. 3: CFST Reinforcing Bar Properties

Specimen	Reinforcing Steel			
	ASTM Spec	f_v (ksi)	f_{vm} (ksi)	f_{um} (ksi)
7	A615	60	72.3	107.8
8	A706	60	68.4	96.7
12	A615	60	71.5	107.6
19	A706	60	68.5	98.4

SPECIMEN CONSTRUCTION

The steel tubes were cut to length using an oxygen-acetylene cutting torch. They were placed vertically on a wood base and strapped down as shown in Figure 3.5a. They were also strapped together to provide stability during the placing and curing of concrete. A plug consisting of two 3/4 in. plywood layers was placed at one end of each tube to offset the concrete from the end and to provide support for the Geokon gauges and the internal reinforcing bars, where present. Specimens 1 through 6 were cast first, on 17 February 2015, followed by Specimens 7 through 13 on 21 May 2015, then Specimens 14 through 21 on 1 July 2015. The concrete was pumped through a 4 in. hose with a maximum freefall height of 4 ft. (see Figure 3.5b). All specimens were left in the vertical position for at least 28 days, except Specimens 1 and 12, which remained vertically for at least twenty days. The top ends of the CFSTs were covered with wet burlap while the concrete was curing.

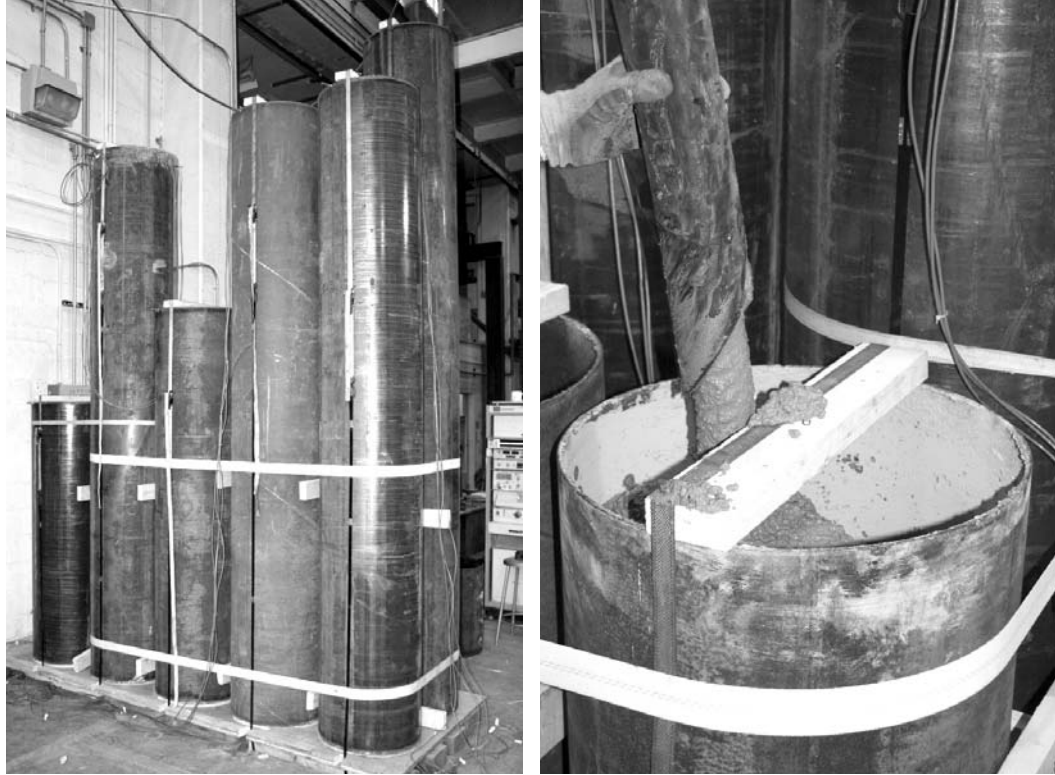


Figure 3. 5: Test Specimen Preparation a) Tubes Prepared for Casting, b) Concrete Placement

No cleaning or special procedure was undertaken to prepare the insides of the tubes at the interface with the concrete, with the exception of Specimens 5 and 9, which were muddied and greased, respectively. The dirt applied to Specimen 5 was of a relatively well-graded aggregate. The tube was placed at an inclined position on rollers, and was then rotated as the wetted dirt coated the inside face of the tube wall until even and thorough coverage was achieved. The grease was applied to Specimen 9 via rags on the end of a pole.



Figure 3. 6: Muddied CFST Interface, a) Creating Surfaces, b) Finished Surface

The Geokon vibrating-wire strain gauges were placed in several of the specimens using a ladder consisting of small-diameter wire rope and mild steel rod. The ladders were secured to the plywood plugs and tightened by tensioning the wire rope once the tubes were in the vertical casting position, so as to locate them more accurately. The wire rope did not provide substantial longitudinal reinforcement as the tensile capacity of the wire rope was approximately 80 lbs.

CHAPTER 4

EXPERIMENTAL RESULTS

This chapter presents the experimental results. For each specimen, the measured force displacement response is presented and images at salient damage states are shown.

Twenty-two tests were performed starting on January 19, 2015 and finishing on August 26, 2015. Analysis of the results is provided in Chapter 5.

LOADING PROCEDURE

A combination of load and displacement control was used to test each specimen to failure. Each test was initiated under load control of the Baldwin testing machine at a 5-kip increment. The 5-kip increment continued until the applied load, which was twice the horizontal force at the supports, reached 40 kips. The increment increased to 10 kips until the applied load reached 80 kips. At 80-kips applied load, the increment was increased again to 20 kips. The 20-kip increment was maintained until the specimen displayed substantial non-linearity in the force-displacement plot (see Figure 4.1 for typical plot). At that point, the Baldwin was operated under displacement control until failure occurred. The initial loading rate of 0.5 kip/sec was maintained until the applied load reached 100 kips. The load rate was then increased to 1.0 kip/sec. The displacement rate was set at 0.002 in./sec.

SPECIMEN FAILURE

Specimen failure was defined as the tube steel tearing, coupled with a significant drop in resistance for CFSTs. Failure for the RCFST specimens was defined as tensile

rupture of at least two layers of the reinforcing steel in addition to the tube steel tearing and a significant drop, approximately 20%, of the peak resistance. After failure the specimens were removed from the test apparatus and the steel tube was cut away from the concrete fill, so that the damage to the concrete fill could be closely examined. Extensive photos were taken of the specimens during and after testing, and the combination of the photographs, notes from visual observations during testing, and the measured data was used to evaluate the test results.

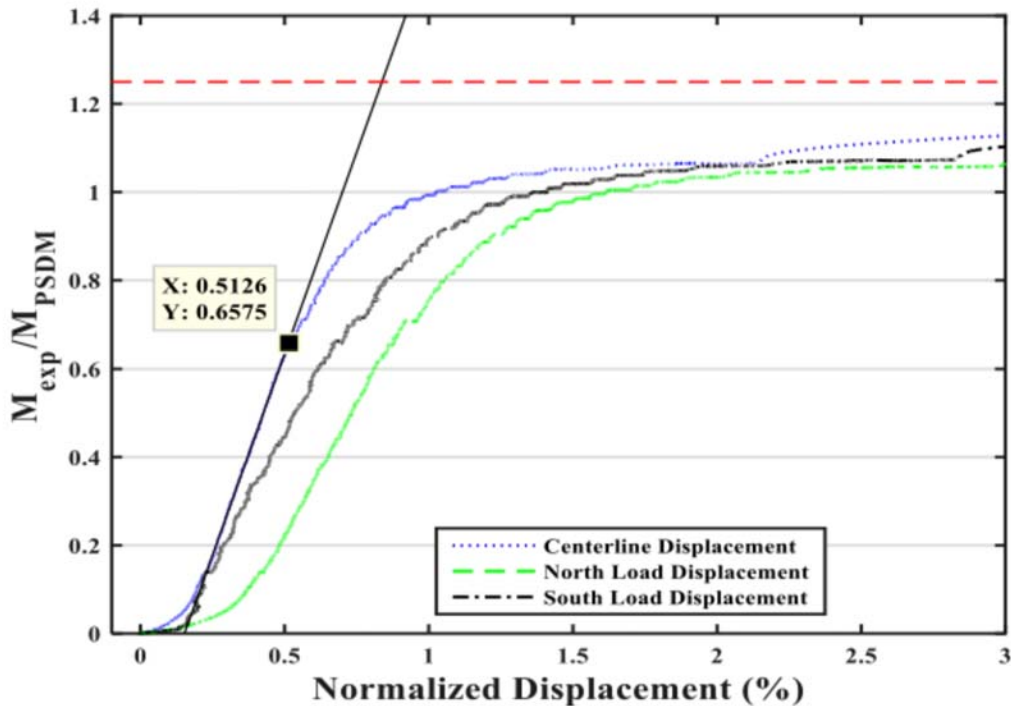


Figure 4. 1: Typical Moment Displacement Curve with Proportional Limit

The applied shear force is directly measured by the Baldwin, but the bending moment depends upon the shear span length. As shown in Figure 4.1 there are several shear span values of potential importance since the load and support are applied over a width of 4 in. and in some cases, that total distance is approximately equal to the clear

space (for the case of the 0.375D the clear span is 7.5 in.). In addition, the length will change with deformation of the specimen, since the mid-height is not the neutral axis depth, and a neutral axis depth is not relevant to the specimens that response primarily in or fail in shear.

The undeformed clear shear span length, a , was used to define the initial a/D ratio. However, the bending moment will control the maximum shear capacity of some specimens, and it is important to have the best possible estimate of the moment for each test specimen to assure whether shear or flexure controls. The forces applied at the load and reaction cradles are distributed over a significant length due to the thickness of the cradles, and a'_o is a better indicator of the bending moment in the specimen. However, due to the high levels of plastic deformation, the short spans, and the vertical location of the support bearing surfaces, the total span, L , and the shear spans, a'_{north} and a'_{south} , varied from the initial lengths, L_o and a'_o during each test (see Figure 4.2). The potential severity of these changes is illustrated in Figure 4.3. These lengths were measured at each time step with the Optotrak instrumentation. The Optotrak system was not be used for these corrections on Specimen 15, and the potentiometer data was used to estimate these changes for that specimen.

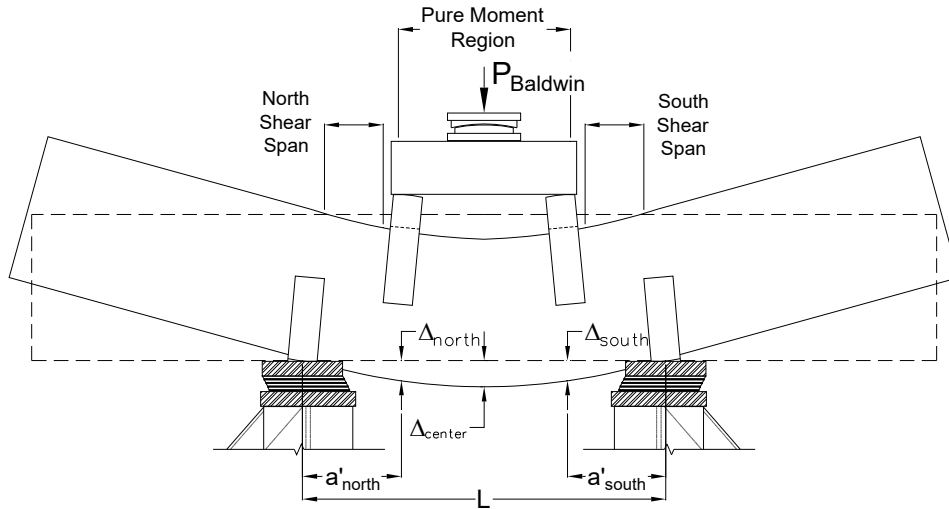


Figure 4. 2: Displacement and Span Measurements

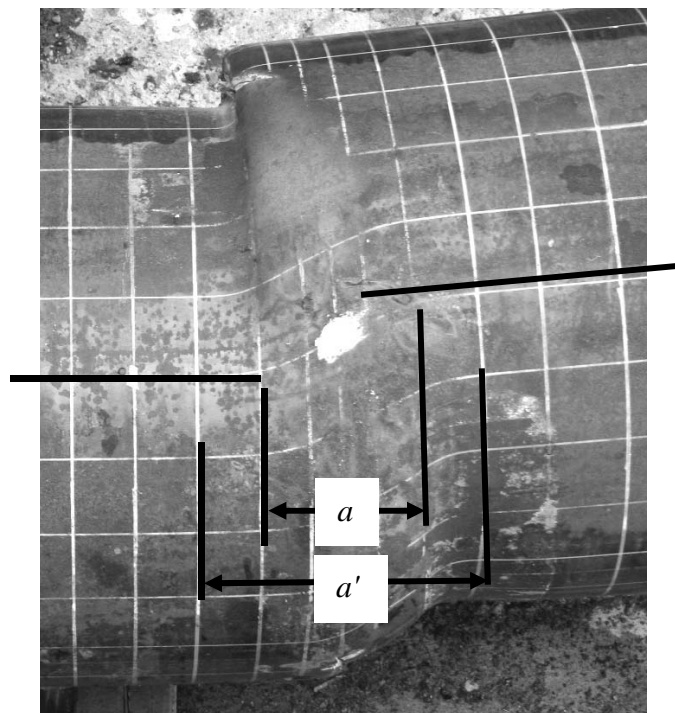


Figure 4. 3: Shear Span Deformation and Restraint

As a result, Equations 4.1 through 4.9 were used to define the behavior characterization summarized in Table 4.1.

$$\bar{\Delta}_{center} = \frac{\Delta_{center}}{L/2} \times 100\% \quad (4.1)$$

$$\bar{\Delta}_{north} = \frac{\Delta_{north}}{a'_{north}} \times 100\% \quad (4.2)$$

$$\bar{\Delta}_{south} = \frac{\Delta_{south}}{a'_{south}} \times 100\% \quad (4.3)$$

where Δ_{center} , Δ_{north} , and Δ_{south} is the measured deflection at the mid-span, north and south load points, respectively. The Baldwin load is applied to the spherical bearing placed in the center between the load cradles, and will ideally be divided evenly between the two load cradles. However, differential movements occur, because more yielding occurs in one span than the other, and the experimental shear and moment at the north and load points and mid-span, V_{north} , V_{south} , V_{center} , M_{north} , M_{south} , and M_{center} , respectively, are adjusted as:

$$V_{north} = \frac{P_{Baldwin}}{2 \times L} (L - a'_{north} + a'_{south}) \quad (4.4)$$

$$V_{south} = \frac{P_{Baldwin}}{2 \times L} (L - a'_{south} + a'_{north}) \quad (4.5)$$

$$V_{center} = \frac{P_{Baldwin}}{2 \times L} (a'_{south} - a'_{north}) \quad (4.6)$$

$$M_{north} = V_{south} \times a'_{north} \quad (4.7)$$

$$M_{south} = V_{south} \times a'_{south} \quad (4.8)$$

$$M_{center} = \frac{M_{north} + M_{south}}{2} \quad (4.9)$$

where $P_{Baldwin}$ is the total force applied by the Baldwin UTM. Table 4.1 summarizes the moment and mid-span displacement and corresponding shear values at first yield, M_{yield} , V_{yield} , and $\bar{\Delta}_{yield}$, at the proportional limit, M_{prop} , V_{prop} , and $\bar{\Delta}_{prop}$, and at the point of maximum moment, M_{ult} , V_{ult} , and $\bar{\Delta}_{ult}$, for each specimen. The mid-span displacement at

failure, $\bar{\Delta}_{fail}$, is also included. The proportional limit is defined by noting the separation from a best-fit line to the linear-elastic portion of the normalized moment-normalized displacement plot as illustrated in Figure 4.1. The bending moment at first yield is established when the bottom strain gauges first reach the yield strain.

Concrete cracking was noted by the audible cracking noted during the test accompanied by sudden changes stiffness or resistance. Table 4.2 shows the shear force, bending moment, and normalized displacement at mid-span when the concrete cracks in the pure flexural region, and as the compression struts in the shear spans form cracks. In specimens with Geokon gauges are noted with an asterisk in the table, because concrete cracking was explicitly measured in those tests.

Table 4. 1: Summary of Key Performance States

Specimen	1	2	3	4	5	6	7	8	9	10	11	12	13
a/D	1.0	0.5	0.5	0.5	0.5	0.5	0.375	0.375	0.5	0.375	0.375	0.5	0.375
D/t	80	80	80	80	80	80	80	80	80	80	80	80	80
ρ_{int}	0%	0%	0%	0%	0%	0%	1.04%	2.00%	0%	0%	0%	1.13%	0%
L_T	2D	2D	D/2	D	2D	2D	2D	2D	2D	2D	D/2	2D	2D
M_{yield} (k-in)	4209	3825	3699	2988	3794	5753	4328	4996	3646	3572	3847	4899	5172
V_{yield} (k)	175	270	264	249	271	409	371	431	261	309	336	346	451
$\bar{\Delta}_{yield}$ (%)	0.331	0.339	0.350	0.286	0.384	0.568	0.360	0.417	0.385	0.452	0.830	0.417	0.484
M_{prop} (k-in)	4209	3930	4025	3915	4027	5916	3903	5432	3647	4316	3665	4539	3784
V_{prop} (k)	175	280	286	280	287	420	335	471	261	372	320	321	330
$\bar{\Delta}_{prop}$ (%)	0.331	0.344	0.375	0.320	0.390	0.570	0.318	0.443	0.383	0.513	0.812	0.380	0.359
M_{ult} (k-in)	7893	8099	8111	8035	8124	11665	8807	9239	6528	8159	7024	9679	8270
V_{ult} (k)	322	550	552	543	556	779	705	802	442	665	600	651	710
$\bar{\Delta}_{ult}$ (%)	9.37	7.96	8.94	10.23	5.60	4.70	12.08	12.71	7.50	6.23	3.26	10.00	22.87
$\bar{\Delta}_{fail}$ (%)	11.40	11.32	11.02	11.56	6.22	9.04	16.19	15.51	17.08	14.57	10.71	11.92	5.66

* Optotrak displacements not used

Specimen	14	15	16	17	18	19	20	21	22
a/D	0.25	0.25	0.375	0.5	0.5	0.5	0.25	0.375	1.0
D/t	80	80	80	80	53.3	53.3	80	80	80
ρ_{int}	0%	0%	0%	0%	0%	1.07%	0%	0%	0%
L_T	2D	5D/8	2D	2D	2D	2D	D/2	2D	4.5D
M_{yield} (k-in)	4894	4052	4764	4536	5980	6626	4244	3479	N/A
V_{yield} (k)	546	450	415	324	430	473	462	305	N/A
$\bar{\Delta}_{yield}$ (%)	0.743	0.162*	0.385	0.557	0.579	0.560	0.484	7.783	N/A
M_{prop} (k-in)	3497	3421	5051	4489	6159	7144	3772	2272	5509
V_{prop} (k)	390	380	441	321	443	511	420	198	230
$\bar{\Delta}_{prop}$ (%)	0.623	0.135*	0.400	0.552	0.590	0.587	0.427	0.392	0.307
M_{ult} (k-in)	76788	7164	9204	8056	12444	13816	6838	5211	11579
V_{ult} (k)	826	796	765	547	832	952	712	449	477
$\bar{\Delta}_{ult}$ (%)	2.58	0.56	6.61	8.25	8.72	7.00	14.37	16.23	6.15
$\bar{\Delta}_{fail}$ (%)	9.48	1.26*	10.36	10.64	10.97	10.72	16.69	17.16	7.06

Table 4. 2: Summary of Concrete States

Specimen	Crack Location	V_{cr} (kips)	M_{cr} (in-k)	$\bar{\Delta}_{cr}$ (%)
1	Mid-span Flexure	36	853	0.05
	North Shear	N/A	N/A	N/A
	South Shear	N/A	N/A	N/A
2*	Mid-span Flexure	60	838	0.091
	North Shear	430	6066	0.652
	South Shear	430	6066	0.652
3*	Mid-span Flexure	60	835	0.132
	North Shear	448	6310	0.792
	South Shear	Unknown	unknown	unknown
4*	Mid-span Flexure	67	939	0.087
	North Shear	451	6327	0.77
	South Shear	456	6395	0.831
5*	Mid-span Flexure	69	969	0.159
	North Shear	440	6223	0.971
	South Shear	487	6881	1.611
6*	Mid-span Flexure	60	837	0.165
	North Shear	461	6487	0.626
	South Shear	438	6167	0.591
7	Mid-span Flexure	110	1281	0.137
	North Shear	308	3590	0.284
	South Shear	308	3590	0.284
8	Mid-span Flexure	135	1555	0.207
	North Shear	Unknown	unknown	unknown
	South Shear	Unknown	unknown	unknown
9	Mid-span Flexure	58	812	0.126
	North Shear	Unknown	unknown	unknown
	South Shear	Unknown	unknown	unknown
10*	Mid-span Flexure	79	911	0.22
	North Shear	403	4674	0.568
	South Shear	373	4318	0.52
11*	Mid-span Flexure	74	851	0.562
	North Shear	390	4473	0.895
	South Shear	380	4357	0.875

12	Mid-span Flexure	75	1062	0.144
	North Shear	322	4556	0.39
	South Shear	322	4556	0.39
13	Mid-span Flexure	140	1606	0.222
	North Shear	unknown	unknown	unknown
	South Shear	unknown	unknown	unknown
14*	Mid-span Flexure	104	929	0.446
	North Shear	390	3499	0.63
	South Shear	391	3502	0.637
15*	Mid-span Flexure	110	989	0.036
	North Shear	450	4050	0.161
	South Shear	480	4327	0.172
16*	Mid-span Flexure	77	887	0.137
	North Shear	440	5051	0.4
	South Shear	451	5166	0.418
17	Mid-span Flexure	69	966	0.262
	North Shear	428	6028	0.823
	South Shear	430	6028	0.823
18	Mid-span Flexure	76	1063	0.302
	N/S Shear	470	6540	0.627
	N/S Shear	560	7792	0.728
19	Mid-span Flexure	74	1080	0.245
	North Shear	unknown	unknown	Unknown
	South Shear	unknown	unknown	Unknown
20	Mid-span Flexure	80	719	0.149
	North Shear	unknown	unknown	Unknown
	South Shear	unknown	unknown	Unknown
22	Mid-span Flexure	47	1137	0.057
	North Shear	N/A	N/A	N/A
	South Shear	N/A	N/A	N/A

PERFORMANCE CATEGORIZATION AND FAILURE MODE

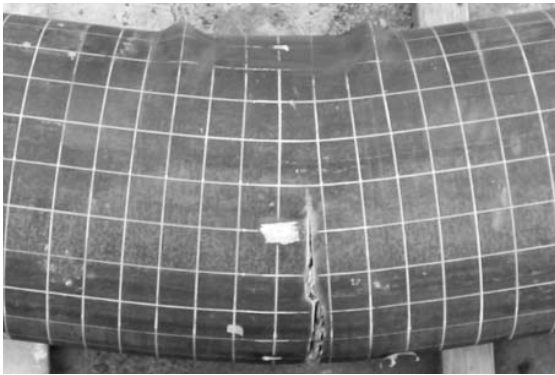
Equations 4.1 through 4.9 were used to estimate the shear span length, a' , bending moment, and the relationship between the moment and 1.25 times the computed moment capacity by the PSDM. The observed strain distribution of the steel, and the damage state of the concrete observed after each test were added to estimate whether the shear capacity was controlled by flexure, shear or combined shear-flexure. Past research shows that the average experimental moment capacity of CFST is 1.25 times the moment capacity predicted by the PSDM, M_{PSDM} . Therefore, the specimen is expected to be shear dominated if $a' V_{\text{exp}} < 1.25 M_{\text{PSDM}}$. The specimen is expected to respond in a flexure-dominated mode if $a' V_{\text{exp}} > 1.25 M_{\text{PSDM}}$. There is uncertainty in this calculation because a' is not known with precision, and the 1.25 is a mean value with some statistical scatter. As a result, the case where $a' V_{\text{exp}} \approx 1.25 M_{\text{PSDM}}$ is viewed as a combined shear and flexural mode. This is not to suggest that the expected shear capacity will be reduced by bending moment, but indicates uncertainty in the zone of behavior.

Bond slip failure was fourth mode of behavior anticipated in this study. The development length needed to assure that CFST can develop its full shear and flexural capacity was evaluated through L_T , the tail length test variable, to examine the length needed to assure this full resistance, and this is related to bond slip. Slip at the steel concrete interface was measured for all specimens, since slip could prevent development of both the shear and flexural capacity of the member.

Flexural Failure in CFST

The predominant characteristics of flexural failures in CFSTs are:

- Flexural buckling of the tube steel due to compressive flexural stresses and rupture of steel tube due to tensile bending stress as illustrated in Figure 4.4a.
- Plane sections remain approximately plane throughout specimen and test with no apparent shear strain in the steel tube.
- Dense, transverse flexural cracking in the concrete fill as shown in Figure 4.4b.
- At most, minor diagonal concrete cracking in the shear spans (see Figure 4.4c).



a) Steel Tearing due Tensile Bending Stress



b) Flexural Cracking of Concrete Fill



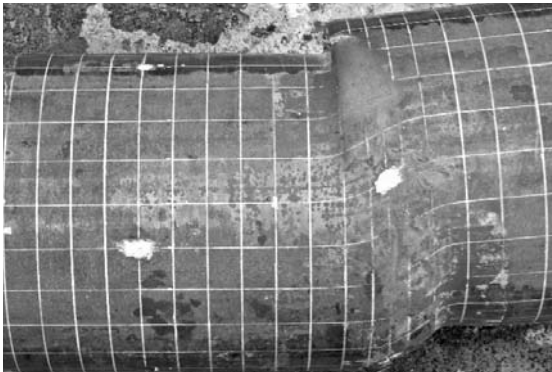
c) Limited Diagonal Shear Cracking of Concrete Fill

Figure 4. 4: Characteristics of Flexural Mode

Shear Failure in CFST

The predominant characteristics of shear failures in CFSTs include:

- Shear strain in the tube steel and inclined tearing of the steel in the shear span (see Figure 4.5a and b).
- Relatively minor flexural cracking in the concrete fill as shown in Figure 4.5c.
- Extensive diagonal cracking in the concrete fill in the shear spans (see Figure 4.5d).



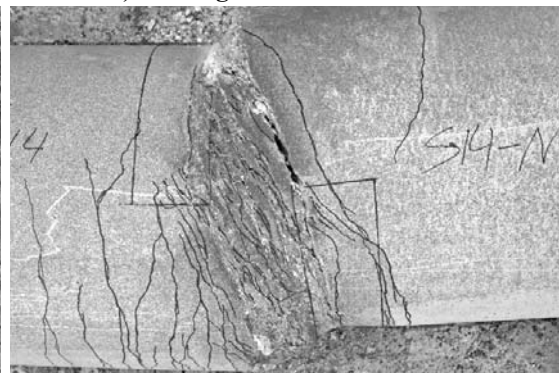
a) Shear Yield Strain



b) Tearing of Steel in Shear Zone



c) Limited Flexural Cracking of Fill



d) Extensive Cracking in Shear Zone

Figure 4. 5: Characteristics of Shear Failure in CFST

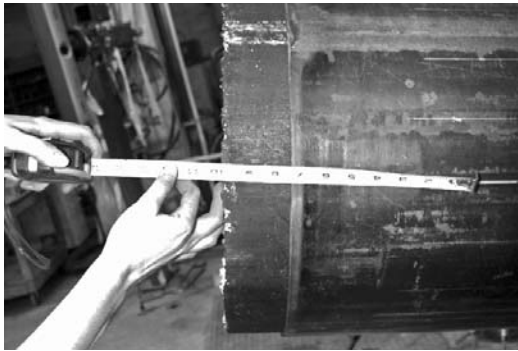
Flexure-Shear Interaction in CFST

As note earlier combined shear-flexural behavior is less a separate failure mode in CFST, than a combination of behaviors. As a result, this behavioral combination is likely to display characteristics from both figures 4.4 and 4.5.

Bond Slip in CFST

CFSTs are composite members, which require stress transfer at the steel-concrete interface. The predominant characteristics of bond slip are:

- Significant slip between the concrete fill and the steel tube as shown in Figure 5.6a.
- Rigid body slip of concrete blocks with limited concrete cracking within the tube may occur as shown in Figure 5.6b.
- A reduction in moment and shear capacity may occur.



a)



b)

Figure 4. 6: Characteristics of Slip within CFST, a) Slip between the Concrete Sill and Steel Tube, b) Rigid Movements of Concrete Blocks with no Shear or Flexural Cracking

Several specimens failed in shear, but most specimens were influenced by flexure. Using the ratio between shear, a' , and MPSDM combined with the observations noted

above, the behaviors and failure modes of the various specimens are categorized in Table 4.3. By this evaluation, nine specimens failed in flexure, five failed in shear (including Specimen 8), six displayed flexure-shear interaction, and two had significant loss of bond stress and bond slip. Several specimens warrant specific comment:

- Specimen 13 had an axial load and was assigned a combined shear-flexure behavior, but some of its characteristics align more closely with the shear specimens.
- Specimen 21 had gravel in the shear spans to document the supplied shear resistance provided by the tube, versus that provided by the concrete. It had a shear failure that was dominated by shear buckling and tension-field action, because the gravel fill did not retain the cross sectional geometry of the tube as well as normal concrete fill does.
- Specimen 8 had 2% internal reinforcement, and it was grouped with the shear failures although some aspects of flexural behavior were noted.

Table 4. 3: Specimen Failure Classification

Specimen	a/D	M_{yield} / M_{prop}	Inclined Tear	Visible Flex Deform.	M_{exp} / M_{PSDM}	V_{exp} / V_n <i>WSDOT</i>	Failure Mode	Max Slip / L_T
1	1.0	1.00	No	Yes	1.30	1.27	Flexure	0.06%
2	0.5	0.97	No	Yes	1.33	2.16	Flexure	0.04%
3	0.5	0.92	No	Yes	1.31	2.14	Flexure	0.44%
4	0.5	0.76	No	Yes	1.30	2.11	Flexure	0.13%
5	0.5	0.94	No	Yes	1.32	2.17	Flexure	0.06%
6	0.5	0.97	No	Yes	1.37	2.20	Flexure	0.02%
17	0.5	1.01	No	Yes	1.16	1.91	Flexure	0.03%
18	0.5	0.97	No	Yes	1.22	1.96	Flexure	0.03%
22	1.0	N/A	No	Yes	1.23	1.24	Flexure	0.02%
7	0.375	1.11	Yes	Yes	1.17	2.74	Flex-Shear	1.46%
10	0.375	0.83	Yes	Yes	1.24	2.42	Flex-Shear	1.71%
12	0.5	1.08	Yes	Yes	1.21	2.38	Flex-Shear	0.07%
13	0.375	1.37	N/A	Yes	1.12	2.60	Flex-Shear	1.07%
16	0.375	0.94	Yes	Yes	1.30	2.62	Flex-Shear	0.22%
19	0.5	0.93	Yes	Yes	1.21	2.24	Flex-Shear	0.08%
8	0.375	0.91	Yes	No	1.03	2.92	Flex-Shear	0.55%
14	0.25	1.40	Yes	No	1.11	2.89	Shear	0.18%
15	0.25	1.18	Yes	No	1.04	2.78	Shear	3.23%
20	0.25	1.10	Yes	No	1.06	2.54	Shear	0.43%
21	0.375	1.53	Yes	No	0.94	1.70	Shear	0.11%
9	0.5	1.00	No	Yes	1.06	1.72	Bond	10.0%
11	0.375	1.05	Yes	No	1.01	2.08	Bond	9.26%

DISCUSSION OF SPECIFIC TEST RESULTS

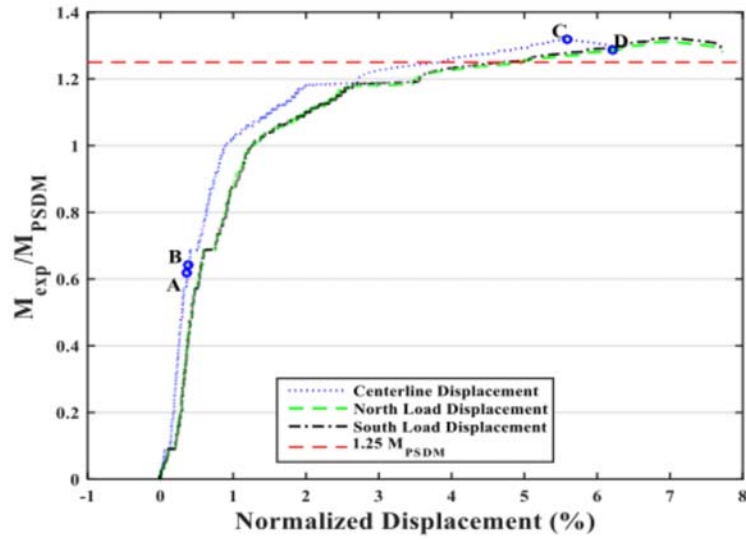
Twenty two tests were completed, and individual description of each test with photos and plots would require a very lengthy report. As a result, specific key tests that illustrate important issues have been selected and will be discussed to demonstrate the effect of different parameters on the shear strength behavior. The selected specimens are:

- Specimen 5 – CFST with muddy interface
- Specimen 8 – RCFST Specimen with combined behavior
- Specimen 9 – CFST Specimen with greased interface
- Specimen 13 – CFST Specimen with axial load
- Specimen 17 – CFST Specimen with flexural behavior
- Specimen 21 – Steel tube with gravel fill

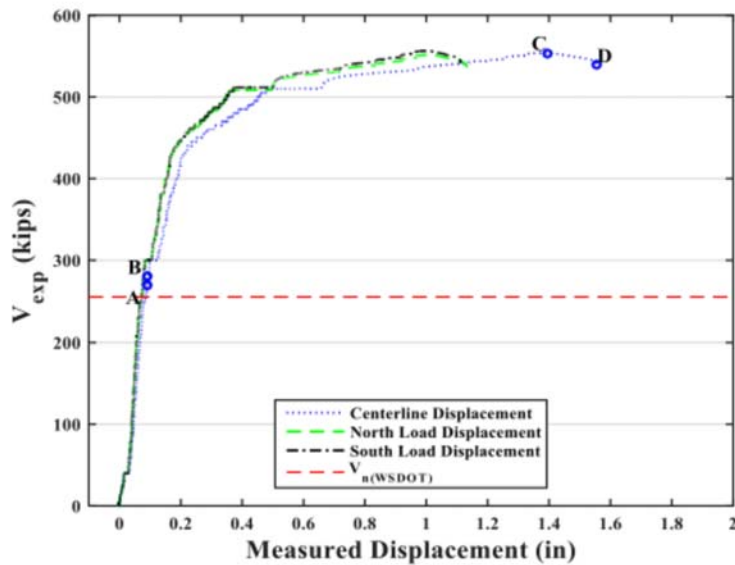
Specimen 5 – CFST with Muddy Interface

Specimen 5 was a tube steel-concrete interface variation of Specimen 2, the baseline specimen for $a/D = 0.5$, and was tested 29 May 2015. It had a muddied steel-concrete interface, a tail length of 40 inches, a straight seam weld, and no internal reinforcement. It achieved 1.32 times M_{PSDM} and 2.17 times $V_n (WSDOT)$ and failed in flexure as shown in Figure 4.7. The tube sustained a vertical flexural tear at the bottom approximately 0.5 inches north of mid-span after significant deformation (see Figure 4.8 a, b, and c). There were no visible shear deformations in the steel but limited diagonal shear cracks formed in the concrete in the shear spans (see Figure 4.8 e and f). The tube steel buckled on both the north and the south ends of the pure moment region symmetrically. Extensive flexural cracking of the concrete fill was also noted in the pure flexural region (see Figure 4.8d). The major goal of this test was to determine whether

surface contamination such as that expected with a pile or drilled shaft would adversely affect CFST performance. Comparison of the resistance and behavior of Specimens 5 and 2, shows that Specimen 5 had slightly larger resistance and easily developed the expected moment capacity, although inelastic deformation may be reduced somewhat.



a) Moment-Displacement



b) Shear-Displacement

Figure 4. 7: Behavior of Specimen 5

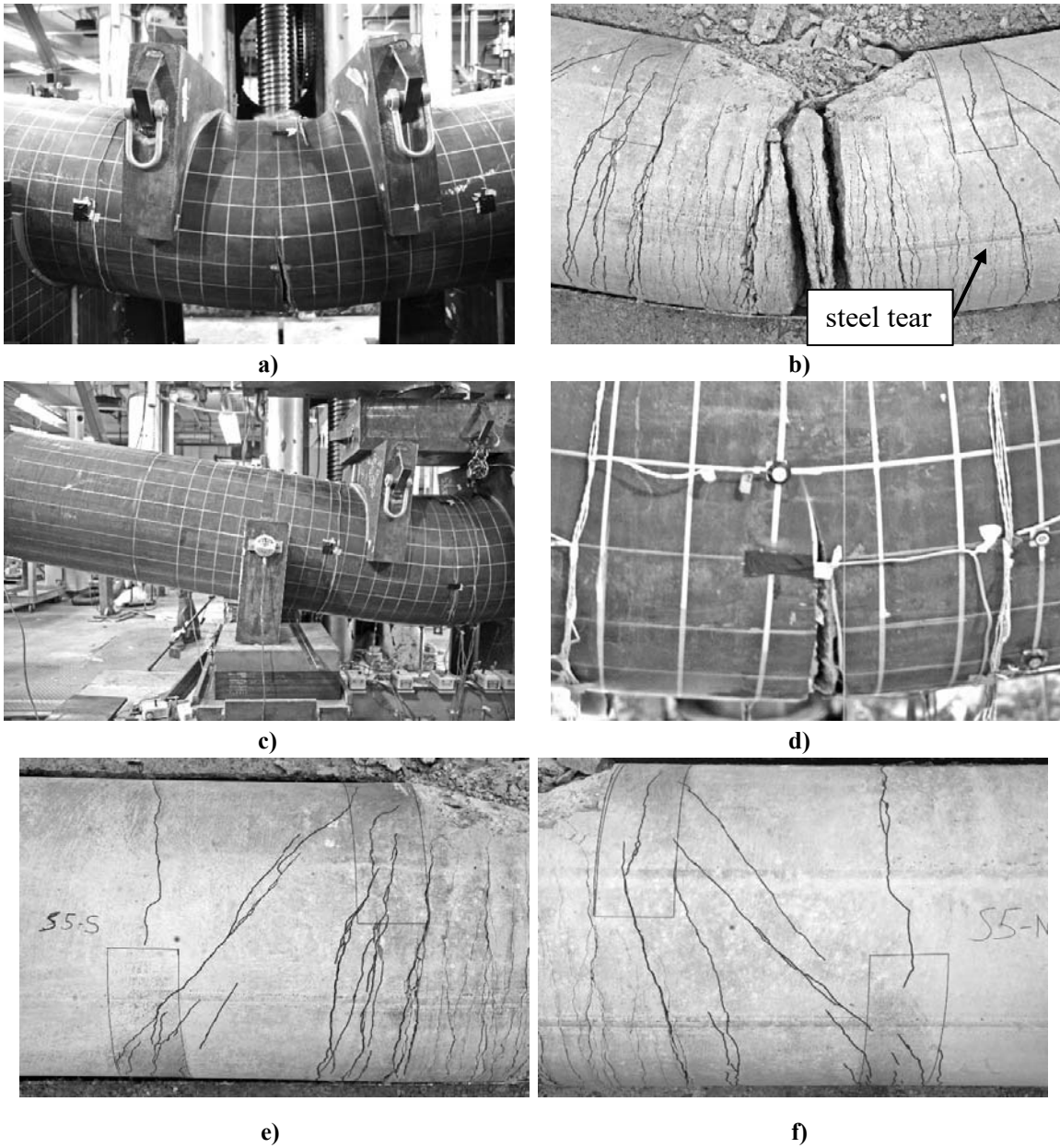


Figure 4. 8: Specimen 5 Photos

Specimen 8 – RCFST Specimen with Combined Behavior

Specimen 8 was an internally reinforced variation of Specimen 10, the baseline specimen for $a/D = 0.375$, and was tested 16 July 2015. It had a clean interface, a tail length of 40”, a straight seam weld, and 2.00% internal reinforcement. The amount of

internal reinforcement was considered a practical maximum for RCFSTs based on discussions with WSDOT engineers. It achieved 1.03 times M_{PSDM} and 2.92 times V_n ($WSDOT$) and failed in shear. The tube tore at the bottom approximately 12 inches south of mid-span after significant shear deformations occurred. The flexural and shear resistance of Specimen 8 was 13.2 and 20.6% larger than Specimen 10, even though the internal reinforcement increased the steel area by approximately 40% (see Figure 4.9). This demonstrates the greater efficiency of the steel tube in reinforcing the CFST. The tear in the steel was inclined from the vertical at generally the same angle as the concrete strut (see Figure 4.10c and e). Three layers of reinforcing bars ruptured along the inclined plane of the tear in the tube steel. Shear strains were observed in the steel in both shear spans (see Figure 4.10 a and b), and the concrete experienced extensive diagonal shear cracking and deformations in both shear spans (see Figure. 4.10 d, e, and f). The tube steel experienced minor flexural buckling on the south end of the pure moment region with no visible buckling on the north end. There was limited flexural cracking in the pure moment region. South is to the left in each photograph.

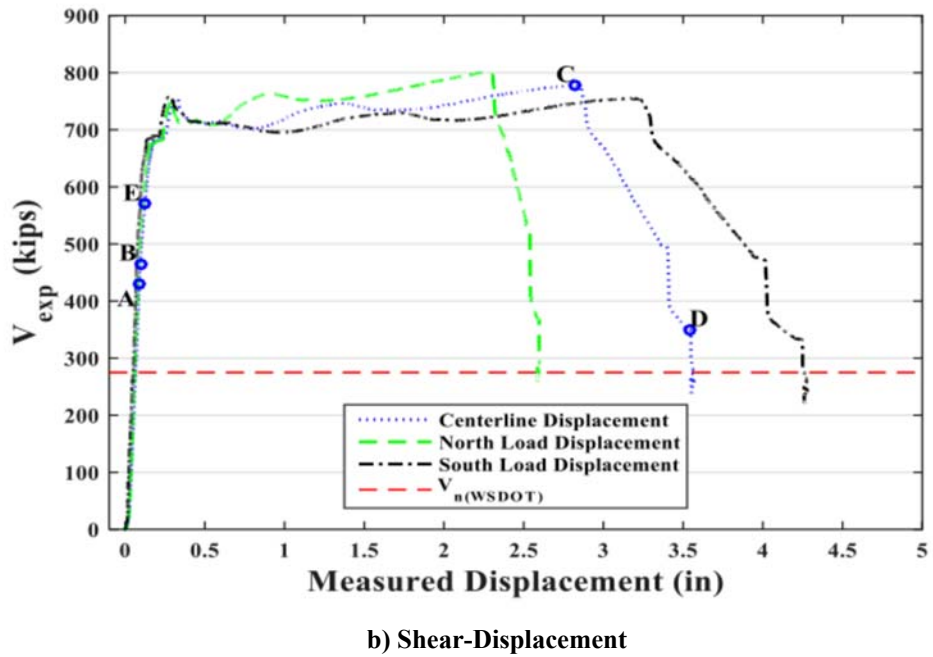
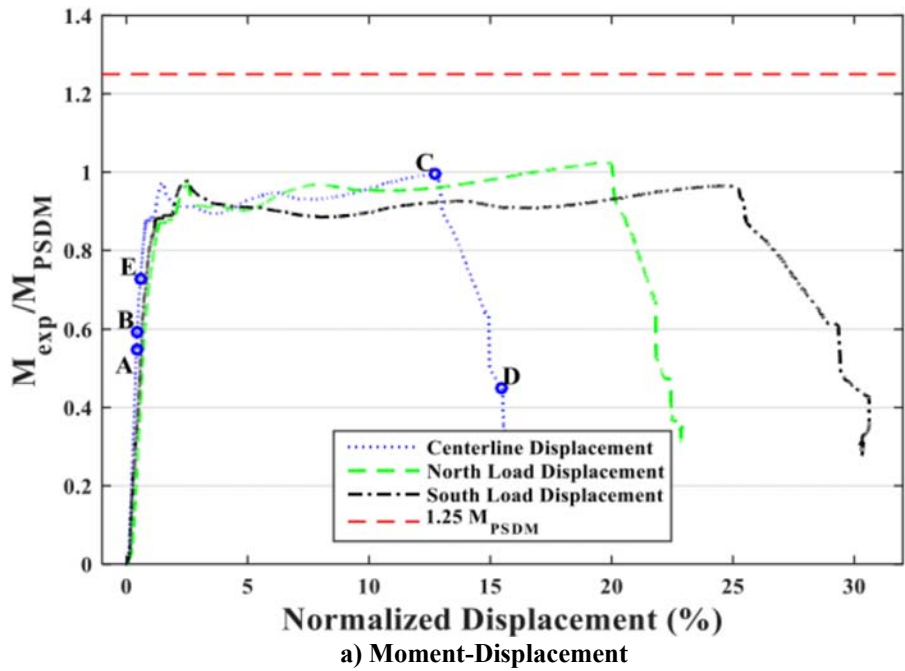


Figure 4. 9: Behavior of Specimen 8

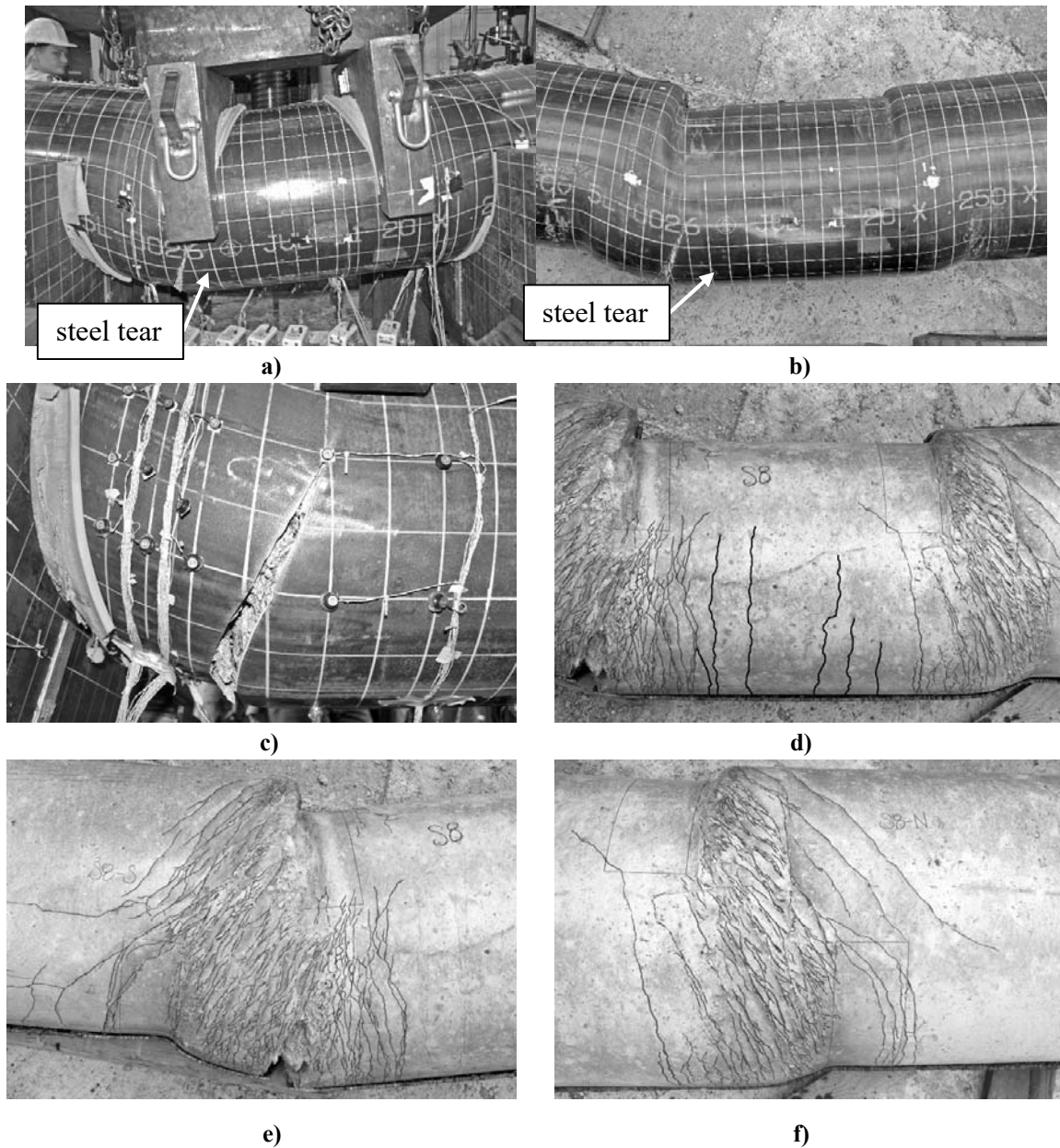
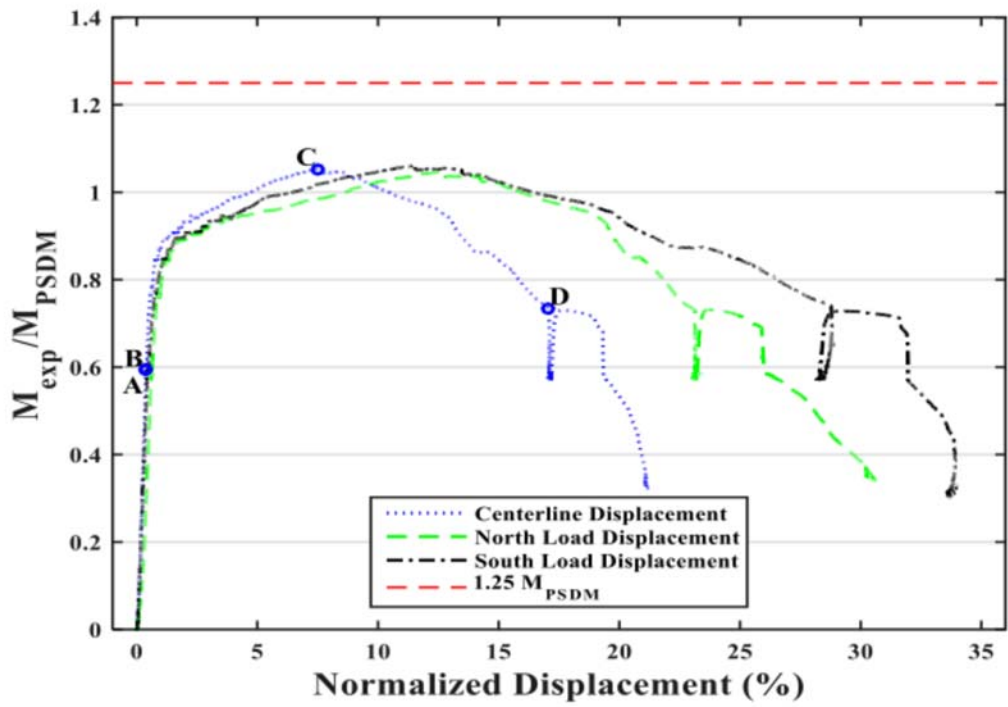


Figure 4.10: Specimen 8 Photos

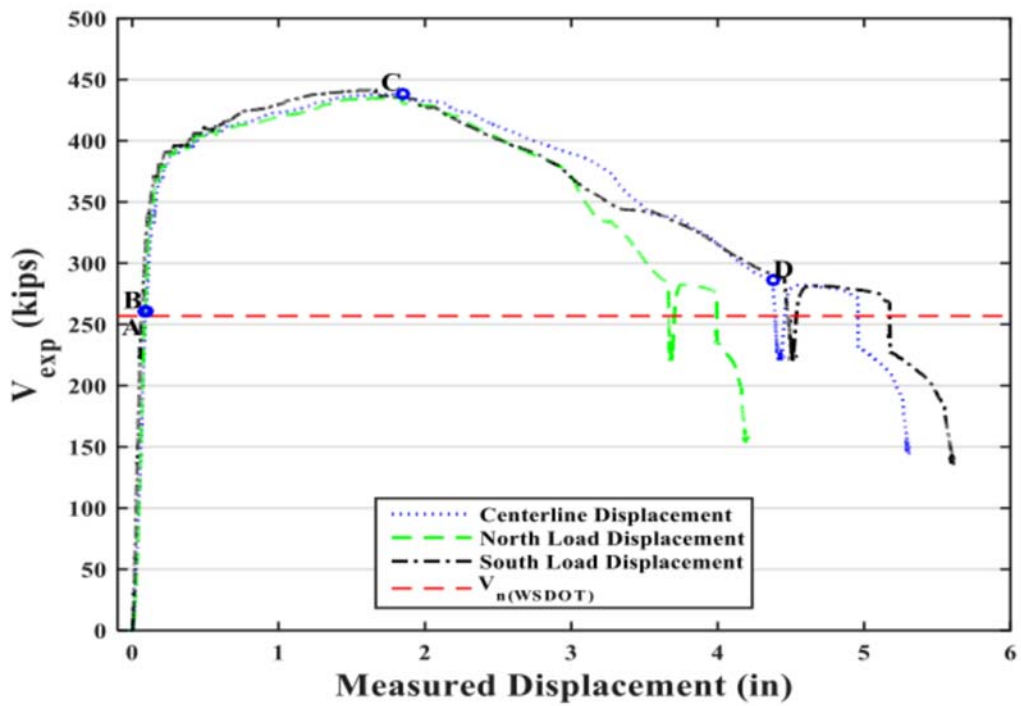
Specimen 9 – CFST Specimen with Greased Interface

Specimen 9 had a greased steel-concrete interface and was a variation of Specimen 2, the baseline specimen for $a/D = 0.5$, and was tested 23 June 2015. It had a tail length of 40 inches, a straight seam weld, and no internal reinforcement. It achieved 1.06 times M_{PSDM} and 1.72 times $V_n (WSDOT)$ and failed in flexure due to a loss of bond as

shown in Figure 4.11. The steel developed the full plastic capacity by the PSDM, but the capacity was clearly reduced by the reduced bond stress and bond slip because the shear and moment capacity 20% smaller than that of Specimen 2. The tube tore at the bottom due to flexure-shear interaction approximately 6 inches south of mid-span after significant flexural deformations, flexural buckling, and shear deformations occurred (see Figure 4.12 a, b, and c). The tear was approximately vertical. Because of the greased interface, the concrete fill had large rigid body displacements, e.g. the concrete in the south tail slipped over 4 inches at the end (see Figure 4.12e). The reduction in composite action effectively concentrated the cracking in the concrete fill into a few, large cracks in contrast to the widely distributed crack pattern seen in the other CFST tests (see Figure 4.12 d and f). North is to the left in each photograph.



a) Moment-Displacement



b) Shear-Displacement

Figure 4. 11: Behavior of Specimen 9

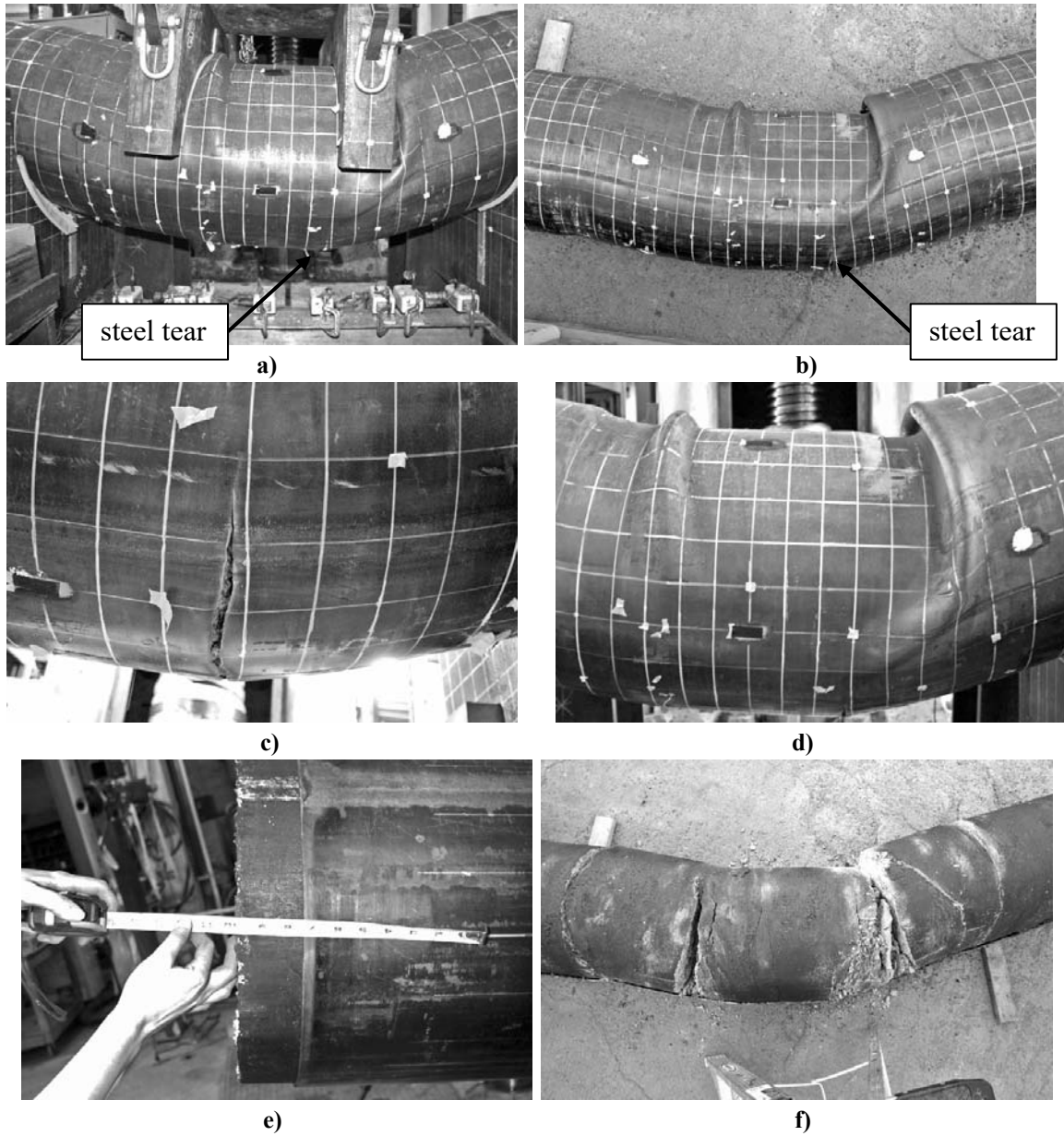
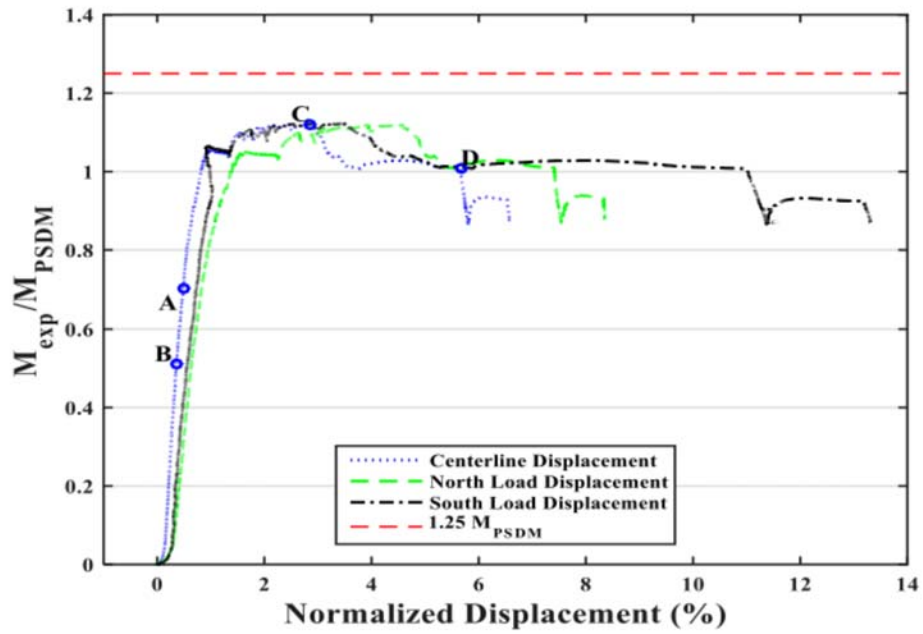


Figure 4.12: Specimen 9 Photos

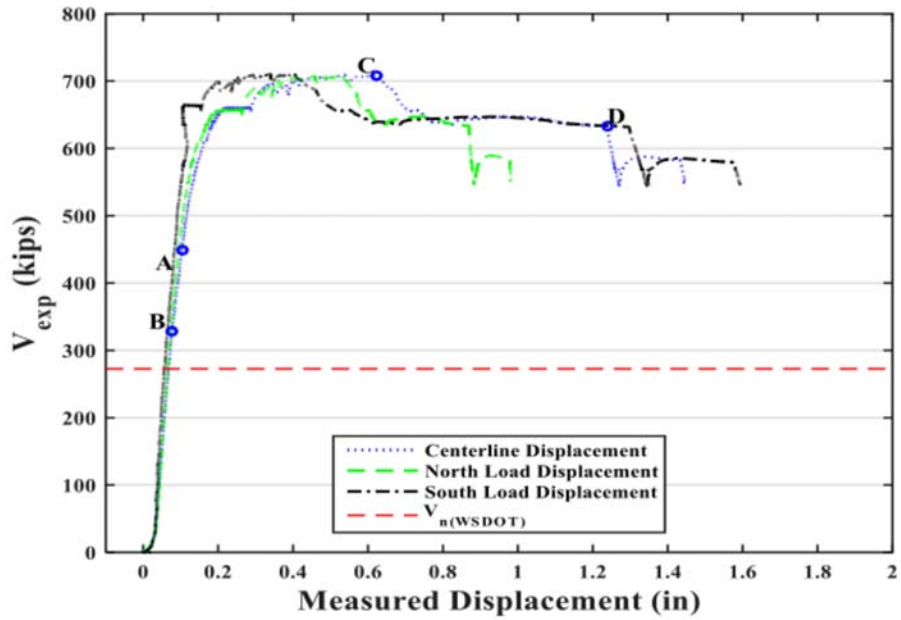
Specimen 13 – CFST Specimen with Axial Load

Specimen 13 was similar to Specimen 11, the $a/D = 0.375$ specimen with the short tail length, but it had an axial load of 8.5% of the compression capacity of the CFST. It had a clean interface, a tail length of 10”, a straight seam weld, and no internal reinforcement. It achieved 1.12 times M_{PSDM} and 2.60 times $V_n (WSDOT)$ and failed due to

flexure-shear interaction as shown in Figure 4.13. The axial load increased the shear and moment capacity by approximately 18% over that of Specimen 11. The tube did not tear since the test was stopped to avoid damaging the Williams rod used to apply the axial load as shown in Figure 4.14c. There were significant shear strains in addition to less severe flexural deformations. The shear strains were seen primarily in the south shear span. Extensive diagonal shear cracking and deformations occurred in the concrete fill in the south shear span while significant diagonal cracking was noted in the north shear span concrete. Flexural buckling just initiated near the end of the test. Moderate flexural cracking was noted in the concrete fill in the pure moment region. The axial load was applied manually via a center-hole hydraulic ram, and was maintained within $\pm 3\%$ of the intended target until the normalized moment reached 1.10, at a normalized displacement of 1.58%, at which point the load dropped to 78% of the target, and it became difficult to control axial load with the manual setup. Pressure was released from the ram four times in an attempt to maintain the axial load as constant as possible, at displacements of 1.58%, 2.17%, 2.48%, and 2.93%, which accounts for some of the saw-tooth pattern in the plots of Figure 4.13. The axial load was released at a displacement of 5.77% and then transverse loading was continued until 6.53%. North is to the left in each photograph of Figure 4.14.



a) Moment-Displacement



b) Shear-Displacement

Figure 4. 13: Behavior of Specimen 13

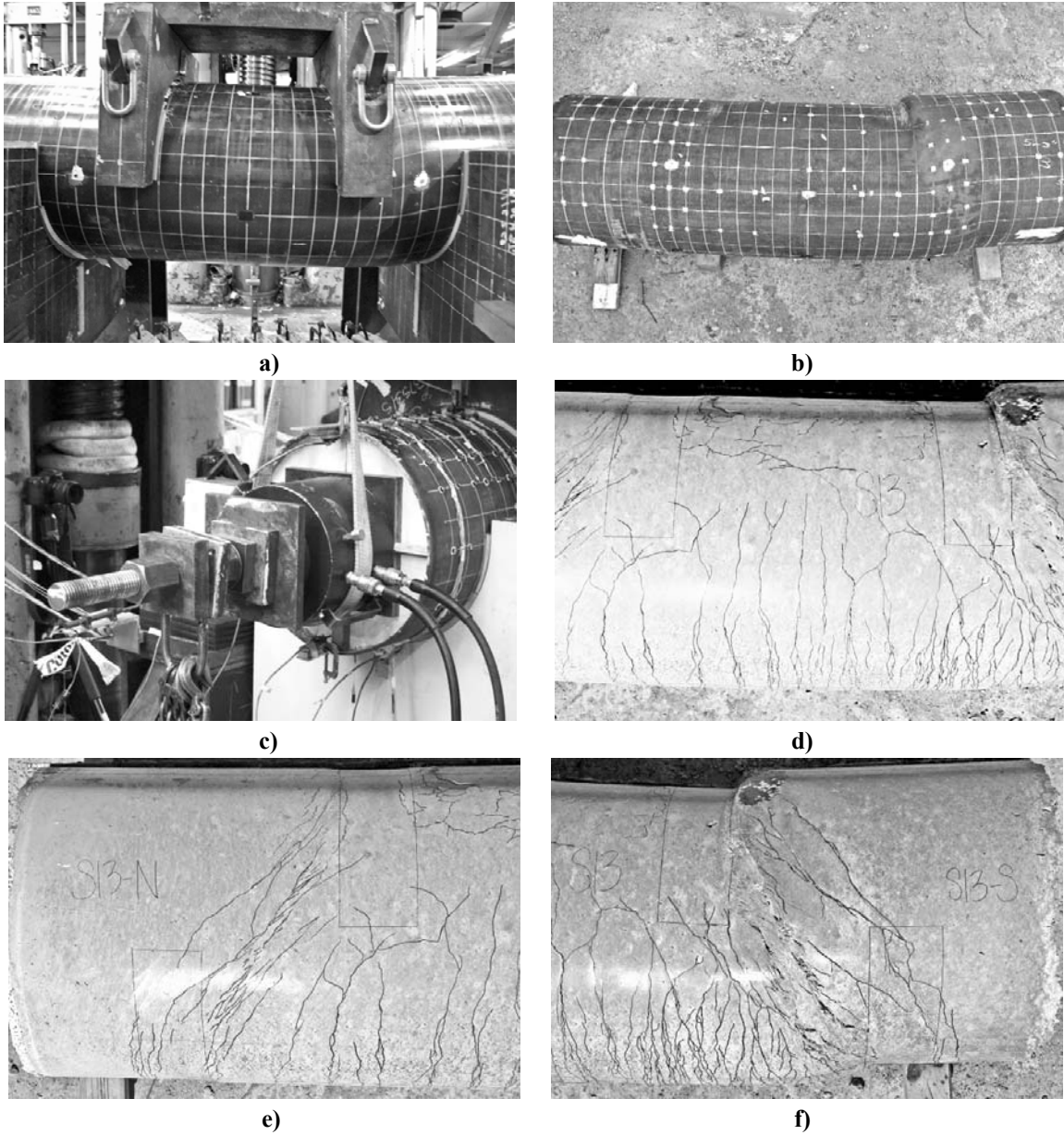
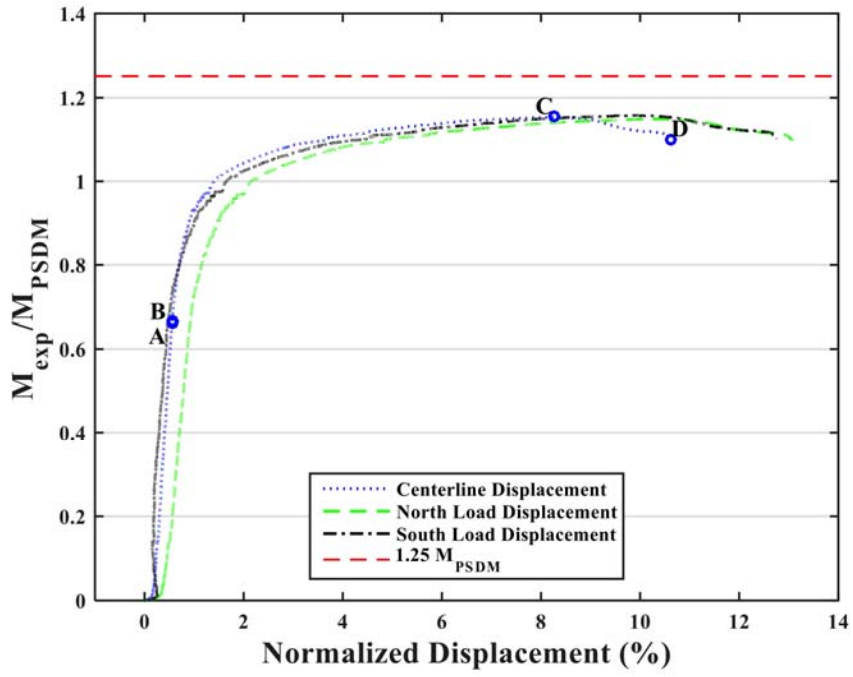


Figure 4. 14: Specimen 13 Photos

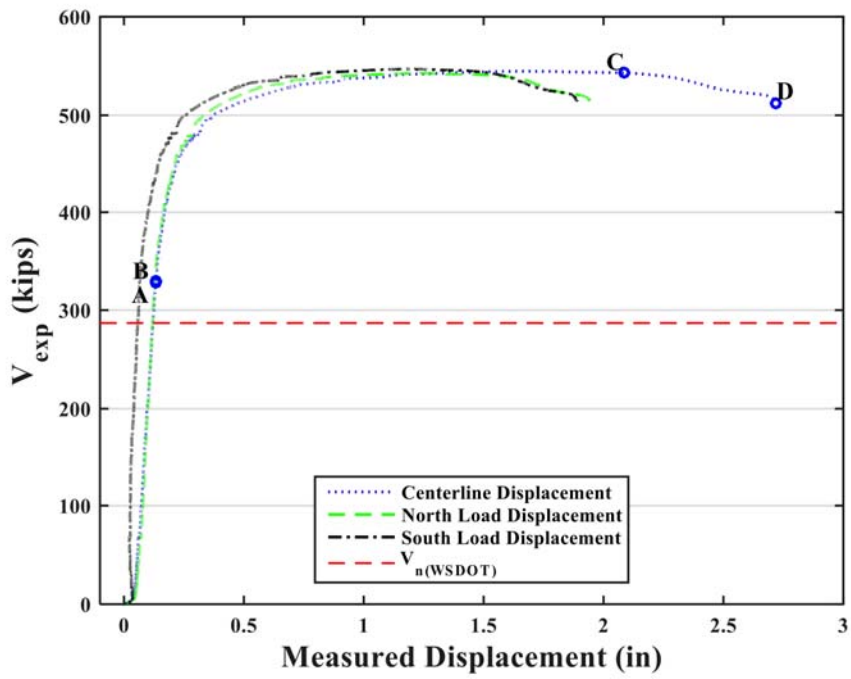
Specimen 17 – CFST Specimen with Flexural Behavior

Specimen 17 was a concrete type variation of Specimen 2, the baseline specimen for $a/D = 0.5$, and was tested 20 August 2015. It had a clean interface, a tail length of 40", a straight seam weld, no internal reinforcement, and a specified 28-day concrete strength of 12000 psi, twice that of Specimen 2. It achieved 1.16 times $M_{p,PSDM}$ and 1.91

times V_n (*WSDOT*) as shown in Figure 4.15 and failed in flexure. The tube tore at the bottom in flexure approximately 2 inches south of mid-span after significant flexural deformations occurred. The tear was oriented vertically as shown in Figure 4.16a and b. The tube steel buckled on both the north and the south ends of the pure moment region symmetrically as shown in Figure 4.15. Extensive flexural cracking of the concrete fill occurred in the pure moment region (see Figure 4.16c), while limited diagonal shear cracking was also noted in the concrete fill in both shear spans (see Figure 4.16 d and e. South is to the left in each photograph of Figure 4.16.



a) Moment-Displacement



b) Shear-Displacement

Figure 4. 15: Behavior of Specimen 17

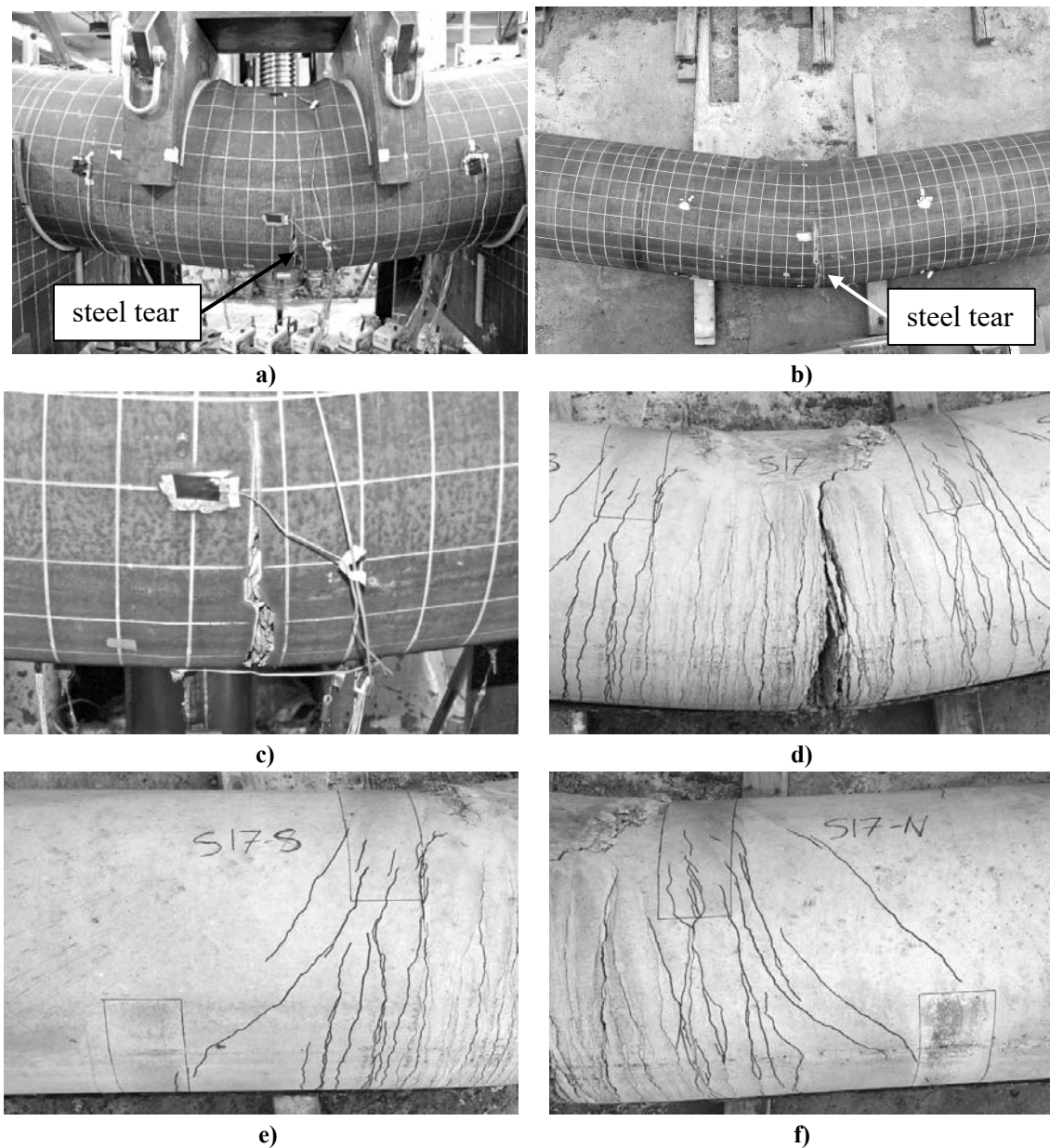
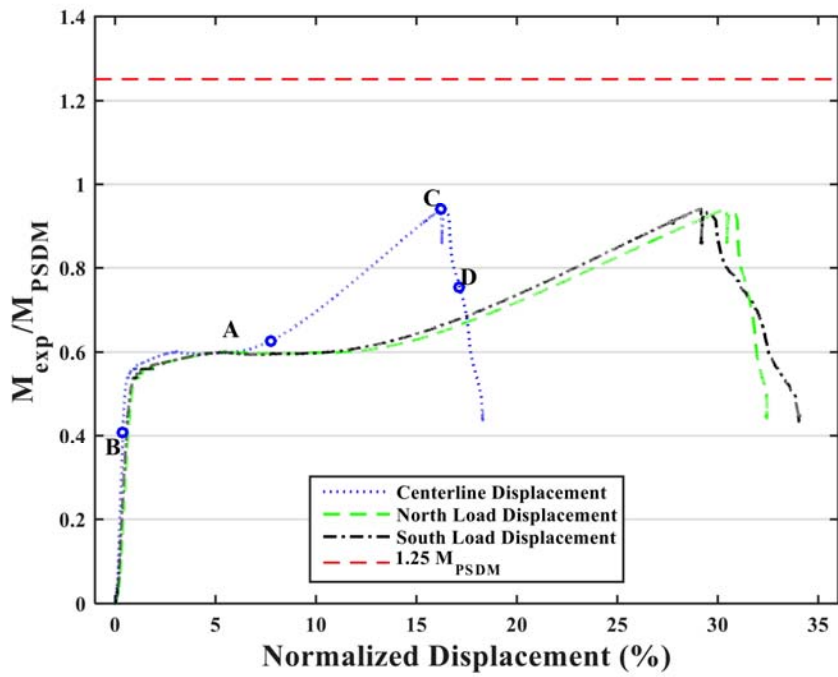


Figure 4. 16: Specimen 17 photos

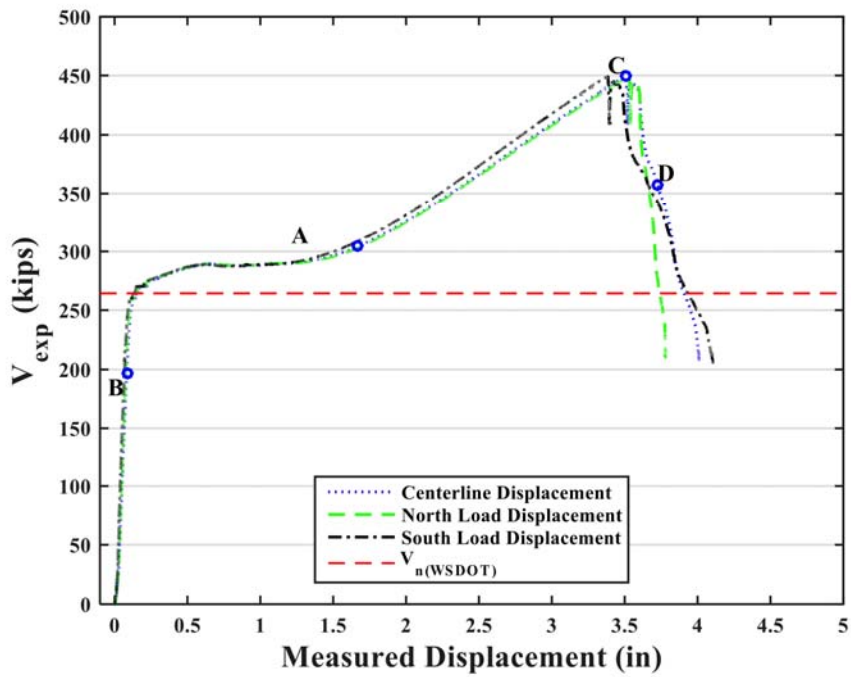
Specimen 21 – Steel Tube with Gravel Fill

Specimen 21 had gravel in the shear spans in lieu of concrete in order to determine the distinct contributions of the concrete and steel to the shear resistance of CFSTs. It was not a true CFST, since it was built to demonstrate the shear resistance contribution of the steel, but it will be compared to the calculated CFST values for

consistency with the rest of the research specimens. It had similarities with Specimen 10, the baseline specimen for $a/D = 0.375$, and was tested 29 July 2015. It had a clean interface, a tail length of 40", a straight seam weld, and no internal reinforcement. It achieved 0.94 times M_{PSDM} of the CFST and 1.70 times $V_n (WSDOT)$ of the CFST as shown in Figure 4.17, and failed in shear. The tube tore at the bottom approximately 11 inches south of mid-span after significant shear deformation occurred as shown in Figure 4.18 a, b, and c. Shear buckling (see Figure 4.18 c) initiated when the normalized moment reached approximately 0.5 and the shear force was approximately 0.9 times $V_n (WSDOT)$. Tension-field action developed and provided increased shear resistance. The tear was oriented at roughly half the angle of the tension field. There was no visible flexural buckling in the pure moment region. The concrete fill experienced very minor cracking and damage (see Figure 4.18d). The gravel fill retain the general volume of the tube but did not perfectly retain the circular shape as shown in Figure 4.18. South is to the left in each photograph.



a) Moment-Displacement



b) Shear-Displacement

Figure 4. 17: Behavior of Specimen 21

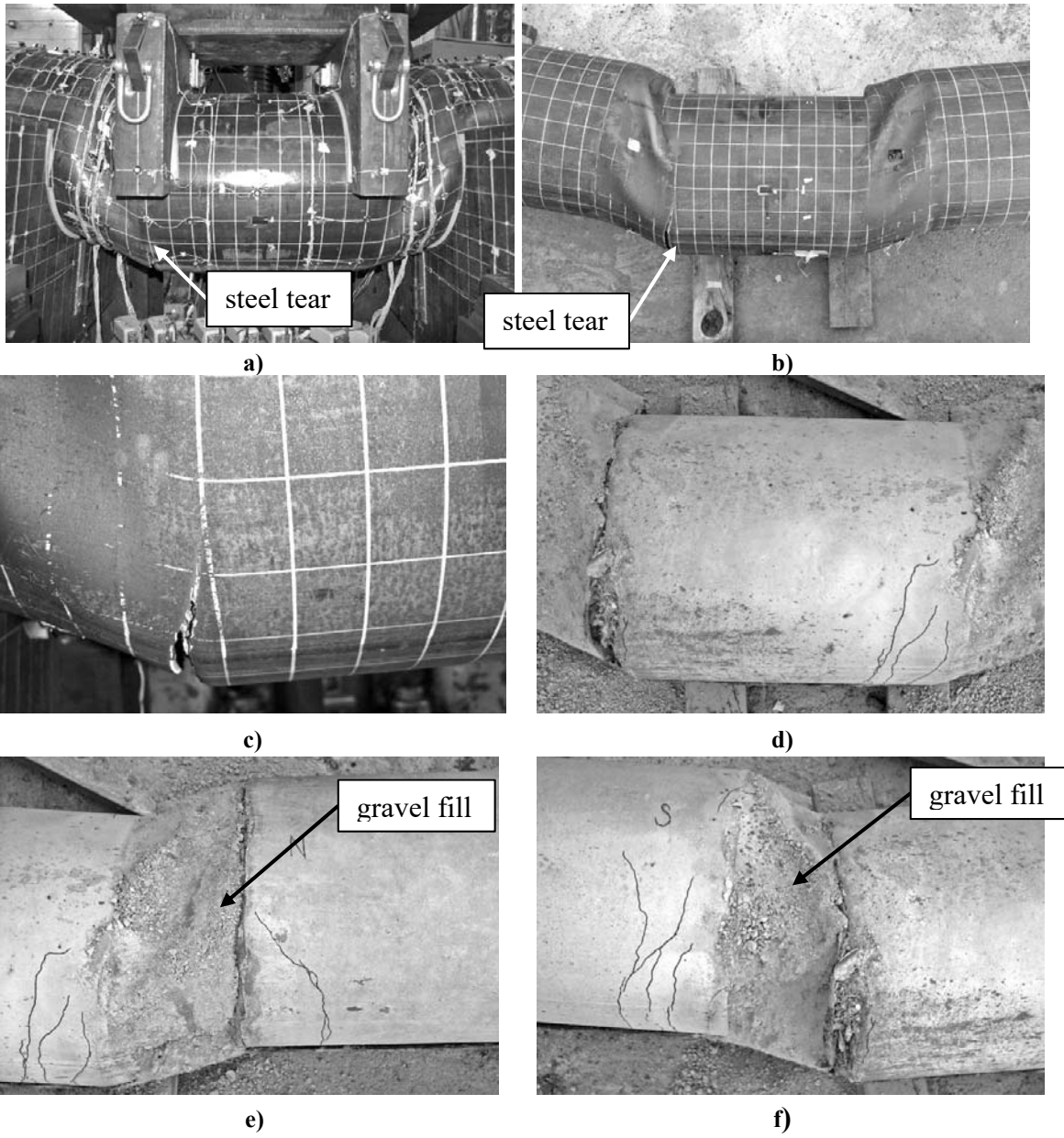


Figure 4. 18: Photos of Specimen 21

CHAPTER 5

FURTHER ANALYSIS OF RESEARCH RESULTS

This chapter combines the data from this research program with prior research programs (discussed in Chapter 2) with the objective of developing recommendations for the design shear capacity of CFST and RCFST members.

COMPOSITE ACTION AND DEVELOPMENT LENGTH

Prior research has shown that composite action of CFST provides a significant increase in strength and stiffness over that achieved by steel or reinforced concrete elements of the same size and geometry (Roeder et al 2008). Composite action requires shear stress transfer between the steel and concrete, and therefore the CFST must have a sufficient length beyond the maximum moment to develop full composite resistance. This length is analogous to the development length of a reinforcing bar.

Much of the prior shear research used end-caps, which do not allow for differential movement of the steel tube and concrete fill and therefore will, ideally, develop full composite action for all cases. However, this end condition does not simulate actual boundary conditions. In the University of Washington test specimens, a tail length, L_T (see Figure 3.1), was used to simulate field boundary conditions and investigate the required length to develop full composite action.

Table 5.1 describes the specimens used in the short tail length series, and compares these results to comparable specimens with longer tail lengths. Most specimens had a L_T equal to two times the diameter of the tube, $2D$, which consistently assured full composite behavior. Five specimens (3, 4, 11, 13, and 15) had shorter tail lengths to investigate the stress transfer mechanism, including failure mode and slip.

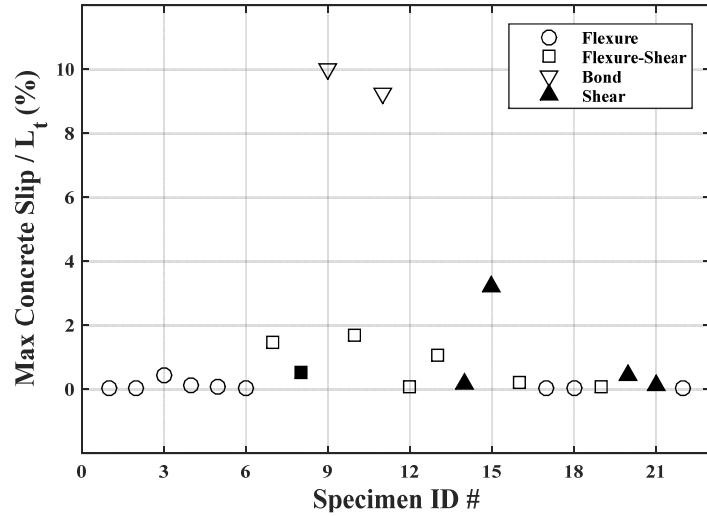
Specimen 13 had a short L_T , but was loaded with an axial load applied through a Williams bar and center hole ram through the center of the specimen, potentially enhancing the bond transfer mechanism (see Figure 4.14c).

Table 5. 1: Tail Length Series Specimens and Comparisons

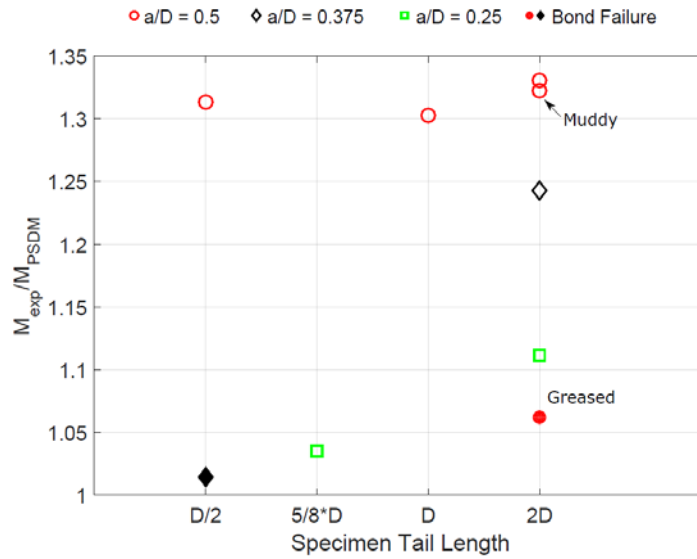
Specimen	2	3	4	6	10	11	13	14	15
a/D	0.5				0.375			0.25	
P/P_0	0%				0%		8.5%	0%	
L_T	2D	D/2	D	2D	2D	D/2	D/2	2D	5/8*D
Failure Mode	flexure	flexure	flexure	flexure	flex-shear	bond	flex-shear	shear	shear
$M_{exp} / M_{p,PSDM}$	1.33	1.31	1.30	1.37	1.24	1.01	1.12	1.11	1.04
$V_{exp} / V_n (WSDOT)$	2.16	2.14	2.11	2.20	2.42	2.08	2.60	2.89	2.78
Max Slip (in)	0.018	0.044	0.026	0.007	0.683	0.926	0.107	0.070	0.404
Max Slip / L_t	0.04%	0.44%	0.13%	0.02%	1.71%	9.26%	1.07%	0.18%	3.23%

The relative slip between the steel tube and the concrete fill was measured at the north and south ends of all specimens. The maximum measured values of slip for all specimens are provided in Figure 5.1a. Of the specimens tested, only two exhibited a bond failure, Specimens 9 and 11 (note that Specimen 9 had a greased interface and, as such, bond failure was expected). However, Specimen 11 had a normal contact surface with a D/2 tail length. The slip clearly affected the performance of this specimen when compared to Specimens 10 and 13, which were nominally identical to Specimen 11 but with longer tail lengths. Both the shear and moment capacity were reduced relative to the comparable specimens, however all specimens developed the full plastic flexural capacity of the member, as indicated in Figure 5.1b. The shear transfer required for composite flexural action is transferred via friction and binding action that occurs as CFST deforms

(Roeder et al. 2009; Roeder et al. 1999). The large slip in Specimen 11 did not occur in other specimens with short tail lengths, which is an issue of concern, since the full flexural resistance (expected to be $1.25M_{psdm}$) was reduced.



a) Maximum Slip (normalized to tail length) for Each Specimen



b) Normalized Moment vs. Tail Length

Figure 5. 1: Tail Length Comparisons

The shorter tail length provides less length for the horizontal shear transfer and allows for more distortion of the cross-section as prying action occurs near the end of the tube. Hence, it is recommended that a minimum development length of one times the

diameter of the tube be used before the CFST is expected to develop its full plastic capacity, M_{PSDM} , as defined by the plastic stress distribution method.

COMPARISON OF RCFST AND CFST

No prior data on the shear behavior of CFST with internal reinforcement, RCFST, was found in literature review. In the UW test program, four (4) RCFSTs with two different shear-span-to-depth ratios and two different tube-diameter-to-wall-thickness ratios were tested. Table 5.2 summarizes the properties of the RCFST specimens and compares their results to the comparable CFST members without internal reinforcing. It is of note that the steel reinforcement has larger yield strength than the steel tube, and as such comparing only the steel area can be misleading. The reinforcement was fully developed in the concrete before it reached the shear span in all the RCFSTs. In all cases, the yield stress of the reinforcement (nominally 60 ksi) is larger than the yield stress of the steel tube (nominally 50 ksi).

- Specimen 12 is similar to Specimen 2 except that it has 22% more steel from the internal reinforcement; this results in an 18% increase in capacity.
- RCFST Specimens 7 and 8 are similar to CFST Specimen 10, except that the RCFST specimens had 20% and 38% increase in the steel area, respectively. However, the capacities of RCFST Specimens 7 and 8 are increased only by 6% and 20.6% relative to Specimen 10, respectively.

Table 5. 2: RCFST Specimen Properties

Specimen	D/t	a/D	ρ_{int}	f'_c (ksi)	$M_{exp} / M_{p,PSDM}$	$V_{exp} / V_{n,WSDOT}$	Failure Mode	A_{sr} / A_s
2	80	0.5	0%	6.22	1.33	2.16	flexure	0%
12	80		1.13%	6.18	1.21	2.37	flex-shear	21.5%
19	53.3		1.07%	9.13	1.21	2.24	flex-shear	13.2%
10	80	0.375	0%	6.15	1.24	2.42	flex-shear	0%
7			1.04%	6.45	1.17	2.74	flex-shear	19.7%
8			2.01%	6.48	1.02	2.92	shear	38.2%

It is of note that the failure mechanism changed with the internal reinforcement, thereby limiting flexural strength to less than the idealized maximum capacity of $1.25M_{psdm}$. However, the measured shear strength of the RCFST specimen relative to the current WSDOT expression is increased, indicating that the internal reinforcement should be included in the proposed shear strength expression.

CONTAMINATION OF THE STEEL-CONCRETE INTERFACE

Four distinct interface conditions were represented in the experimental program: 1) clean interior tube surface with a straight-seam welded tube, 2) clean interior tube surface with a spirally welded tube, 3) muddied interior tube surface with a straight-seam welded tube, and 4) greased interior tube surface with a straight-seam welded tube. The normalized moment-normalized displacement curves for each of the four specimens are shown in Figure 5.2. All of the specimens had an $a/D = 0.5$, and so it would be expected that they would respond in a primarily flexural mode and the shear developed would be determined by the flexural capacity.

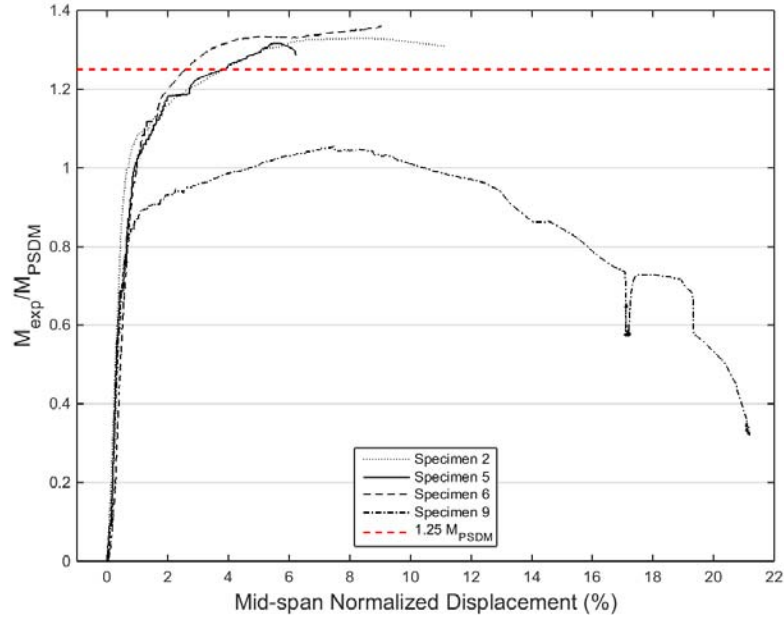


Figure 5. 2: Moment-Displacement Behavior of Interface Series Specimens

The CFST with the greased interface, Specimen 9, developed some composite behavior since it attained 106% of the plastic moment of the composite section, but it had a significantly smaller resistance than the other 3 comparable CFST specimens (Specimens 2, 3 and 6).

Table 5. 3: Interface Series Specimen Properties

Specimen	2	5	6	9
a/D	0.5			
Interface	clean SS	muddied SS	clean SW	greased SS
L_T	2D			
Failure Mode	flexure	flexure	flexure	bond
$M_{exp} / M_{p,PSDM}$	1.33	1.32	1.37	1.06
$V_{exp} / V_n (WSDOT)$	2.16	2.17	2.20	1.72
Max Slip (in)	0.018	0.024	0.007	4
Max Slip / L_t	0.04%	0.06%	0.02%	10%

The ultimate moment capacities of the other three specimens in the series were all similar. The primary difference was that the spiral-welded tube was stiffer (after

cracking) between yield moment and peak moment than the straight-seamed tubes. The interlock between the concrete and the internal weld seam adds significant force transfer between the tube and the concrete and therefore this response was expected.

The muddied interface also appears to have increased the force transfer as the post-yield stiffness for Specimen 5 is slightly greater than the clean interface of Specimen 2.

There was little difference in the behavior of the CFSTs for all of the surface conditions, but all of the failures were flexural in nature. The same conditions should be tested at an a/D ratio smaller than 0.5 to achieve shear behavior and impose different stress conditions on the interface.

EFFECT OF CONCRETE STRENGTH

Several important questions relate to the effect of concrete strength on shear resistance. First, it is necessary to establish how much of the shear resistance is provided by the steel and how much is provided by the concrete fill. Given that the concrete fill does provide shear resistance, these tests also provide a basis for quantifying the contribution of the concrete fill.

Table 5.4 outlines the properties of the specimens used in this series, and compares these results. Specimen 21 had gravel in the shear spans, and it could be said to have a concrete with zero strength at those locations. Specimens 2, 10, 14, 16, 17, and 20 demonstrate the effect of variation in the compressive strength of the concrete fill on shear resistance of CFST.

Table 5. 4: Concrete Strength Series Specimen Properties

Specimen	a/D	D/t	f'_c (ksi)	f'_{cm} (ksi)	$M_{exp} / M_{p,PSDM}$	$V_{exp} / V_{n,WSDOT}$	$\bar{\Delta}_{fail}$ (%)
2	0.5	80	6.0	6.22	1.33	2.16	11.32
17		53.3	12.0	9.45	1.16	1.91	10.64
10	0.375	80	6.0	6.15	1.24	2.42	14.57
16			12.0	8.61	1.30	2.62	10.36
21			0	0	0.94	1.70	17.16
14	0.25	80	12.0	8.60	1.11	2.89	9.48
20			2.5	2.79	1.06	2.54	16.69

The sample size is small, but the table clearly shows that the steel tube provides the bulk of the shear resistance. Specimen 21 achieved a large shear resistance even though its capacity was limited by shear buckling, because the gravel fill did not develop shear and did not fully retain the circular shape of the tube. Comparison of Specimens 2 and 17, as well as Specimens 10 and 17 and Specimens 14 and 20, show that a significant increase in the compressive strength of the concrete results in a relatively modest increase in total shear resistance.

EVALUATION OF DESIGN EXPRESSIONS

Chapter 2 presented several equations that have been used or proposed to calculate the shear resistance of CFST and RCFST. It is clear from the experimental research that the shear resistance of CFST is significantly larger than currently permitted in US design provisions.

Further, the research shows that for most of the specimens, the shear demand is controlled by the flexure capacity. Only the smallest aspect ratio specimens (0.5, 0.375, and 0.25) sustained shear failure and therefore only those specimens can be used to

quantify the shear resistance. The research also demonstrates that the steel tube likely provides a much larger portion of the shear resistance than the concrete fill.

The shear resistance does not appear to be overly influenced by the surface conditions of the steel-concrete interface, although a greased interface did result in a clear reduction in shear resistance. Axial load results in clear increase in shear resistance, but very limited reliable test data is available to quantify this increase. RCFST has somewhat larger shear resistance than CFST of the same size and geometry, because of the added internal reinforcement, but the research suggests that the internal reinforcement is less efficient in providing this resistance.

Prior discussion has clearly shown that shear capacity is often controlled by flexural capacity of the CFST. Prior research has also shown that on average the experimental moment capacity of CFST is 1.25 times moment capacity predicted by the plastic stress distribution method, M_{PSDM} . Hence specimens with measured flexural strength, M_{exp} , greater than $1.25 M_{PSDM}$ are clearly controlled by flexure, and only specimens with M_{exp} significantly smaller than $1.25 M_{PSDM}$ are controlled by shear. Specimens in the intermediate range are in the intermediate shear-flexure zone of behavior where both shear and flexure are noted.

This and prior experimental research show no evidence that large bending moments reduce shear resistance or that large shear forces reduce flexural resistance. The shear forces in the beam are either limited by the flexural capacity of the beam or the maximum shear resistance, V_n . The use of experimental data controlled by flexure or by combined shear-flexure would therefore underestimate V_n . Hence, only experimental results with M_{exp} less than $1.15 M_{PSDM}$ are used to evaluate the equations for predicting

V_n . As noted in prior discussions, the high applied loads required to cause shear failure of CFST make the determination of M_{exp} imprecise. This 1.15 limit is quite conservative in that it still will include some specimens limited by flexure, but conservatism is necessary in view of the uncertainty in evaluation of M_{exp} .

Considering this parameter, Specimens 8, 11, 14, 15, and 20 were used in the following evaluations. Most other specimens were not considered because they had an M_{exp} that exceeded $1.15 M_{PSDM}$. Specimen 9 was not used because was a greased specimen and it developed a bond slip failure. Specimen 21 was not included because it was filled with gravel, and was not a CFST specimen. Specimen 13 had an axial load, and, therefore, was not included in the comparison, as sufficient data is not available to include the effect of axial load on shear strength.

Evaluation of Current WSDOT Provisions

As discussed in Chapter 2, the current shear strength design equation combines the shear strength of the two materials and neglects the benefits of the composite action present in CFST members. Recognizing this deficiency in Equation 2.1, Figure 5.3 shows that the current provisions from WSDOT underestimate shear capacity by over 250% on average, when compared to the relevant University of Washington experimental results. That is, the mean and standard deviation of this data are 2.64 and 0.35, respectively.

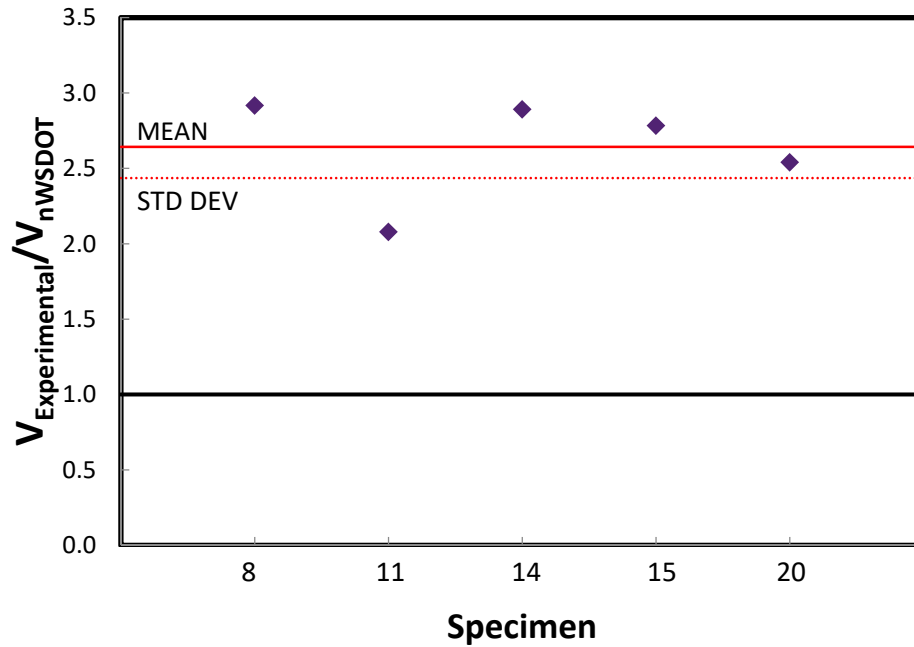


Figure 5. 3: Comparison of Current WSDOT Design Equation to UW Experiments

To extend this evaluation further, extensive tests were performed by Xu, Xiao, Nakahara and Qian (references) prior to this research study. Chapter 2 mentions that the tests were all on small diameter tubes and there was great scatter in their research results, but a comparison was made of relevant research results from their tests to further evaluate the WSDOT equation in Figure 5.4. The mean and standard deviation of this data are 3.1 and 0.69.

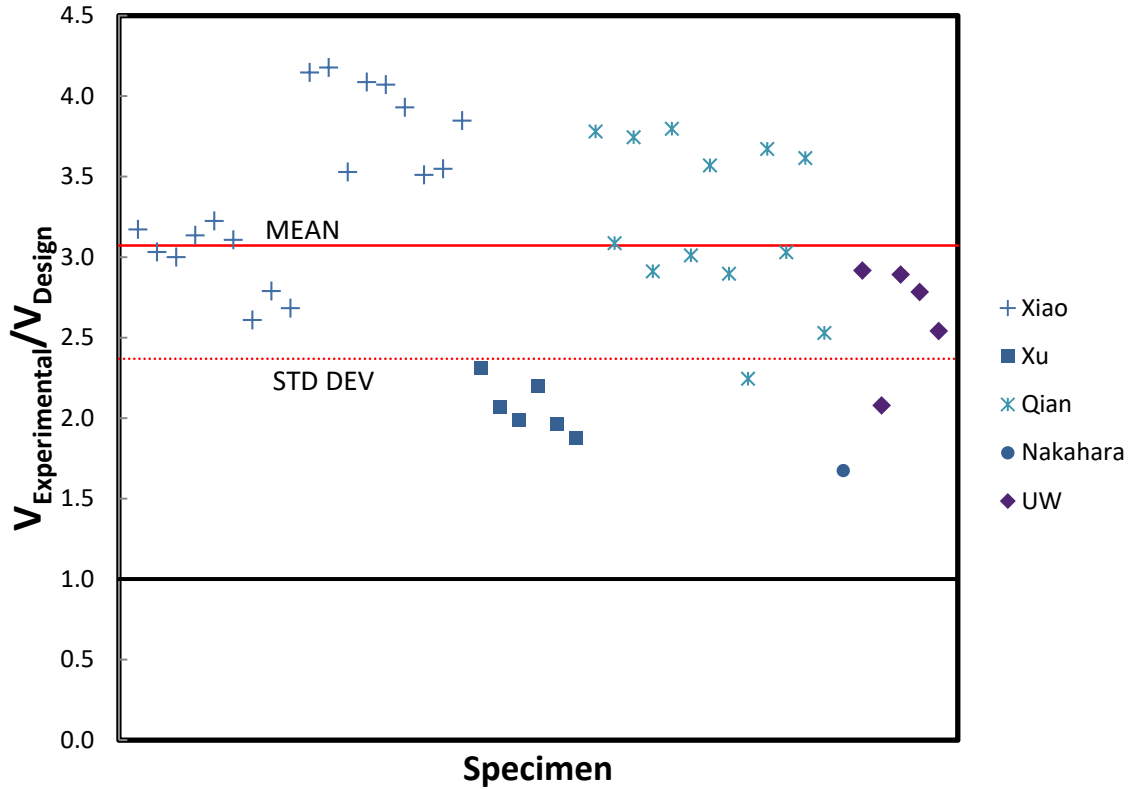


Figure 5. 4: Comparison of Current WSDOT Design Equation to Prior Experimental Results

Although the applicability of some of these specimens could be questioned, as discussed in the next section, these comparisons show that the estimation of shear strength, as it stands currently, is quite conservative and can be approved upon.

Recommended Provisions

Equations for predicting shear resistance were developed in prior research and these equations were used as a starting point for developing improved resistance equations. Specimen 21 showed that the steel tube filled with gravel developed a nominal shear resistance, V_n , of:

$$V_n = 1.7 \cdot 0.5 \cdot A_s \cdot 0.6 F_y \tag{5.1a}$$

In the expression, A_s and F_y are the total area and yield stress of the steel tube, respectively. The gravel fill did not provide any shear resistance in this test, but instead served to approximately retain the circular shape of the tube so that the steel tube developed shear buckling and a diagonal tension field. Hence this resistance is viewed as a lower bound on the shear resistance of CFST, which can be achieved even with extensive damage to the concrete fill under the most severe cyclic deformation. If this shear capacity of the steel is used as a basis of strength for the composite section, the nominal shear capacity can be evaluated as:

$$V_n = 1.7*0.5*A_{st}*0.6 F_y + 0.85*A_{sr}*0.6 F_{yr} + 4*A_c*0.0316*\text{SQRT}(f'_c) \text{ (ksi units)} \quad (5.1b)$$

where A_{sr} and F_{yr} are the total area and yield stress of the internal reinforcing in RCFST, while A_{st} and F_y correspond to the tube contribution, and A_c and f'_c are the total area and compressive strength of the concrete fill.

Figure 5.5 illustrates the comparison of this design equation with the University of Washington experiment results. The mean experimental value is 1.40 and the standard deviation is 0.17.

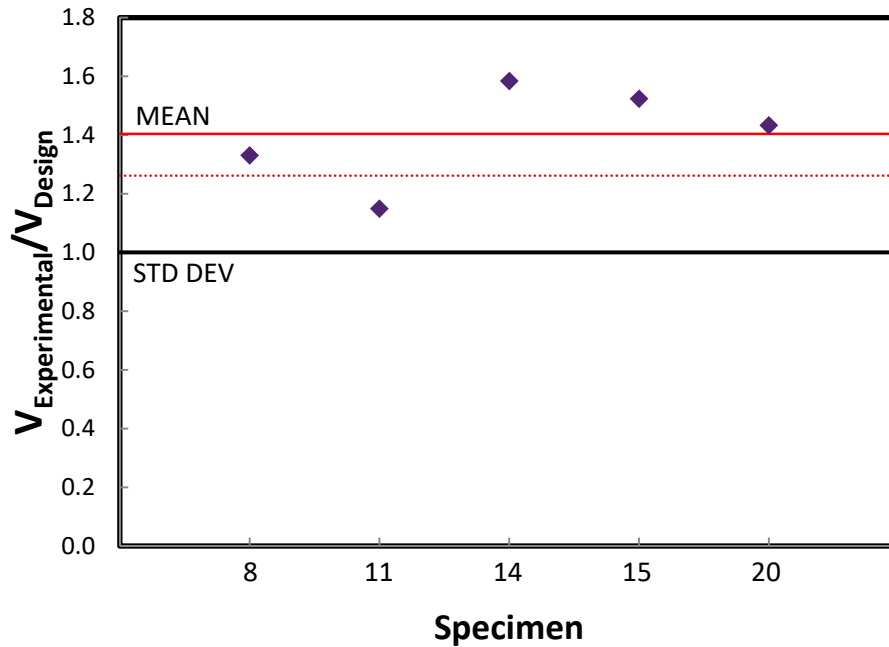


Figure 5. 5: Comparison of Possible Design Equation to UW Experiments

In general, the possible equation is conservative with a fairly large standard deviation. Then, turning attention to previous researcher efforts, Figure 5.6 compares the possible equation to relevant past data. The mean value of this data is 1.76 and the standard deviation 0.4 for a total of 43 specimens in the data set.

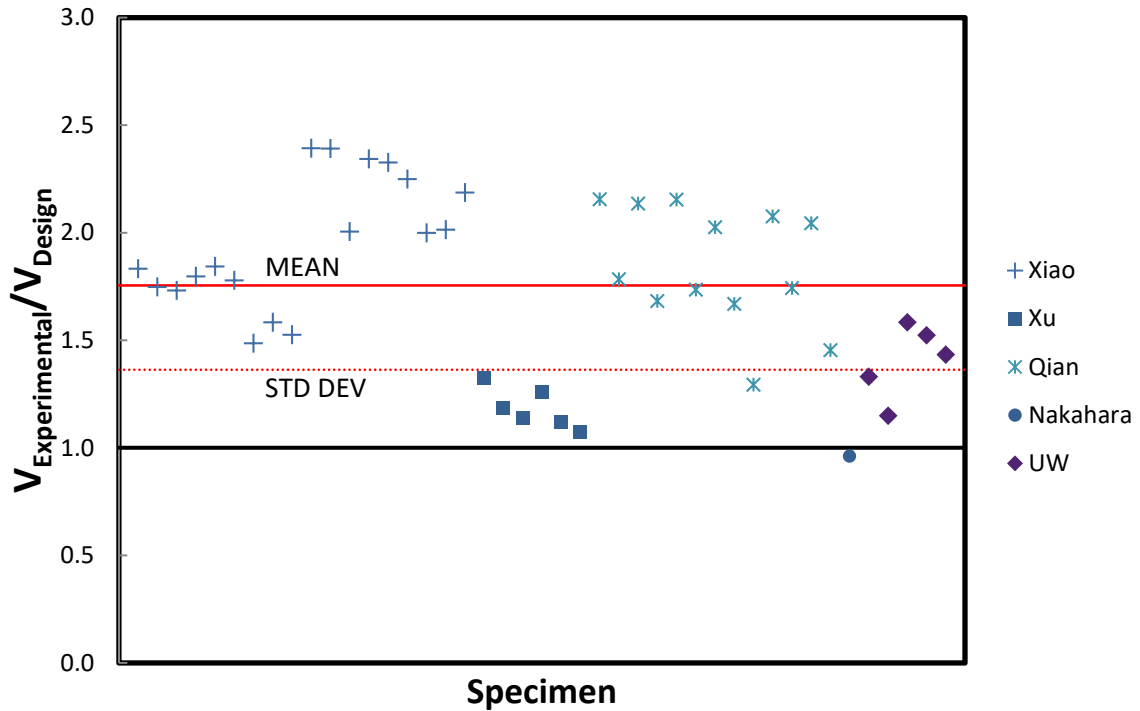


Figure 5. 6: Comparison of Possible Equation to Prior Experimental Results

There is considerable scatter in this data. The tests by Nakahara consistently achieve smaller experimental shear than predicted by the proposed equation. This is to be expected. Nakahara indicated that all his specimens were controlled by shear, but photos of his specimens do not support this claim. It is expected some of his tests were affected by flexure because the moment is larger within the grips of the specimen, and the flexural yielding limited the shear developed in the specimen. Note though, that only one specimen was included from this set, as the others were loaded axially. The current strength equation analysis by UW is not intended to specifically analyze this particular effect.

The tests by Xiao have tremendous scatter. The majority of these specimens had large axial load, and it is clear that axial load increases shear capacity. However, as

mentioned, this aspect is not considered in the possible design equation. Nevertheless, the data shows to be pertinent to the proposed equation, while still being largely conservative.

Xu used expansive concrete in many of his specimens and, consequently, were not considered in this comparison. Only those specimens with normal concrete were considered. However, the expansive concrete did show an increase in shear capacity in Xu's research program, suggesting that the proposed equation would be conservative in this case, but some of the benefits were reduced by short tail lengths and failure of end caps. This was true for the normal concrete specimens as well. This data is somewhat stronger than the UW data, but more comparable than the data by Nakahara and Xiao. In the end, all data points remained above the proposed design equation's estimate.

Qian's data is most comparable to the UW test results.

In general, the prior data suggests that the proposed equation is generally conservative but the scatter and deviation is quite large.

In view of these observations, a number of other alternatives were considered.

The final proposed equation for predicting shear resistance of CFST is:

$$V_n = 2*0.5*(A_{st} + A_{sr})*0.6 F_y + 3*A_c*0.0316*SQRT(f'_c) \quad (\text{ksi units}) \quad (5.2)$$

Here, F_y corresponds to the tube steel yield strength, with the assumption that the reinforcement steel has a larger yield strength. That is, the reinforcement is understood to be less effective than the steel tube in resisting shear, so by using the smaller yield strength, its contribution is limited. The equation is compared to UW experimental data in Figure 5.7. The mean and standard deviation of this data are 1.2 and 0.17, respectively. As with the earlier equation, the prediction is generally conservative, but the

standard deviation is still a bit larger because this model does not separate the tube and reinforcement steel areas, as the sample size of experiments able to distinguish their individual contributions is limited.

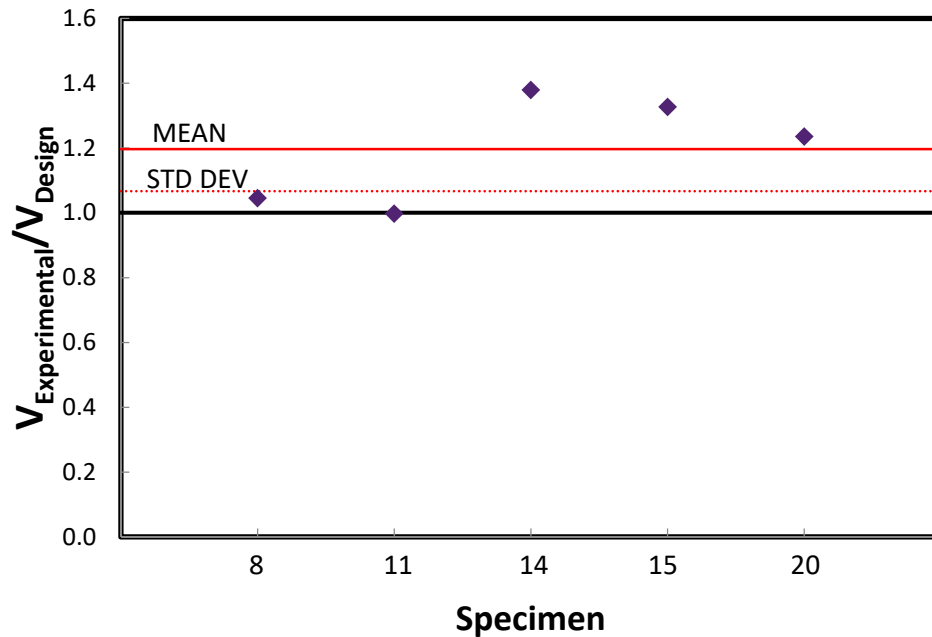


Figure 5. 7: Comparison of Proposed Design Equation to UW Experiments

The data was again compared to the prior experimental results, as shown in Figure 5.8. The variation with respect to individual researchers remains much the same with this proposed equation, but the mean and standard deviation are 1.51 and 0.35, respectively. Again, there is scatter, but the equation is still quite conservative for design. The low values on Figure 5.7 and 5.8 are likely influenced by bending moment, and their apparent shear resistance is reduced accordingly. This then results in the large standard deviation with respect to the accuracy of the proposed equation.

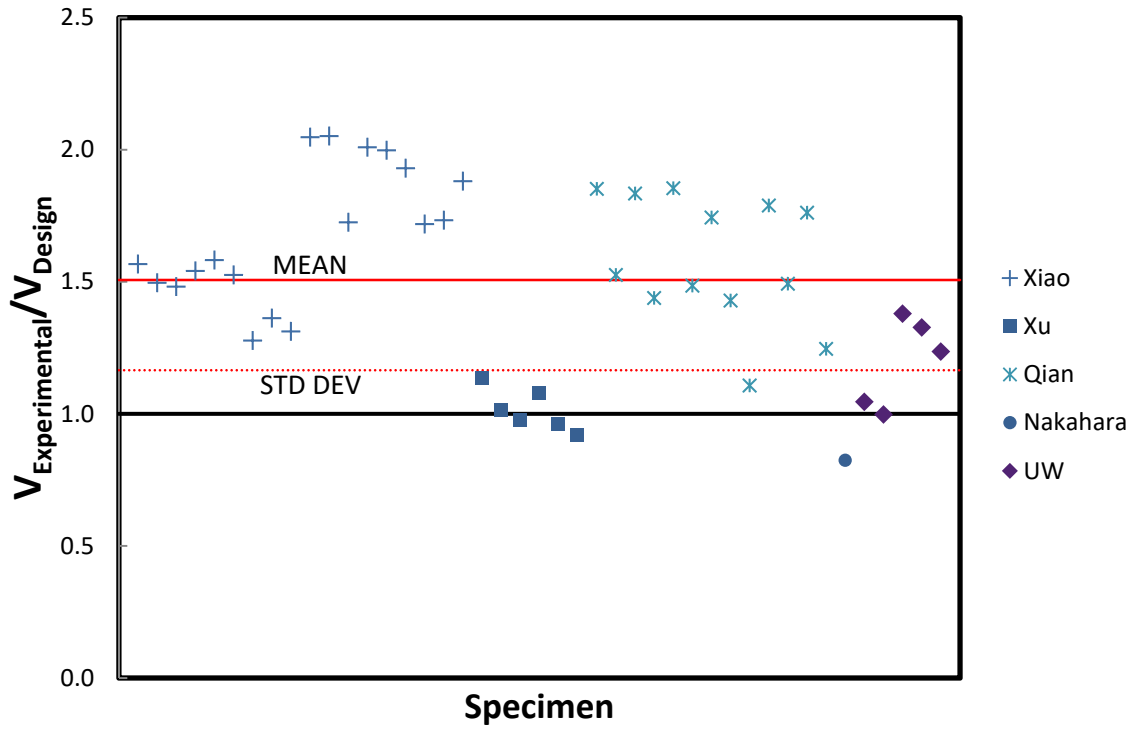


Figure 5. 8: Comparison of Proposed Equation to Prior Experimental Results

CHAPTER 6

NONLINEAR ANALYSIS AND PARAMETER STUDY

Nonlinear finite element models were developed in the ABAQUS computer program, and parameter studies were performed to extend the experimental results. This chapter provides a description of the model, its validation and the results of a parametric study, which was used to develop a design model based on a wider range and other design parameters, including axial load ratio and internal reinforcement ratio.

THE MODEL

The initial ABAQUS model was created based on recommendations from previous research conducted by the PIs (Moon et al. 2012, Moon et al. 2013), in particular the constitutive relations, the steel-concrete interface and the element types. The base model is illustrated in Figure 6.1. In addition to the concrete filled tube specimens, the test setup was simulated, including the load cradle, support cradle, cotton duck bearing pads, and elastomeric bearing with steel top plate; each are indicated in the figure.

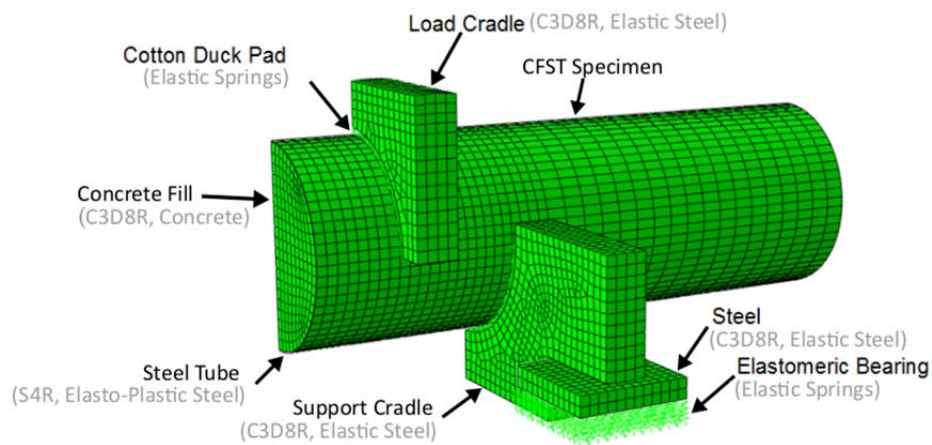
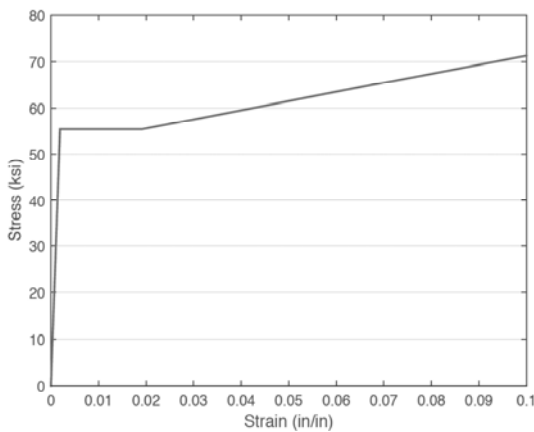


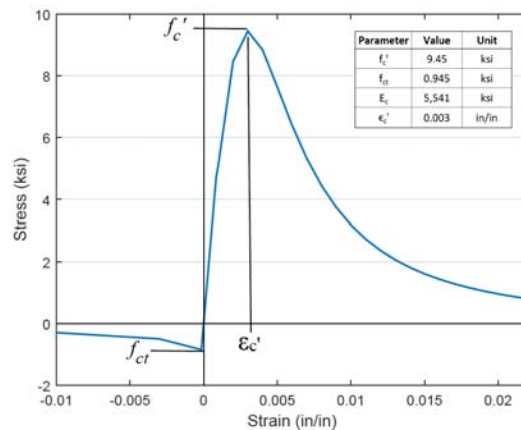
Figure 6.1. Base Model in ABAQUS

The steel tube was modeled using SR4 shell elements, with reduced integration schemes (S4R). A trilinear stress-strain relationship, including Von Mises yield function and isotropic hardening, was used to model the steel. The elastic modulus was 29,000 ksi and Poisson's ratio was 0.3. The nonlinear stress-strain relationship is illustrated in Figure 6.2a.

The concrete fill was modeled using solid 3D quadratic elements with reduced integration (C3D8R). The nonlinear constitutive relationship as illustrated in Figure 6.2b. In compression, the concrete model displays a relatively subtle decrease in strength after reaching its peak stress. The elastic modulus of concrete was defined by ACI, 2011, $E_c = 57,000\sqrt{f'_c}$ (psi) and the Poisson's ratio was 0.2. In this initial model, confinement of the concrete was not explicitly modeled but instead accounted for through the normal stress developed in the tube and the interface model. The peak tensile stress strength was $0.1f'_c$. The post-peak behavior under tension was simulated with a bilinear descending branch to avoid numerical issues.



a) Steel



b) Concrete

Figure 6.2 Material Models

The Concrete Damaged Plasticity model in ABAQUS was used to simulate cracking damage in the concrete and to provide flow rule for the concrete. This model requires five parameters: f_{bo}/f_{co} , K_c , dilation angle, eccentricity, and a viscosity parameter, which are defined in Table 6.1.

Table 6.1. Concrete Damaged Plasticity Parameters

f_{bo}/f_{co}	K_c	Dilation Angle	Eccentricity	Viscosity Parameter
1.12	0.666	20°	0.1	0.001

Bond stress between the steel tube and concrete fill develops through friction and binding action. This was modeled using surface-to-surface contact condition between the tube steel and concrete fill. A “Hard Contact” pressure normal to the interface was defined to prevent penetration, but separation was permitted. A 0.37 coefficient of friction was used to simulate shear transfer under a compressive normal stress. (Note, this coefficient of friction was smaller than that used by Moon et al. (2012) because Moon’s value was for spiral-weld tubes and the majority of the tests used straight-seam welded tubes.

The load and support cradles were modeled with 3D solid quadratic elements (C3D8R) and dimensioned to match the experimental setup. However, the support was cradle was not modeled with its full vertical depth to reduce computation time. Both cradles were elastic materials with E_s of 29,000 ksi and a Poisson’s ratio of 0.3. The surface-to-surface interaction between steel surfaces used Hard Contact normal pressures with a tangential Mohr-Coulomb coefficient of friction, μ , of 0.6.

Elastomeric bearings and cotton-duck bearing pads were used in the test setup to distribute stress under concentrated load to permit local deformation of the specimen near these cradles (See Chapter 3 for further description of the test setup). The behavior of these bearings was highly nonlinear with different characteristics in shear and compression. Normal and diagonal springs were used to measure the compressive and shear behavior of both the elastomeric bearings and cotton duck pads. The elastomeric bearing springs spanned the 2.5-inch thickness between the bottom of the steel top plate and fixed support of the bearing. The vertical and diagonal elastomeric bearing springs were modeled with stiffness values of 19 and 10 kips/in, respectively. These values were determined from a parameter study with stiffness values between 5 and 19 kips/in where this range of stiffness values was determined from prior research on elastomeric bearings (Roeder et al., 1987) and axial compression tests performed on the bearings used in research.

The steel top plate was modeled with 3D solid elements (C3D8R) with an elastic steel material ($E_s = 29,000$ ksi and Poisson ratio = 0.3). The cotton duck springs were also arranged normal and diagonal to the tube surface, and spanned approximately 0.5 in. between adjacent mesh nodes of the cradle and the mid-thickness of the steel tube. The vertical and diagonal spring stiffness were 41.9 and 15 kips/inch based upon parameter analyses between 10 and 41.9 kips/inch limits, which were based upon prior research recommendations (Lehman et al. 2003).

The model included one quarter of the test specimen, since symmetry about the longitudinal and midspan axes was employed. A mesh refinement study was performed to determine the finite element mesh that provide accuracy of the response and efficiency

in the solution. In addition the aspect ratio of various was considered, since this ratio affects the accuracy and reliability of the elements. The final resulting mesh was approximately 1 inch by 1 inch for the shell elements of the steel tube. The solution time for various analyses varied between 2 and 3 hours to over 2 days, using 4 CPUs and a total of approximately 5 gigabytes of RAM. Additional information about the modeling approach can be found in Heid 2016.

INITIAL VERIFICATION AND IMPROVEMENT OF THE MODEL

The models were verified by detailed comparison of the simulated response and behavior (e.g., deformed shape) with the measured. Six test specimens were used, as illustrated in Table 6.2. The specimens varied in their response mode (flexure, shear or flexure-shear), their a/D ratio, and their concrete strength.

Table 6.2. Specimens for Verification Study

a/D	Specimen	F_{ym} (ksi)	f'_{cm} (ksi)	V_{exp} (kips)	V_{ed} (kips)	$M_{ed}/$ M_{PSDM}	Failure Mode
1.0	1	49.6	6.012	322.0	322.0	1.27	Flexure
0.5	17	55.4	9.450	549.3	544.5	1.10	Flexure
	2	49.6	6.220	550.8	549.0	1.26	Flexure
0.375	16	56.8	8.609	759.2	760.5	1.24	Flex-Shear
	10	53.9	6.151	668.9	660.0	1.16	Flex-Shear
0.26	14	55.4	8.596	874.9	788.4	1.03	Shear

A total of three flexural specimens (Specimens 1, 2 and 17) were used. The results from the simulation provided relatively good accuracy for several aspects of the response, as shown in Table 6.2 and Figure 6.3. First, the force-deflection behavior is well approximated as shown in Figure 6.3e. Second, the model accurately captures local

deformation and buckling, as seen by comparing figures 6.3a and 6.3b. Finally, the extensive flexural cracking in the flexural span compared well with experimental observations, as shown by comparison of figures 6.3c and 6.3d.

However, comparing the simulated response of the shear specimens, indicates that this initial model did not simulate shear response accurately, as shown in Table 6.3 and Figure 6.4. For example, the maximum computed shear force in the model underestimated the measured shear force in Specimen 16 ($a/D = 0.375$) by 26%. Table 6.3 shows that similar discrepancies were noted for other specimens strongly influenced by shear, Specimen 10 and 14. As such, significant changes to the numerical model as described below.

Three significant differences between the model and the experiments were noted. First, the deformed shape of the test specimens dominated by shear indicates that one side sustained significant deformations while the other did not, as illustrated in Figure 6.5. This asymmetric behavior likely occurs because of minor eccentricities in the test setup of slight variations in the material properties of a specimen; either will cause damage to concentrate on one side. This is not captured by the analytical model. Second, very large shear strains were noted in the experiments failing in a “shear” model, however the base model utilized an small engineering strain approximation. Finally, severe nonlinear shear deformations of the specimens resulted in severe rotation demands on the support cradles and large deformations the elastomeric bearings and cotton duck pads. In many cases these deformations permanently damaged the cotton-duck bearing pads (they were replaced after every test); the model is not capable of capturing the nonlinear response of the bearing pads throughout the history. Instead, a different approach was taken with the

objective of optimizing the model to accurately approximate the shear strength of the specimens, since the objective of the numerical study was to extend the experimental study to further validate and extend the shear design model.

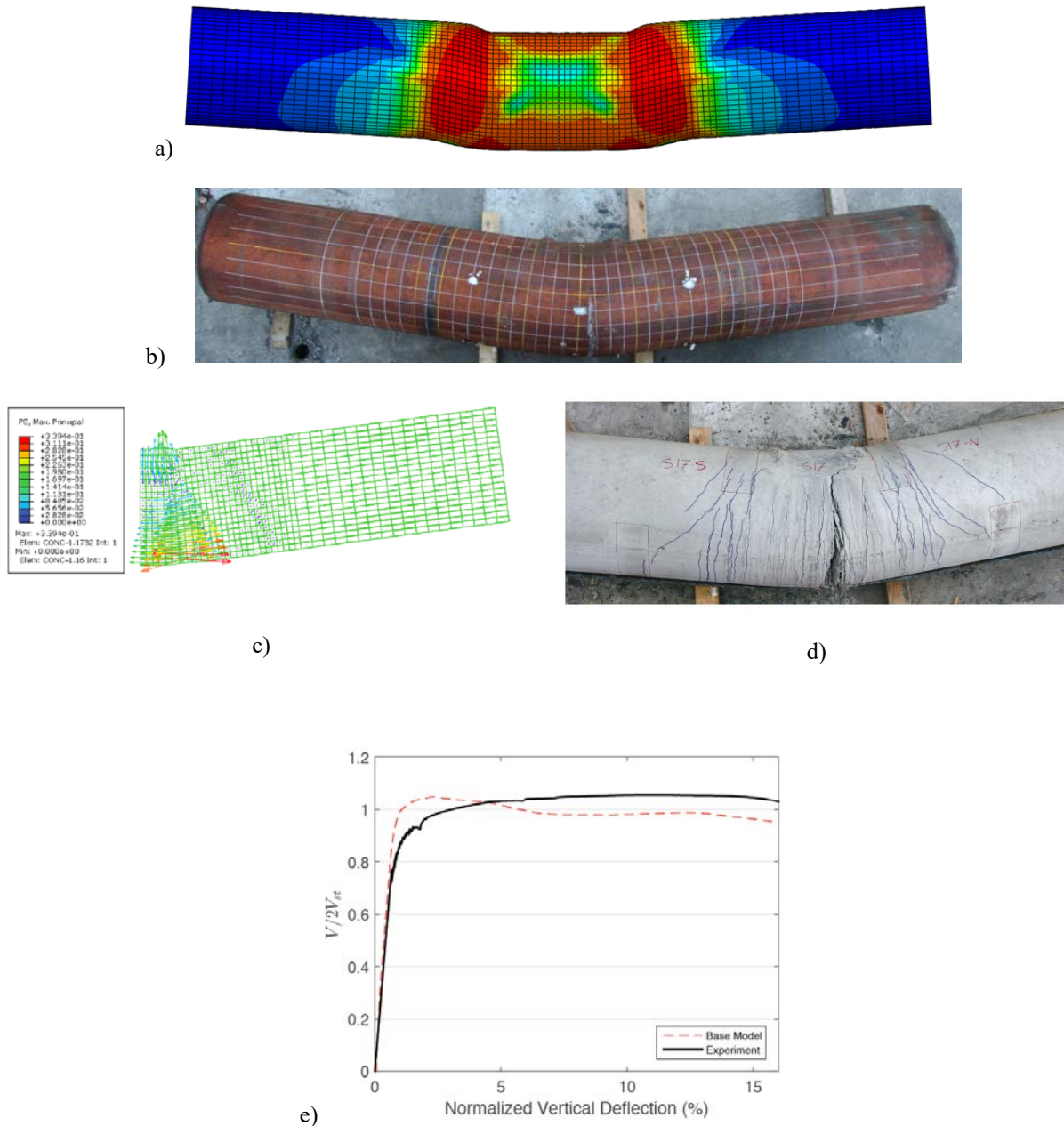


Figure 6.3. Computed and Measured Response of Specimen 17

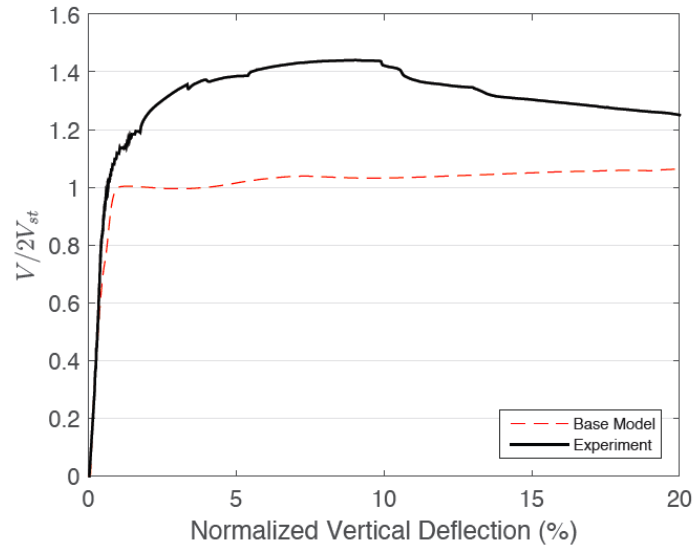


Figure 6.4. Force-Deflection Behavior of Specimen 16



Figure 6.5 Observed Asymmetric Deformations of Shear Dominated Specimen

The initial model was changed to address these issues, and Specimen 16 was used to validate the revisions as follows:

1. Because large local shear strains were observed, finite strain definitions were used for the steel and concrete with the Cauchy stress and logarithmic strain deformations employed in the ABAQUS model.
2. The concrete elastic modulus was defined the Eurocode, $E_c=10,000(f'_c+8)^{0.33}$ (MPa) as recommended by Hanneson (2010), since this definition results in more

strain hardening and better prediction of shear resistance.

3. The cotton-duck bearing pads were removed from the model, because these pads experienced extremely high strains and did not remain in position under high shear loads and had no effect on the test results at maximum load.
4. The support cradles had very large rotations with shear dominated tests, but these rotations were not predicted in the initial ABAQUS model. As a result, the support cradles were replaced by axial springs, which were rotated at an angle as observed in the experiments and illustrated in Figure 6.6, and had a spring stiffness of 100 kip/inch.

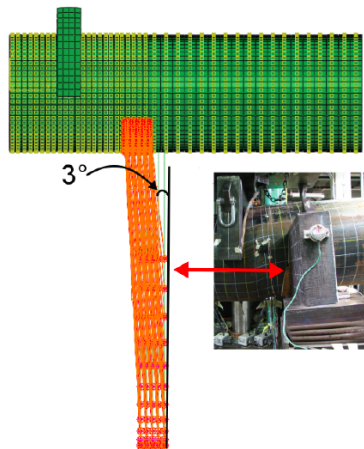


Figure 6.6. Replacement of the Support Cradle with Axial Springs

5. Finally, the concrete confinement was not achieved in the initial model because of the extremely large local strains in specimens with shear deformation. As a result, the confinement model proposed by Han (2007b) was used to simulate concrete confinement in the improved model. This approach better simulated the confinement effects for shear dominated specimens, as illustrated in Figure 6.7.

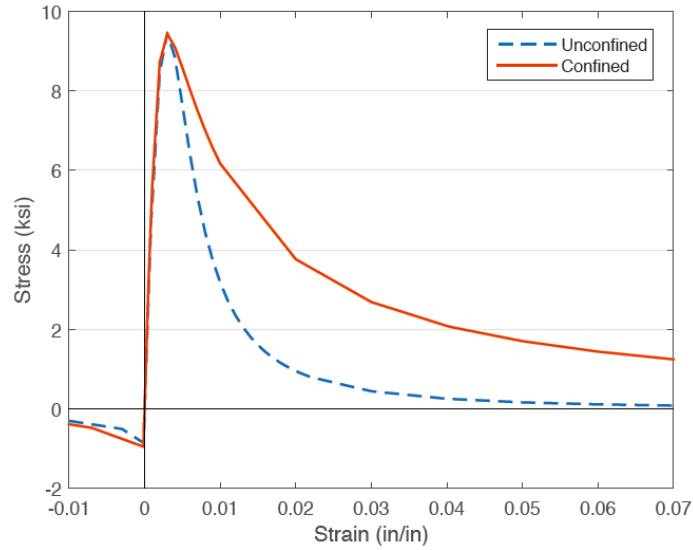


Figure 6.7. Confinement Model Used for Specimen 17 Based on Han 2007b

VALIDATION OF THE FINAL MODEL

Using the techniques in the final ABAQUS model, simulations of the specimens listed in Table 4.3 were created and validated using maximum experimental shear forces. A summary of the simulated values compared to the experiments is found in Table 4.4. With the final model, the average error in the predicted shear was approximately 8%. A positive value in the table reflects underestimation and a negative value, overestimation. Table 4.4 shows that larger errors are found with the intermediate shear span ratios of 0.5 and 0.375, where a combined shear-flexural behavior is expected.

Table 6.3 Summary of Error in Predicted Ultimate Shear Resistance

a/D	Specimen	Failure Mode	V _{ed} (kips)	V _{pr} (kips)	% Error
1.0	1	Flexure	322.0	327.9	-1.83 %
0.5	17	Flexure	544.5	624.8	-14.7 %
	2	Flexure	549.0	496.0	9.65 %
0.375	16	Flex-Shear	760.5	655.6	13.8 %
	10	Flex-Shear	660.0	628.1	4.83 %
0.25	14	Shear	788.4	764.7	3.01 %

PARAMETER STUDY

The experiments demonstrate the behavior of CFST members under shear and provide a basic estimate of the shear resistance of CFST, but it does not prove a good basis for separating the contributions the steel tube and concrete fill. The improved ABAQUS model was calibrated to the experimental results, and the calibration shows that the model provides an (conservative) accurate of the shear resistance. As a result, this model was used to complete a parameter study which primarily evaluated the effects of axial load ratio, P/P_0 , the effect of changes in the strength of the concrete and steel (f'_c and F_{yt}), the D/t ratio, and the effect of the internal reinforcement ratio, ρ_{int} .

All models had a diameter of 20 in., a tail length, L_T , of $2D$, to ensure full composite action, and either a/D of 0.375 or 0.25, since these specimens were strongly influenced by shear in the experiments. All steel tubes were assumed to be straight seamed with a clean interface between the steel tube and the concrete fill. In this evaluation the shear resistance is defined as:

$$V_n = 2V_{st} + V_{srl} + \eta V_c \quad (6.1)$$

with the concrete contribution estimated as:

$$\eta = \frac{V_{pr} - 2V_{st} - V_{srl}}{0.0316A_c \sqrt{f'_c}} \quad (f'_c \text{ is in ksi units}) \quad (6.2a)$$

$$\text{where: } V_{st} = 0.6F_{yt}(0.5A_{st}) \quad (6.2b)$$

$$V_{srl} = 0.6F_{yrl}(0.5A_{srl}) \quad (6.2c)$$

Axial Load Ratio

Axial compression can increase the shear-strength contribution of the concrete; this is used in the shear strength of concrete column in the ACI Building Code (ACI 2014). However axial load ratio increases the moment capacity, which can also increase the shear demand for a CFST responding in flexure alone. In addition, large axial loads can result in global and local stability issues. As such, it is difficult to conclude the impact of axial load, in particular since only one test examined the impact of axial load.

A parameter study was conducted to evaluate this effect further. Axial load ratios of 0%, 5%, 8.5%, 10%, 15%, 20%, 30%, 40%, and 50% were simulated as a uniform pressure applied to CFST as a uniform pressure on the tail surface of the concrete fill and line load on the edge of the steel tube. The line load was equivalent to the pressure applied to the concrete surface since the shell element application does not explicitly model a finite thickness. The yield stress of the steel was 56.8 ksi and f'_c was 6 ksi in this study. Both a/D of 0.375 and a/d of 0.25 were considered.

Figure 6.8 shows that the shear resistance increases with increasing axial load, with the rate of increase tapering off around 20% of the axial capacity. The models with a/D equal to 0.25 have a larger resistance at a given axial load ratio, suggesting as shear becomes more dominant the ultimate resistance increases, but the a/D ratio is not

precisely controlled because the large concentrated loads necessary to cause shear failure of CFST can only be applied over a finite length because of the large stress concentrations involved.

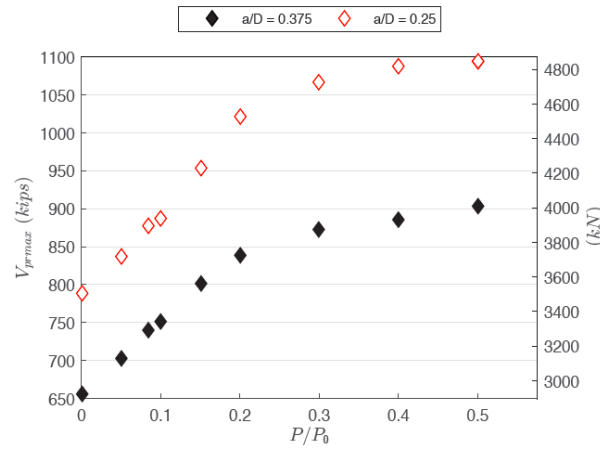


Figure 6.8: V_{prmax} vs. Axial Load Ratio

Figure 6.9 shows how the concrete contribution to the shear strength, η , increases with axial load for this CFST. This was approximated with a bilinear relationship, with a significant decrease in slope occurring at approximately 20% axial load. For example, considering only the a/D of 0.375 models, η begins at 4.7 and increases with a slope of 33.2. At an axial load ratio 20%, this value approaches 11 and increases with a slope now of 2.2, as shown in Figure 6.10.

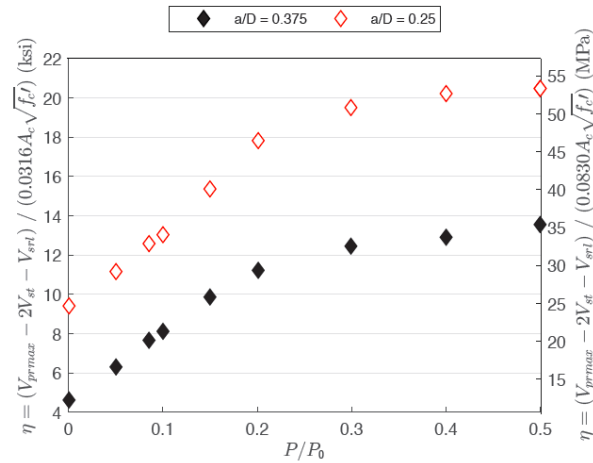


Figure 6.9. η vs. Axial Load Ratio

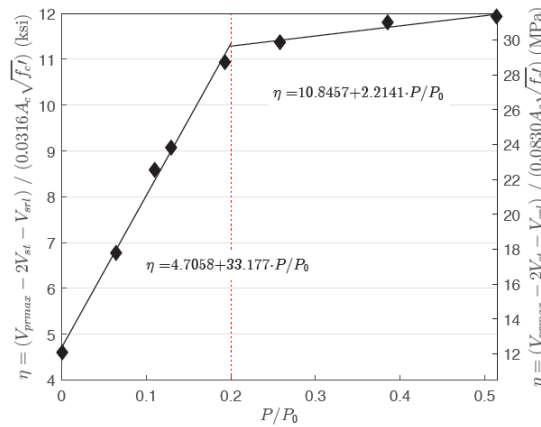


Figure 6.10. Bilinear Relationship of η vs. Axial Load Ratio for $a/D = 0.375$

Diameter to Thickness Ratio, D/t

The D/t ratio of the tube has a significant influence on the relative quantities of the steel and concrete. The ratio of tube diameter to thickness, D/t, is used to define the slenderness of circular CFSTs, and large (typically over 100) D/t ratios are more susceptible to local buckling than stockier members. Three values of D/t were considered: 53.3, 80 and 100, since this covers that maximum range of applicability for CFST bridge components.

The bending moments calculated for each analysis were compared to M_{PSDM} predictions, and maximum moment ratios, M_{max}/M_{PSDM} , less than 1.1 were clearly dominated by shear resistance. Ratios larger than 1.1 were often limited by flexure and as a result had reduced maximum shear values. Analyses were performed with different D/t ratios and various axial load ratios, and the results show that behavior was dominated by shear for all axial loads with the 0.375 and 0.25 a/D ratios.

Figures 6.11 and 6.12 show the increase in resistance and η values as a function of axial load, but this increase is significantly smaller with the lower D/t ratio, because the steel plays a greater role in developing the shear resistance of those sections. Compressive stress increases the shear capacity of concrete but it does increase the shear capacity of steel.

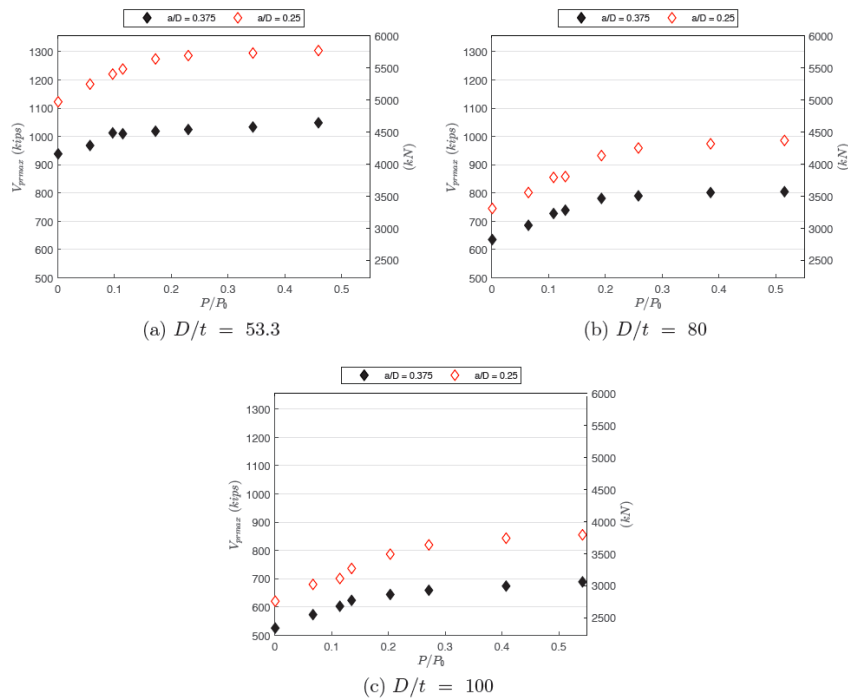


Figure 6.11. Shear Resistance vs Axial Load with Different D/t Ratios

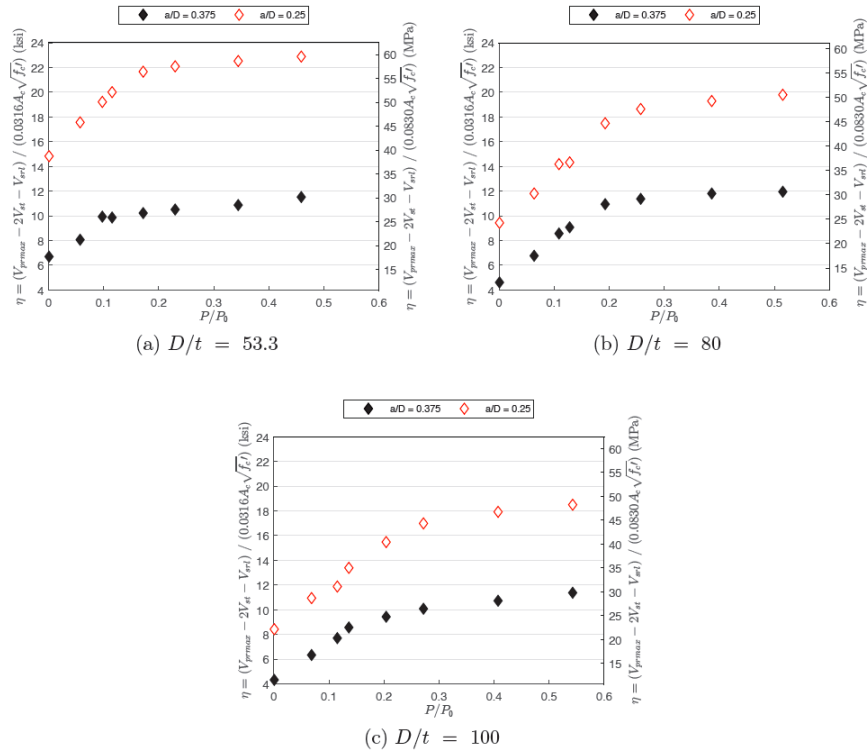


Figure 6.12. η vs. Axial Load Ratio with Different D/t Ratios.

Concrete Strength, f_c'

In this study, f_c' varied between 3, 6, 8.6, and 12 ksi while the steel remained at a 56.8 ksi yield stress. The maximum bending moments were again evaluated for these specimens, and specimens with f_c' of 3 ksi frequently had M_{\max}/M_{PSDM} ratios larger than 1.1 and were dominated by flexure rather than shear resistance. Figure 6.13 shows the η value as a function of axial load for different concrete strengths. Comparison of these figures shows that η does vary for different concrete strength.

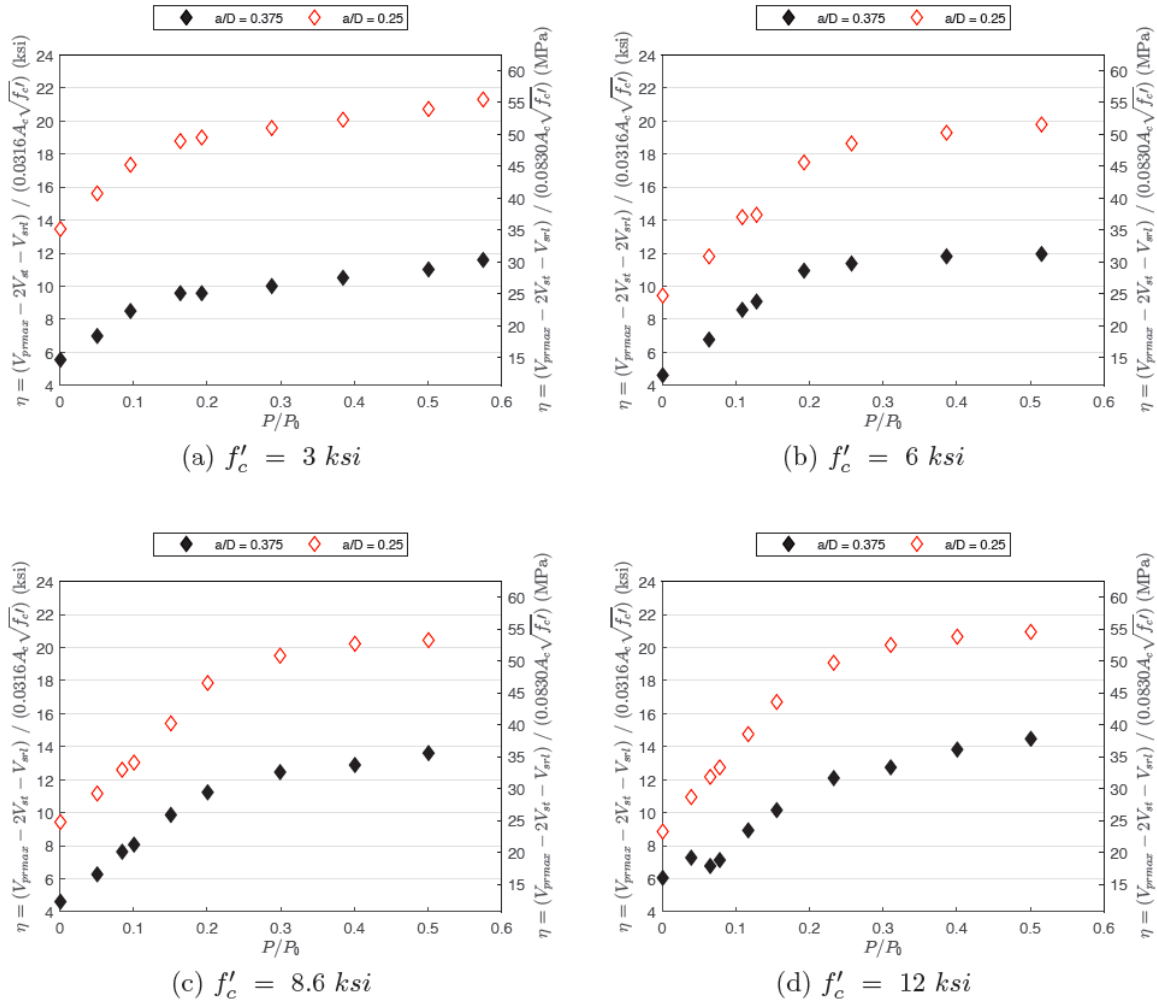


Figure 6.13. η vs. Axial Load Ratio with Different Concrete Strength

Yield Stress of Steel Tube, F_{yst}

Increased yield strength of the steel nominally decreases the relative contribution of concrete fill. The yield stress of the steel was varied between 35, 56.8 and 70 ksi, since is a reasonable for bridge construction. The concrete strength was 6 ksi for all analyses in this part of the study.

Analysis of the maximum computed bending moments showed that all analyses had M_{\max}/M_{PSDM} ratios less than 1.1 with higher yield stress steels and were dominated by shear resistance. However, the lowest steel strength has larger M_{\max}/M_{PSDM} ratios and

the shear force was limited or influenced by flexure. Figure 6.14 clearly shows that the maximum shear resistance is strongly influenced by the yield stress of the steel.

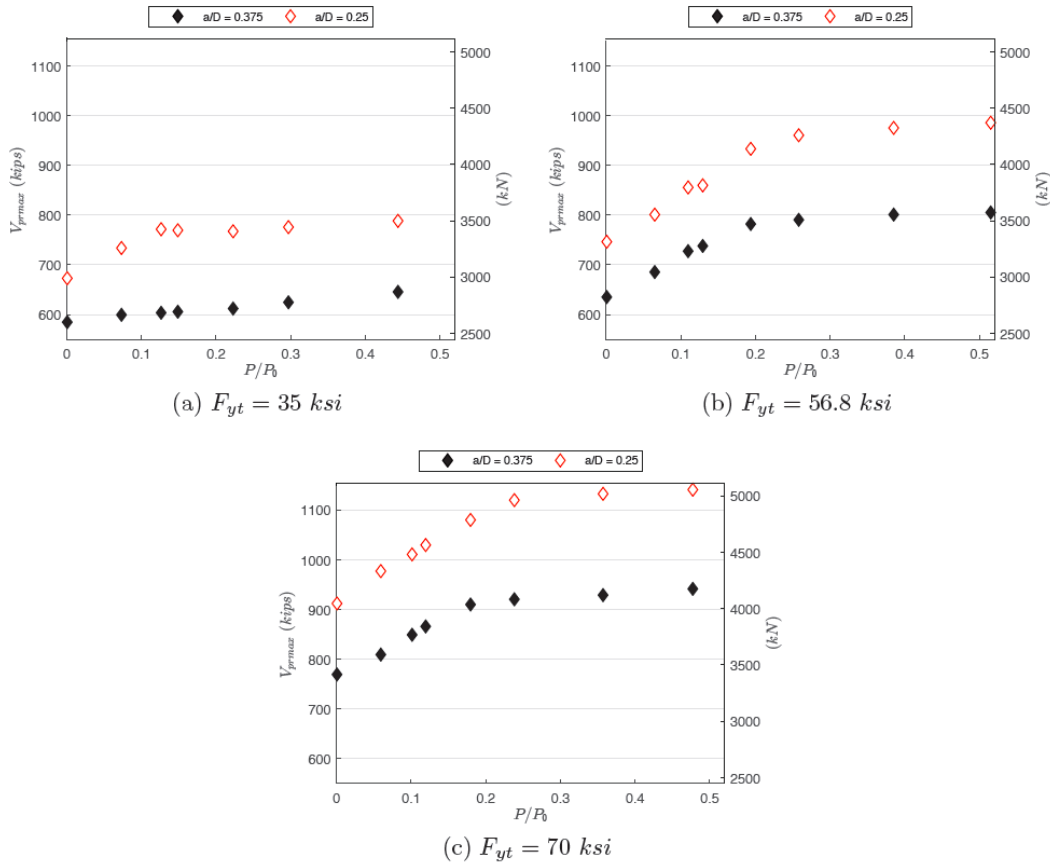


Figure 6.14. Shear Resistance vs. Axial Load Ratio with Different Yield Stress, F_{yst}

Figure 6.15 shows the concrete contribution factor, η . The lowest steel tube strength models showed a smaller increase in η over a smaller range than the other two groups. This observation is consistent with observations with higher axial load ratios, where it is suspected that flexural behavior has a larger impact. Among the two tube steel strengths where shear was observed, η varied significantly relative to previous models. The concrete factor was greatest with the largest steel tube strength, 70 ksi, and decreased with tube strength. Because η was derived to estimate the concrete contribution, these large factors would appear to contradict the notion that the concrete fill does not provide as

much strength to the CFST section as the steel tube. However, because the concrete strength parameter study showed the term η to vary little between f_c' values of 3 and 12 ksi. This suggests that the factor of 2 being used for V_{st} is an underestimate of the contribution of the steel tube for CFST.

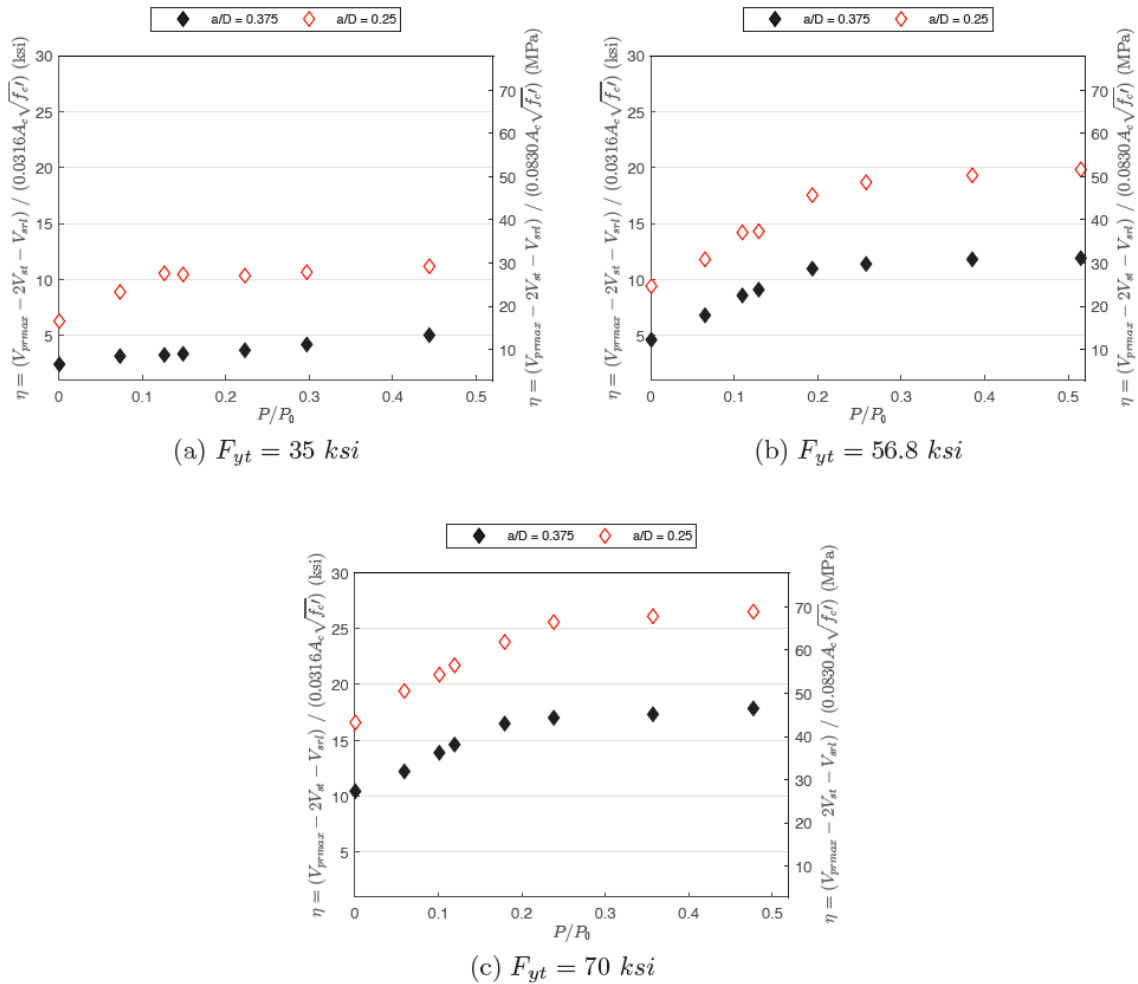


Figure 6.15. η vs Axial Load Ratio for Various Steel Yield Stresses

Effect of Internal Reinforcement Ratio, ρ

Reinforced concrete-filled steel tubes (RCFSTs) are CFSTs with internal longitudinal reinforcement. For this part of the study, internal reinforcement with individual bars modeled as truss elements (T3D2) perfectly bonded (“Embedded Region

Constraint”) to the concrete, and arranged in the concrete fill uniformly in the circumferential direction with a bar located at the top and bottom of the cross-section centerline and a distance of 1.75 in. from the interior surface of the tube.

The material properties for the reinforcing bar used the same trilinear material behavior the tube steel, with a yield strength of 60 ksi and ultimate strength of 90 ksi.

The internal reinforcement ratio, ρ_{int} , was varied from 1% to 2%. The 1% design used 10 No. 5 reinforcing bars, each with a cross-sectional area of 0.31 in.², and the 2% design used 10 No. 7 reinforcing bars, each with a cross-sectional area of 0.6 in.². Because the simulation only models half of the RCFST cross-section, only 6 bars were actually included in the model, with the top and bottom bars each given an area equal to half of the designated bar area. (The yield stress of the steel tube was 56.8 ksi, and the concrete strength, f'_c was 6 ksi as used in prior models.)

The maximum computed moments were again compared to the M_{PSDM} for all models, and all models with M_{max}/M_{PSDM} less than 1.1 were deemed a shear failure. Figure 6.16 shows the computed maximum shear resistance for the specimens in this series. The effect of concrete is quite significant for the CFST without internal reinforcement. The figure shows that axial has a significant effect on the shear resistance of CFST but significantly reduced effect on the RCFST specimen. Nevertheless, the internal reinforcement increased the shear resistance, but the increase is relatively small with the increased area of steel for the RCFST specimens is considered.

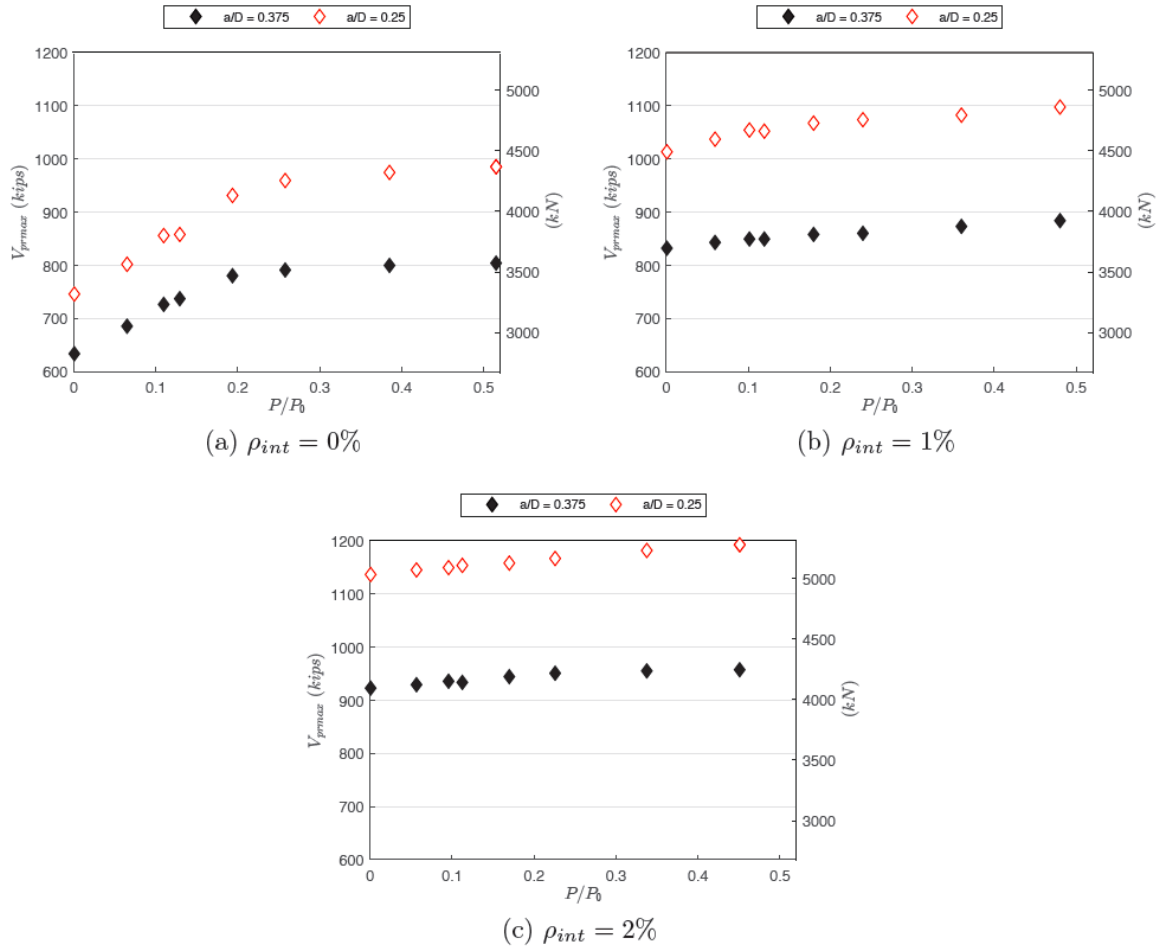


Figure 6.16. Shear Resistance vs. Axial Load Ratio for RCFST Specimens

The model results were used to calculate the normalized contribution of the concrete, η , were are presented in Figure 6.17. The following observations are made:

- There is little change of η in RCFSTs with increasing axial load
- The value of η increases with an increase in internal longitudinal reinforcement
- Larger η values are noted for the 1% RCFST without axial load than the CFST with an axial load ratio of 50.

Clearly, the introduction of reinforcement allows the concrete to contribute to the resistance of the member by restricting large cracks from developing in the concrete as quickly. So, as ρ_{int} increases, not only does that RCFST benefit in terms of moment and

shear capacity from the added steel bar area, but also from the concrete crack arresting behaviors. However, the reinforcement was not particularly effective in providing shear strength. The reinforcement increased flexural resistance and this resulted in increased shear deformations.

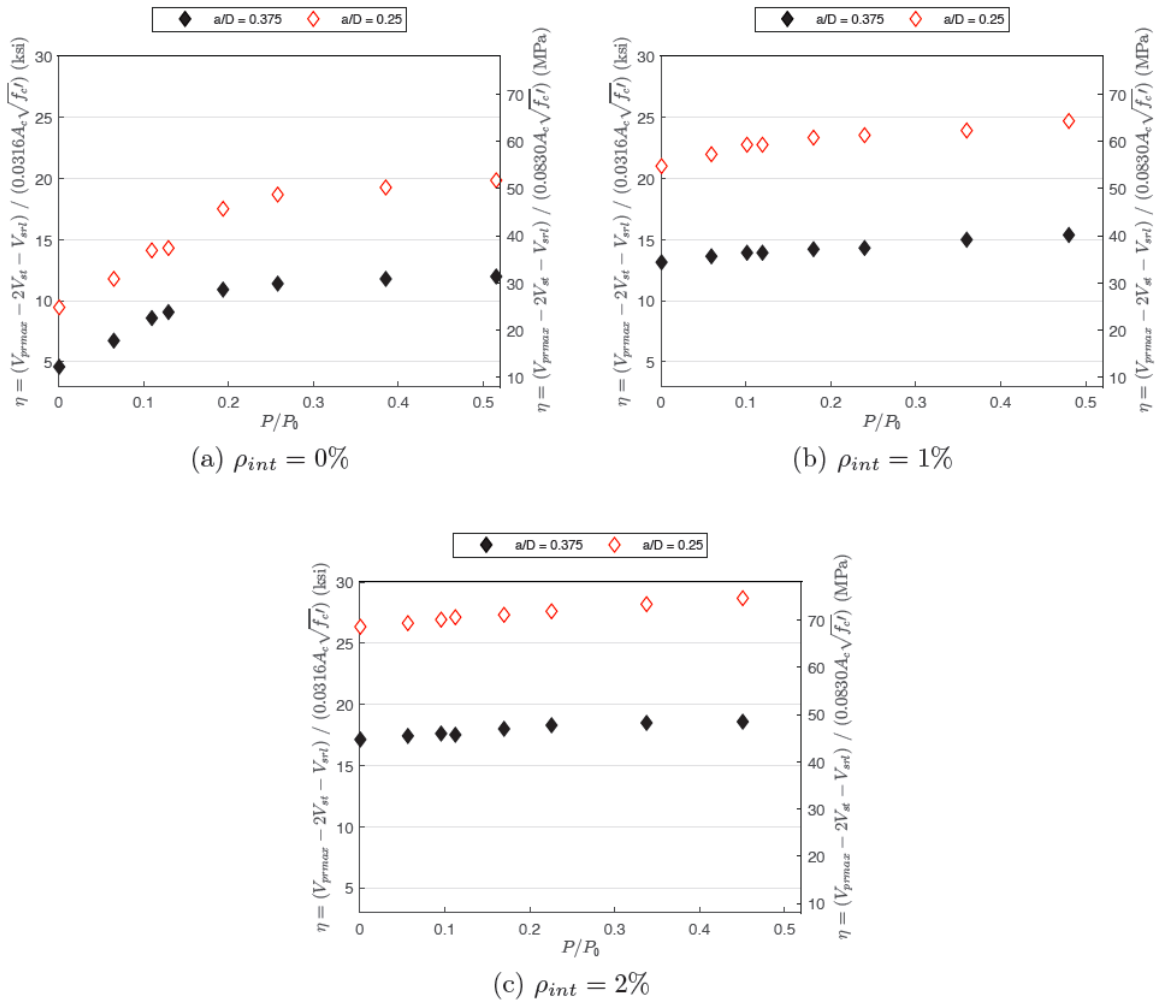


Figure 6.17. η vs Axial Load Ratio of RCFST Specimens

IMPROVED DESIGN EXPRESSIONS

The design expressions that were developed in earlier chapters based entirely upon experimental results. These expressions provide no consideration of axial on the

shear resistance although experimental results clearly showed that some benefit existed. Further, the parameter studies show that as axial load increases, the maximum predicted shear force increases linearly until about 20% axial load, where the rate of this increase then decreases. This increase in shear resistance with axial load is typically attributed to concrete, because concrete cracking is restrained by axial load. Using these results, a relationship between axial load and the contribution of concrete can be developed and a refined shear capacity expression can be formed.

Simulations of the CFST resistances from shear controlled failures (i.e., $M_{pr} < 1.1M_{PSDM}$) and were subject to 20% axial load or less were evaluated. A linear, least-squares regression analysis was performed; Figure 6.18 illustrates the results.

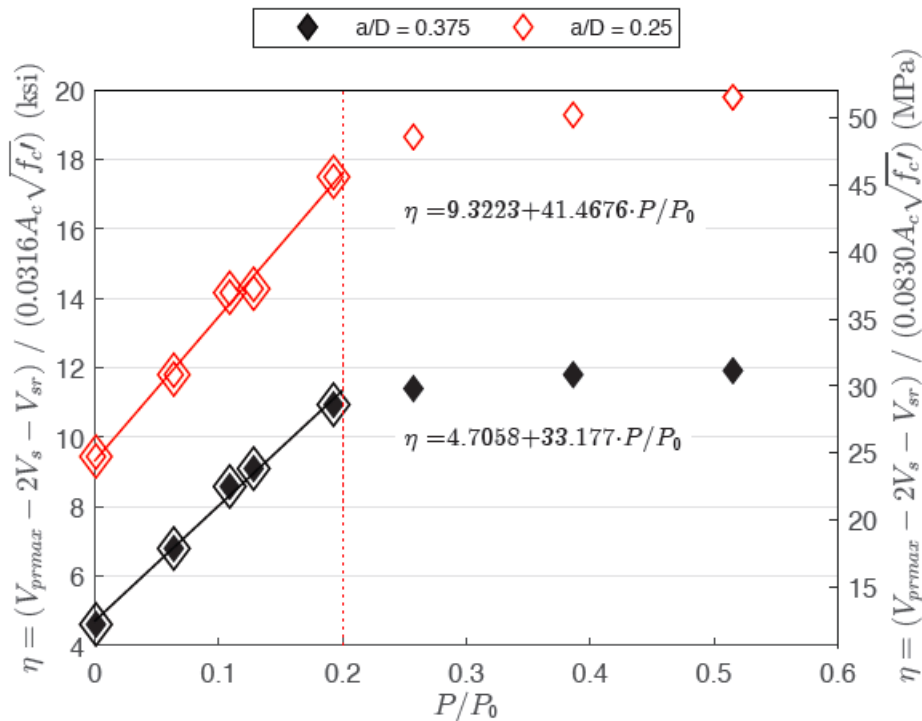


Figure 6.18: Example of Least Squares Linear Regression Fit Line using CFST with $D/t = 80$, $f'_c = 6$ ksi, $F_{yt} = 56.8$ ksi, and $\rho_{int} = 0\%$

Using the relationships developed through this process, a final expression for η was estimated, with a maximum η of 10 set at the 20% axial load marker, where a notable decrease in the slope of the η - P/P_0 was observed in most models. Figure 6.19 shows that the new η relationship better reflects the concrete contribution compared to those found in the previously discussed provisions, while remaining conservative.

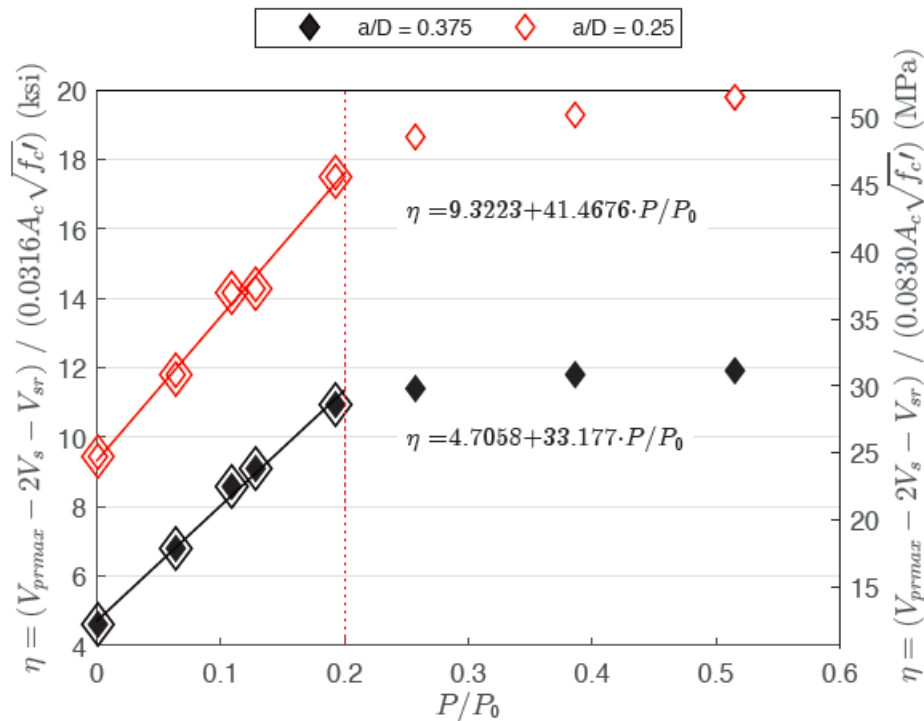


Figure 6.19. Comparison of $\eta = 5(1 + 5 \cdot P/P_0) \leq 10$ for Shear-Controlled Models

The total data set (simulation and experimental results) were compiled for test specimens computational models controlled by shear; these were compared using the proposed limit state criterion of Eq. 6.4, both with and without axial load are evaluated here. Although four specimens by Xiao met the criterion presented, this data was excluded from analysis because the researcher reported that the end plates experienced significant deformations, with some specimens designated to fail by the end plate weld, and specific

specimens with these issues were not identified. With the behavior of the weld plates being so influential on the behavior of the specimens, this data was found unreliable for determining shear capacity. Nakahara also had one specimen that fell into the shear category with the proposed criterion. However, the results from this program also exhibited significant flexure-like behaviors and, therefore, was eliminated from this evaluation.

$$V_{n(prop)} = 2V_{st} + V_{srl} + \eta V_c \quad (6.4a)$$

$$where : \eta = 5 \left(1 + 5 \cdot \frac{P}{P_0} \right) \leq 10 \quad (6.4b)$$

$$V_{st} = 0.6F_{yt}(0.5A_{st}) \quad (6.4c)$$

$$V_{srl} = 0.6F_{yrl}(0.5A_{srl}) \quad (6.4d)$$

$$V_c = 0.0316A_c\sqrt{f'_c} \quad (6.4e)$$

(f'_c is in ksi units)

The sample size is still quite small, and the scatter relatively large, as demonstrated in Figure 6.20. The Xu data is low compared to other shear controlled specimens. These specimens are thought to be influenced by flexural action, and Xu reported the lowest specimen on the plot to be dominated by flexure. Other flexurally dominated specimens could also be mistakenly put into this analysis because of the underestimated moment arm in calculating M_{ed} . On the other hand, the data reported by Ye shows to be the most conservatively estimated. These specimens had large axial loads applied to them, more than typical of CFST use, where the η value was capped, and the maximum η value in this recommendation was based on models that allowed for relative movement between that tube steel and concrete fill. The experimental program by Ye used end plates that restricted this behavior. By restricting this slippage, the composite behavior of the CFST is maintained throughout testing, allowing it to resist larger forces

and therefore making the estimation with $V_{n(prop)}$ more conservative. In spite of these variations among experimental programs, the proposed design expression still shows reasonable capacity estimation with a mean $V_{ed}/V_{n(prop)}$ of 1.13 and standard deviation of 0.158

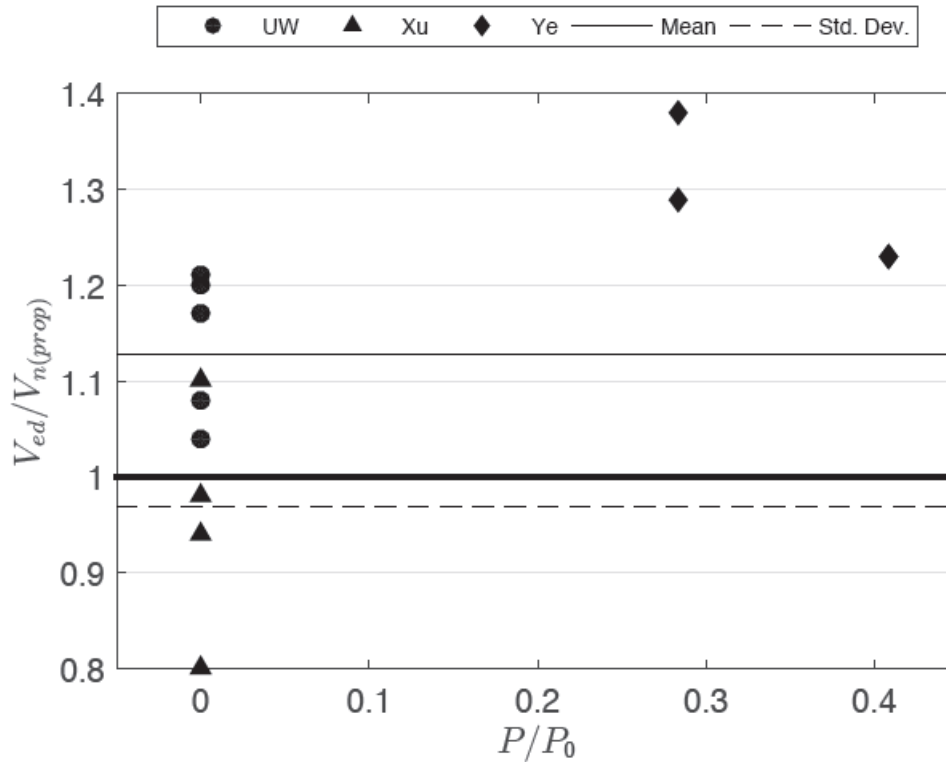


Figure 6.20: Comparison of $V_{n(prop)}$ to Experimental Results Meeting Proposed Limit State Criterion, Including Axial Load

Figure 6.21 shows comparisons of the proposed shear resistance to the predicted resistance from analytical simulations that resulted in shear-dominated response. This evaluation shows the mean effective ratio, $V_{ed}/V_{n(prop)}$, and standard deviation to be 1.17 and 0.134. Overall the expression is shown to be conservative.

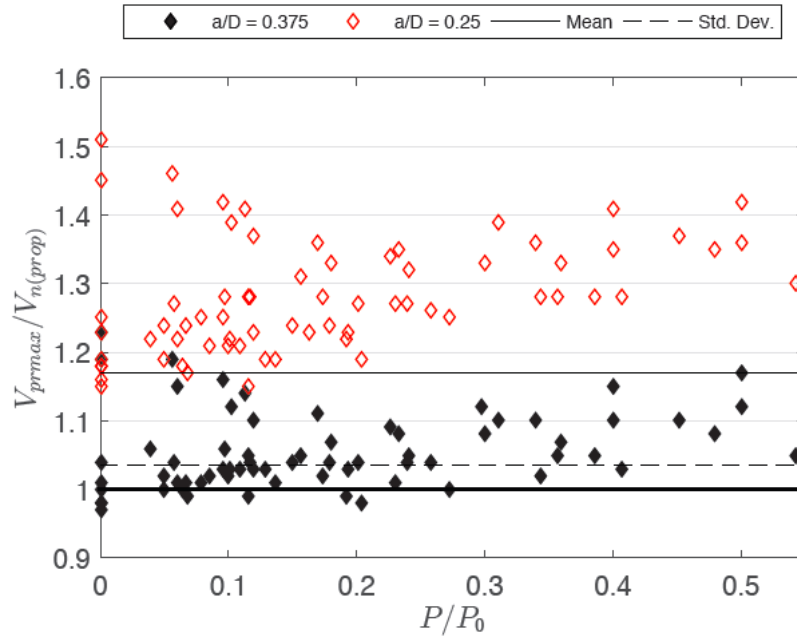


Figure 6.21: Comparison of $V_{n(prop)}$ to Shear Controlled Models, Meeting Limit State Criterion

The longitudinal reinforcement in the proposed equation has been estimated to contribute to the total CFST capacity with only half of its total cross-sectional area being utilized. This was largely based qualitatively on experimental and parametric study data that suggested the reinforcement is less effective than the steel tube in terms of reinforcing the CFST member. Even though explicit quantitative analysis was not used in estimating this, $V_{n(prop)}$ shows to conservatively estimate the shear capacity of RCFSTs in the experiments and models meeting the proposed limit state criterion, as shown in Figure 6.22. All points are above 1.0, and the mean and standard deviation of $V_{ed/pr}/V_{n(prop)}$ are approximately 1.2 and 0.15, respectively.

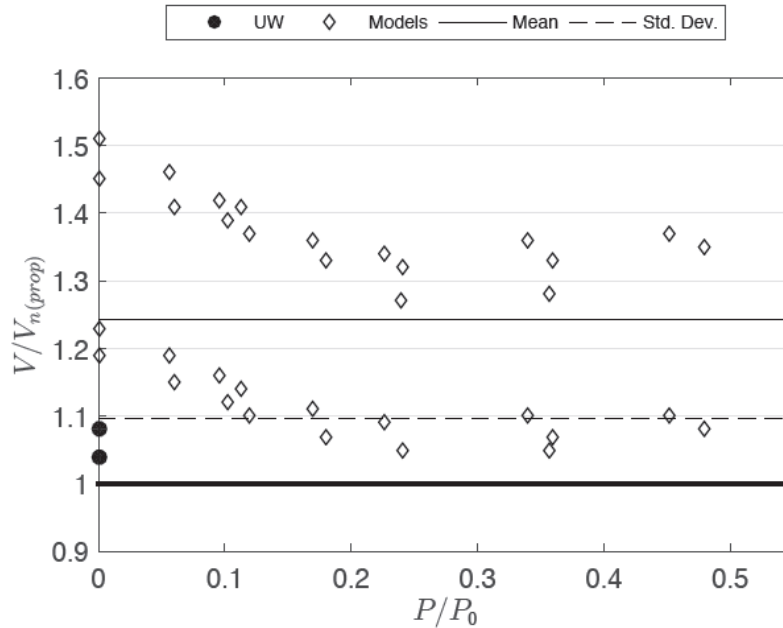


Figure 6.22. Comparison of $V_{n(prop)}$ to Experimental and Analytical RCFST Shear Specimens, Meeting Proposed Limit State Criterion

Figure 6.23 summarize the results for both experimental and analytical data that meet the proposed limit state criterion for shear. Altogether, the data demonstrates conservatism and more precise shear capacity estimation than seen with previous design expressions, with a mean effective ratio of approximately 1.2 and standard deviation of 0.14. A few results do fall below unity in the figure due to the incidental inclusion of flexural response from underestimated moments. Moreover, nominal capacity is being estimated here and in design application, factored loads would be analyzed and an additional resistance factor would be applied to this value, establishing further conservatism.

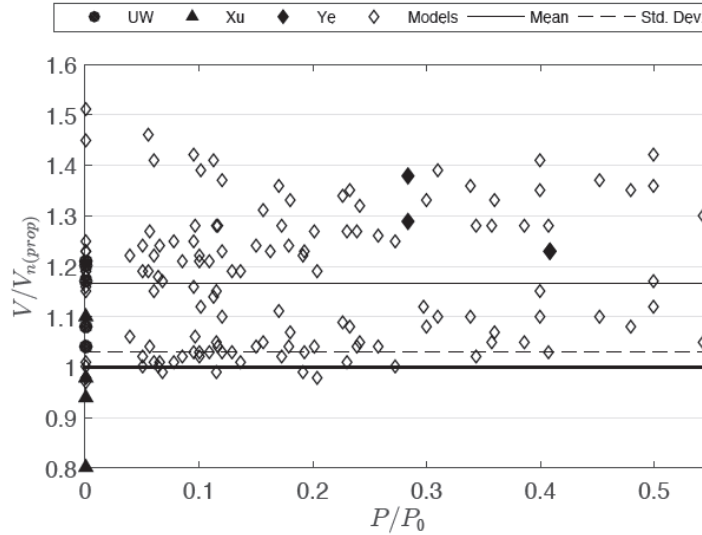


Figure 6.23: Comparison of $V_{n(prop)}$ to Experimental and Analytical Shear Specimens, Meeting Proposed Limit State Criterion

Using the proposed equation, $V_{n(prop)}$, an evaluation of a potential resistance factor, ϕ , that could be used for LRFD design based on Ravindra and Galambos (1978) was completed. Based on this probabilistic calculation, a ϕ of 0.90 is recommended.

Designers must make decisions that yield an efficient solution. This research has shown that the tube steel provides most of the shear resistance to CFST members. The experimental results show that on average the steel tube provides approximately 83% of the total shear resistance, while the concrete and reinforcement only contribute 15 and 13%, as shown in Figure 6.24a. When using the larger spectrum of material strengths, component areas, and axial load in the simulations (Figure 6.24b), the average steel tube contribution lessens to 70%, largely due to the low strength steel (35 ksi) and D/t of 100 models. The concrete then increases in participation to 26% due to the effect of axial load, and not the increases in f'_c of some models. And finally, the reinforcement moves down to 10% contribution. With all results considered (Figure 6.25), the tube steel provides 72% of

total shear resistance on average, with the concrete following with 25% average contribution, and finally, the reinforcement with 10%.

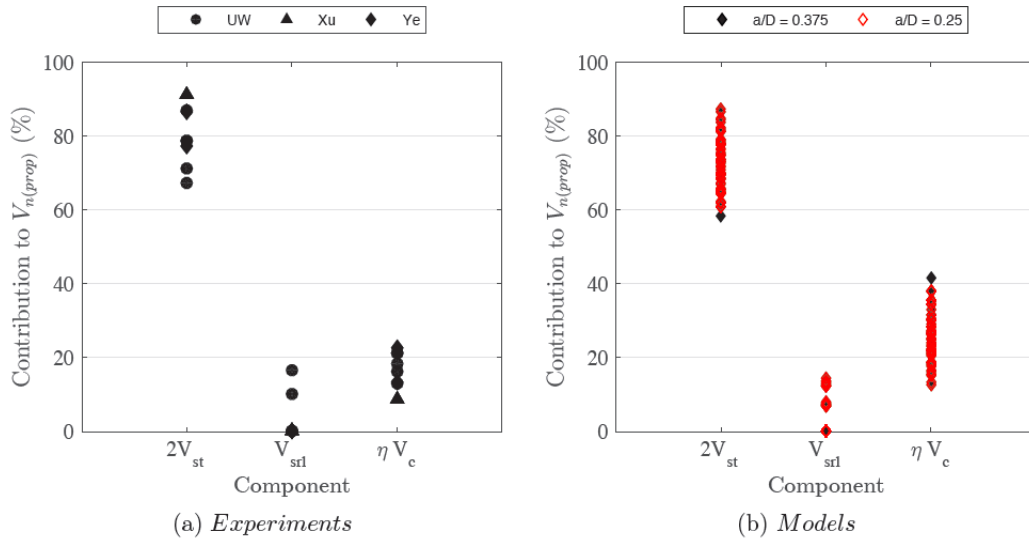


Figure 6.24. Contribution of Tube Steel, Internal Reinforcement, and Concrete to Total Shear Resistance According to $V_{n(prop)}$

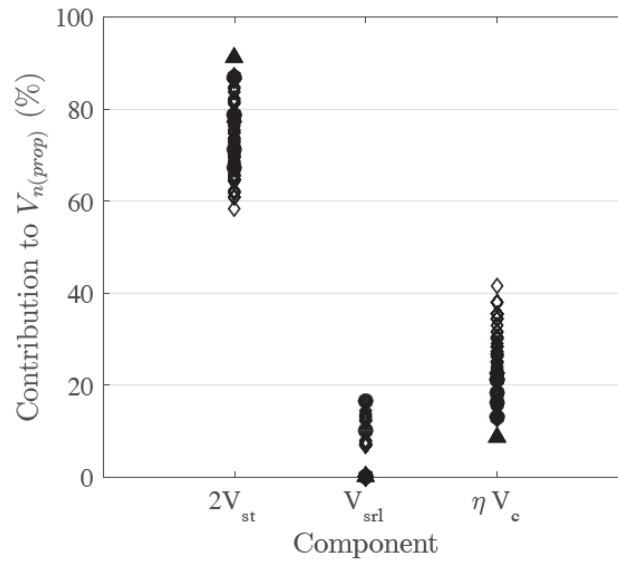


Figure 6.25: Contribution of Tube Steel, Internal Reinforcement, and Concrete to Total Shear Resistance According to $V_{n(prop)}$ using All Data

As noted, the data sets presented look at large ranges of CFST component design. However, if only parameters common to CFST and RCFST design are considered, that is, a D/t of 80, $F_{yt} \approx 50$ ksi, $f_c' \approx 6$ ksi, and $P/P_0 \leq 0.2$, the average contributions are more commonly 70.5% from the tube, 22% from the concrete fill, and 10.7% from the internal reinforcement, as shown in Figure 6.26.

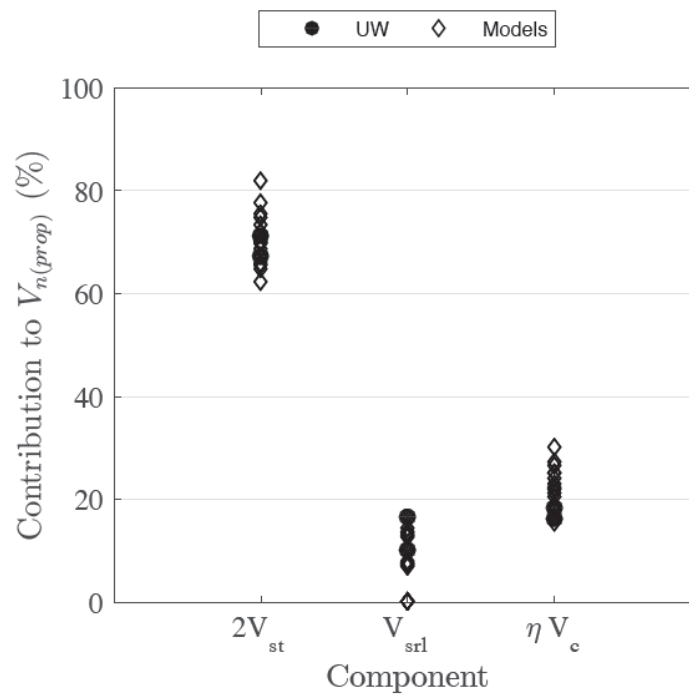


Figure 6.26. Contribution of Tube Steel, Internal Reinforcement, and Concrete to Total Shear Resistance According to $V_{n(prop)}$ using Typical CFST Design

CHAPTER 7

SUMMARY, CONCLUSIONS, AND RECOMMENDATIONS

SUMMARY

This research has evaluated the shear resistance of CFST and RCFST members. The research was conducted in three phases: (1) literature review, (2) experimental study, and (3) analysis of test results.

The literature review culled and analyzed the results from several prior studies. These studies were typically performed on small diameter tubes (less than 6 inches). The results of these prior experiments were evaluated and compared to establish and research models for predicting shear resistance. There was great scatter in these results, and a significant portion of this scatter appears to be associated with the inability to separate shear and flexural yielding as the controlling response mechanism. In addition to the size and misinterpretation of the behavior, several study parameters also contributed to the uncertainty in shear strength prediction including: (1) use end caps, (2) large axial loads, (3) expansive concrete, and (4) very overhang/tail length (length beyond the support).

The experimental study consisted of 22 large-scale (20 in. diameter, D) tests. The study parameters included: (1) shear span to diameter ratio (between $0.25D$ and $1D$), (2) concrete strength, (3) internal reinforcement, (4) tube type (spiral or straight seam), (5) condition of internal concrete (gravel or cured concrete), (6) axial load, (7) internal surface condition (muddied, clean or greased), and (8) the overhang/tail length (length of the specimen beyond the support). In all, seventeen CFST specimens, 4 RCFST specimens, and one steel tube with gravel in shear spans were built.

The tests were completed, and the test data was compared to prior test results and various design models for predicting CFST behavior.

Finally nonlinear analyses with the *ABAQUS* computer program were performed. These analyses were initially performed as an aid in designing the test apparatus. Later analyses were compared to experimental results to evaluate the accuracy of the predictions and hopefully extend the experimental results to a wider range of conditions. This later goal has not yet been realized, as the analytical model is not able to accurately predict the displacement and resistance of shear yielding specimens in a complete manner, and, as a result, the report only addresses modeling and simulated results in a limited way.

A new shear strength expression was developed based on the test results. The shear strength expression was also compared with prior test. Both provided very good agreement. This new shear strength expression provides a total shear strength of 2 times the current CFST shear strength expression used by WSDOT.

CONCLUSIONS

A number of conclusions are available from this research, including:

1. Shear yielding of CFSTs results in very ductile behavior with large inelastic deformation capacity. CFST members controlled by shear yielding developed large inelastic deflections prior to tearing of the steel in the shear region. This is in contrast to RC members which do not develop ductility when responding in shear.
2. The shear force carried by a member can be determined by the plastic flexural capacity or shear yield capacity. That is, if the member yields in flexure, the flexural

strength, approximated as $1.25M_{psdm}$, will control the shear demand. In some cases, the member will begin to yield in flexure and, upon further loading, the steel will also yield in shear. This flexure-shear response mode is an interface between two different behaviors. It does not result in a unique failure mode.

3. Bond slip was noted in 2 of the 22 specimens. One specimen used a grease interface in a straight seam welded tube. The second specimen that sustained large slip had a very short ($D/2$) tail length, the length beyond the support. In both cases, the bond slip limited the ultimate capacity of the specimen, but the specimens still developed the moment capacity predicted by the plastic stress distribution method, M_{psdm} .
4. The specimen with muddied interface had no apparent adverse effect from this contaminated bond surface.
5. The tail length was varied between $D/2$ to $2D$, and specimens with tail length greater than D showed no adverse effects on the CFST performance. A minimum length of one diameter beyond the support is recommended for developing the plastic capacity of CFST.
6. Specimen 13 had axial compressive load which was less than the axial load at balance. Application of the axial load increased the resistance of the CFST member (approximately 18%). However, because only one specimen evaluated the impact of this parameter, the impact of the axial load was not included in the shear design expression.

7. Use of internal reinforcement resulted in an RCFST specimens were stronger than identical CFST without internal reinforcement, but the effect of internal reinforcement was not significant.
8. Because of the loads and shear spans required to develop shear yielding of CFST, it would appear very difficult to actually have shear yielding behavior in practice.

RECOMMENDATIONS

Design recommendations were developed from this research, including:

1. The ultimate shear yield capacity of CFST is defined by the following set of equations:

$$V_{n(prop)} = 2V_{st} + V_{srl} + \eta V_c$$

$$where : \eta = 5 \left(1 + 5 \cdot \frac{P}{P_0} \right) \leq 10$$

$$V_{st} = 0.6F_{yt}(0.5A_{st})$$

$$V_{srl} = 0.6F_{yrl}(0.5A_{srl})$$

$$V_c = 0.0316A_c\sqrt{f'_c}$$

$$(f'_c \text{ is in ksi units})$$

where the mean experimental resistance from the UW test program was 1.2 times the nominal value, as shown here, and the standard deviation was 0.17.

2. The minimum development (beyond the point of zero moment) to achieve the full plastic capacity of CFST is 1.0D.

3. RCFST develops increased resistance compared to CFST with identical tube, concrete fill and geometry but without internal reinforcement. The shear strength equation accounts for this increase.

REFERENCES

- American Association of State Highway and Transportation Officials (AASHTO) (2016) "AASHTO LRFD Bridge Design Specifications," 7th Edition with 2016 Interims, AASHTO, Washington, D.C.
- American Concrete Institute (ACI). (2011). Building Code Requirements for Structural Concrete and Commentary. ACI, Farmington Hills, MI.
- American Institute of Steel Construction (AISC). (2010). Specification for Structural Steel Buildings. AISC, Chicago, IL.
- Bishop, E. (2009). Evaluation of the Flexural Resistance and Stiffness Models for Circular Concrete-Filled Steel Tube Members Subjected to Axial-Flexural Loading. MSCE Thesis, University of Washington . Seattle, WA.
- Brown, N., Kowalsky, M., & Nau, J. (2015). Impact of D/t on seismic behavior of reinforced concrete filled steel tubes. *J. Constr. Steel Res.*, 107 , 111-123.
- Lehman, D., & Roeder, C. (2012). Initial Investigation of Reinforced Concrete Filled Tubes for use in Bridge Foundations. WSDOT Research Report WA-RD 776.1 . Olympia, WA.
- McGann, C. (2013). Numerical Evaluation of Forces on Piled Bridge Foundations in Laterally Spreading Soil. PhD Dissertation, University of Washington . Seattle, WA.
- Moon, J., Lehman, D., Roeder, C., & Lee, H. (2012). Strength of Circular Concrete-Filled Tubes with and without Internal Reinforcement under Combined Loading. *J. Struct. Eng.*, 139(12) , 1-12.
- Nakahara, H., & Tokuda, S. (2012). Shearing Behavior of Circular CFT Short Columns. *Proc. of the 10th Intl. Conf. on Advances in Steel Concrete Composite and Hybrid Structures*, (pp. 362-369). Singapore.
- Qian, J., Cui, Y., & Fang, X. (2007). Shear strength tests of concrete filled steel tube columns. *China Civil Engineering Journal*, 40(5) , 1-9.
- Roeder, C., Cameron, B., & Brown, C. (1999). Composite Action in Concrete Filled Tubes. *J. Struct. Eng.*, 125(5) , 477-484.
- Roeder, C., Lehman, D., & Bishop, E. (2010). Strength and Stiffness of Circular Concrete-Filled Tubes. *J. Struct. Eng.*, 136(12) , 1545-1533.

- Roeder, C., Lehman, D., & Thody, R. (2009). Composite action in CFT components and connections. *Engineering Journal*, 47(4) , 229-242.
- Thody, R. (2006). Experimental Investigation of the Flexural Properties of High-Strength Concrete-Filled Steel Tubes. MSCE Thesis, University of Washington . Seattle, WA.
- Washington State Department of Transportation. (2012). Design Memorandum: Structural Design Recommendations of CFT and RCFT for Bridge Foundation. Olympia, WA.
- Xiao, C., Cai, S., Chen, T., & Xu, C. (2012). Experimental study on shear capacity of circular concrete filled steel tubes. *Steel Compos. Struct.*, 13(5) , 437-449.
- Xu, C., Haixiao, L., & Chengkui, H. (2009). Experimental study on shear resistance of self-stressing concrete filled circular steel tubes. *J. Constr. Steel Res.*, 65 , 801-807.